Estimating Diffusion Coefficients and Visualizing Interactions in Propane-Heavy Oil Systems

by

Khan Sameem Athar

A thesis submitted in partial fulfillment of the requirements for the degree of

Master of Science

in

Petroleum Engineering

Department Of Civil & Environmental Engineering
University of Alberta

Abstract

Unconventional oil (mainly heavy oil, extra heavy oil and bitumen) represents a significant share of global oil reserves. Due to their high viscosity, efficient recovery of oil from these reserves is challenging and remains an issue of ongoing global research. Thermal recovery methods are generally accepted as viable and successful. These methods rely on heat for viscosity reduction. Their high energy requirement has lead the industry to investigate solvent based recovery methods as alternatives. Among solvent based recovery methods, vapour extraction (VAPEX) is gaining most attention.

VAPEX has immense potential for heavy oil recovery due to its low energy requirement and low GHGs emission. Experimental and numerical studies of VAPEX have indicated its technical and economic viability. In VAPEX, in-situ viscosity reduction is due to molecular diffusion of solvent in heavy oil. One of the most important uncertainty of VAPEX is the mixing rate of light hydrocarbon solvent molecules with heavy hydrocarbons (high density and high viscosity). This mixing rate is quantified as diffusion coefficient (D) or diffusivity and determines the effectiveness of VAPEX.

Measuring diffusion coefficient is difficult, especially at in-situ conditions, i.e. at high temperature and pressure. There is no universally acceptable method of measuring diffusion coefficient. Therefore, it is inferred through the data obtained from experimental methods, with the pressure decay (PD) technique being the most convenient and simple.

In the first part of this research, numerical and experimental approaches are used to estimate unknown parameters from PD data. The results provide new insights from PD data analysis

including the identification of different stages in diffusion process. PD data from high temperature and high pressure tests is analyzed and divided into three regions based on different slopes; early-time, transition and late-time regions. Due to very limited data available in literature, solubility and diffusivity of propane and butane in heavy oil at high temperatures and high pressures are also estimated. Also, the effects of i) temperature and solvent type on diffusion coefficient of solvent in heavy oil, ii) solvent solubility and diffusion time in heavy oil, and iii) the corresponding viscosity reduction are investigated and discussed in this study.

In the second part of this research, we conduct visualization tests in a customized visual cell to investigate interactions between liquid propane ($C_{3(l)}$) and a heavy oil sample during soaking process at different experimental conditions. The results show how different mechanisms lead to the complete mixing of heavy oil with $C_{3(l)}$.

The results of this study are of direct relevance to in situ recovery of heavy oil. They help in understanding propane-based recovery processes and diffusion processes in heavy oil and bitumen systems. Also, the results can be applied in the simulation of VAPEX and other solvent-based recovery processes.

Preface

This thesis is original work by Khan Athar. Some parts of this research in Chapter 1, 2 and 4 of this thesis have been published or presented as:

- Athar, K. S., Yassin, M. R., & Dehghanpour, H. (2018, December). Non-Equilibrium Interactions Between Heavy Oil and Liquid Propane. In SPE International Heavy Oil Conference and Exhibition. Society of Petroleum Engineers.

The necessary approval to include the conference paper as chapter 4 in this work is provided in Copyright Permissions section.

Dedicated to my parents

Athar and Faiza

Acknowledgements

ALLAH, The first and foremost, Who is beneficial and merciful, with Whose blessings I have been able to accomplish my work.

I am sincerely grateful and would like to offer my earnest gratitude to my supervisor, Dr. Hassan Dehghanpour for his persistent support, guidance and encouragement for my research throughout my Masters. I pay my deepest appreciation to him and I am deeply indebted for all his efforts and help. His valuable suggestions have always been very helpful during the course of my project.

I would also like to acknowledge the Cenovus Energy, Imperial Oil and National Sciences and Engineering Research Council of Canada (NSERC) for providing the heavy oil samples and funding this study.

I gratefully acknowledge the help and contributions from colleagues (Yingkun Fu, Taregh Soleiman, Sara Eghbali, Mahmood Yassin, Lin Yuan, Ali Habibi, Ashkan Zolfaghari, Yanmin Xu, Obinna Ezulike, Son Tran, Tamer Moussa, Mingxiang Xu, Mohammad Yousefi, Mohammad Hossein and Maryam Eghbalvala). I would also like to thank Todd Kinnee, for his guidance and support in conducting the experiments.

Finally, I would like to express my love and gratitude to my family back home, my parents, my brother and my sisters. I would also like to thank all my friends in Edmonton especially; Maheen, Shaheryar, Subbor, Onaib, and Khubaib for sharing their time and joy with me.

Table of Contents

List of Figures

List of Tables

Nomenclature

A	Area of cross-section of the cell, cm^2
C	Molar concentration of component gas, mol/cm^3
$C_{eq(p)}$	Oil-gas interface molar concentration, mol/cm^3
D	Diffusion coefficient, m^2/s
EF	Expansion Factor
h	Height of gas in cell, cm
m	Slope of line intercept in graphical method, m^2/s^2
MW	Molecular Weight,
n_i	Number of moles of gas at initial pressures, mol
n_f	Number of moles of gas at equilibrium pressures, mol
P(t)	Pressure of cell at time t, kPa
P(eq)	Equilibrium pressure, kPa
R	Universal gas constant
t	Time, s
T	Temperature, ^oC
V	Volume of gas, cm^3
wt	Weight, kg
z	Interface position, cm
z_o	Initial height of oil-gas interface, cm
z_g	Gas compressibility factor
β	Constant defined by Eq. 3.14
μ	Viscosity, cP

Abbreviations

API	American Petroleum Institute
CHOPs	Cold Heavy Oil Production with Sand
CSS	Cyclic Steam Simulation
DI	De-Ionized
DPDVA	Dynamic Pendant Drop Volume Analysis
ES-SAGD	Expanding Solvent SAGD
NMR	Nuclear Magnetic Resonance
PD	Pressure Decay
PDT	Pressure Decay Technique
SAGD	Steam Assisted Gravity Drainage
THAI	Toe to Heel Air Injection
VAPEX	Vapor Assisted Petroleum Extraction

Chapter 1: Introduction

1.1 Background

Global energy consumption is expected to increase at 1.2% per annum from 2016-2040 due to population and economic growth (British Petroleum Outlook, 2018). Oil is an important source of energy and will play an important role in responding to this increasing energy demand. However, available statistics reveal that more than 65% of proven oil resources are heavy oils, bitumen and oil sand (British Petroleum Outlook, 2018). Heavy oil (9°API to 14°API) is highly viscous and immobile at reservoir conditions (Butler and Mokrys, 1991; Yazdani and Maini, 2005; Roopa and Dawe, 2007; Pathak et al., 2012). Therefore, improving heavy oil mobility at in situ conditions is required to obtain economical flow rates (Butler, 1991). This is achieved by employing Enhanced Oil Recovery (EOR) methods.

EOR methods for heavy oil reservoirs can be classified into thermal (i.e. steam stimulation, cyclic steam injection, steam flooding, steam assisted gravity drainage, etc.) and non-thermal methods (i.e. water flooding, solvent flooding, caustic flooding, vapour extraction, etc.). Typically, thermal EOR methods reduce the viscosity of in-situ heavy oil by increasing temperature of in-situ heavy oil whereas, viscosity reduction in non-thermal methods is due to diffusion and dispersion of solvents into heavy oil (Hart, 2014).

Although thermal EOR processes are effective, they are not economically feasible in some reservoirs due to overlying gas cap, low porosity, thin pay zone, and low thermal conductivity (Kok and Acar, 2008). EOR processes in such reservoirs result in considerable heat losses (Karmaker, 2003; Vargaz-Vasquez, 2007). In addition to heat losses, thermal EOR process causes depletion of water resources, emission of greenhouse gases and production of waste water. These result in additional cost, thus making alternate EOR techniques more economically feasible and environmentally friendly (Luhning et al., 2003; Moghaddam, 2009; Pourabdollah and Mokhtari, 2013). Therefore, considering the amount of energy consumed during EOR process, the efficiency of the implemented method and its environmental impacts are crucial for heavy oil recovery.

Among non-thermal EOR methods, Vapour Extraction (VAPEX) method has gained a lot of attention from researchers as it requires lesser energy for its operation. In addition, VAPEX has a

good potential for down-hole heavy oil upgrading and requires less capital investment compared to Steam Assisted Gravity Drainage (SAGD) (Al- Hadhrami et al., 2014; Jiang et al., 2014; Pourabdollah and Mokhtari, 2013; Vargas-Vasquez and Romero-Zerón, 2007; Karmaker, 2003; Luhning et al., 2003). In VAPEX, viscosity of the heavy oil is reduced through mass transfer phenomena by injection of light gaseous hydrocarbons such as propane (C_3) and butane (C_4) into reservoirs (Yazdani and Maini, 2005).

VAPEX mimics Steam Assisted Gravity Drainage (SAGD) because two horizontal wells are drilled in the pay zone, one above the other (Figure 1-1). Gaseous solvent (light hydrocarbons, CO_2 or mixture of gases) is injected from an upper horizontal well into a heavy oil reservoir and as a consequence, heavy oil is diluted by injected solvent and its viscosity decreases dramatically. Thus, the diluted heavy oil drain downwards into the production well by the gravity drainage (Bayat et al., 2015; Moghadam, 2009; Das, 1998).

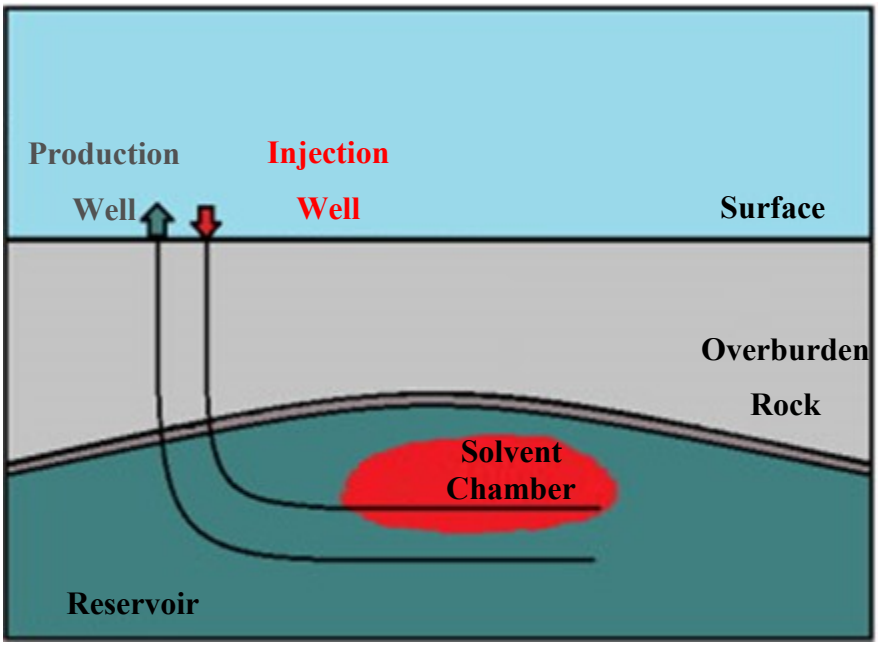

Figure 1-1: Schematic of the production and injection well patern in the VAPEX process. (Bayat et al., 2015)

In VAPEX, solvent mass transfer into heavy oil occurs at the boundary layers of the vapor chamber as shown in Figure 1-2. Diffusion is the dominant mechanism for mass transfer in VAPEX and thus results in viscosity reduction of heavy oil (Etminan, 2009).

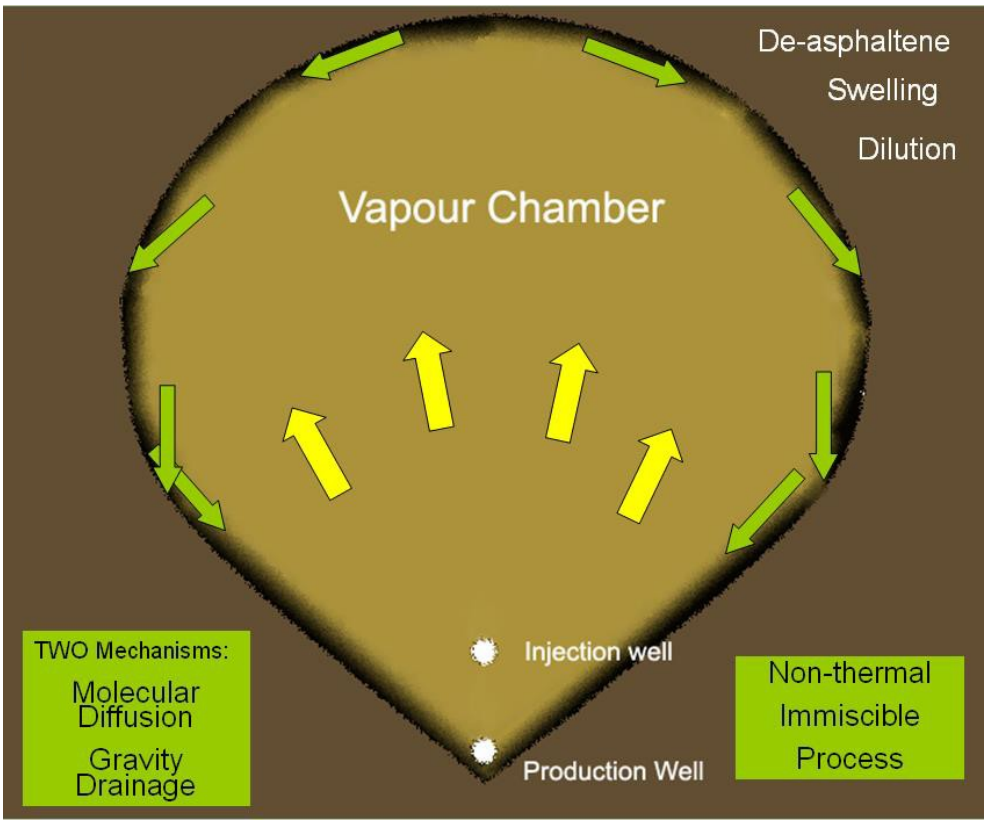

Figure 1-2: Cross section of VAPEX solvent chamber. (Etminan, 2006)

The factors controlling the drainage rate of heavy oil in VAPEX include reservoir temperature, reservoir pressure, reservoir rock properties, solvent rate of injection, types of solvent, solvent diffusion coefficient, swelling tendency of oil in presence of solvent, molecular diffusivity of solvent vapor and heavy oil, interfacial tension between heavy oil and solvent, well configuration and well spacing (Abdolkarim et al., 2011; Butler and Jiang, 2000; Singhal et al., 1996). The selection of the solvent for VAPEX is also an important factor that determines the oil production rates. Criteria for solvent selection also depends on solubility, diffusivity, density difference between oil and solvent, reservoir temperature and pressure (Ramakrishnan et al., 2003).

1.2 Research Gap

To develop and understand solvent-based recovery methods such as VAPEX, it is important to quantify the mass transfer between solvent and heavy oil (Civan et al., 2009). Diffusion coefficient (D) of solvents into heavy oil is a key parameter controlling mass transfer and production rates in VAPEX and other solvent-based recovery processes (Etminan, 2014; Butler and Mokrys, 1989, 1991). Another important parameter is solubility. Diffusion coefficient controls the rate at which

gas dissolves in oil while solubility specifies amount of gas dissolution in oil (at specific temperature and pressure).

Abdolkarim et al., 2011 and Das, 2005 reported the effects of *D* on production rates and growth of vapor chamber. Figure 1-3 shows viscosity profile of VAPEX after 5 days with and without diffusion coefficients, respectively. Comparing both profiles, Abdolkarim et al., 2011 reported that the simulator (CMG) was able to simulate lateral extension of vapor chamber and prevent fingering due to the input of diffusion coefficient. Thus, in order to effectively design and simulate VAPEX and other solvent-based recovery processes, we need to determine the type, rate and amount of solvent to be injected (Tharanivasan et al., 2006). This requires the diffusion coefficient (also termed as diffusivity by some researchers) and solubility of a solvent in heavy oil. In this study we aim to estimate diffusion coefficients of light hydrocarbon solvent into heavy oil.

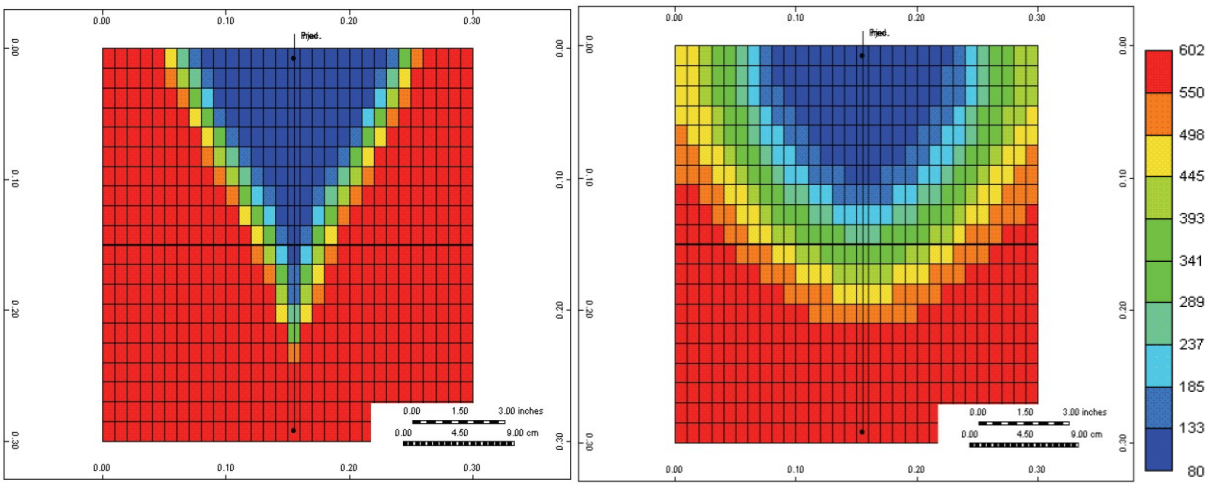

Figure 1-3: Viscosity (cP) profile of VAPEX after 5 days (a) without diffusion coefficient and (b) with diffusion coefficient (Abdolkarim et al., 2011).

For measuring the diffusion coefficient of solvents into heavy oil samples, the researchers have applied different experimental techniques which can be generally categorized into two groups: direct and indirect methods. In direct methods, liquid samples are taken from the heavy oil-solvent mixtures and analyzed at different times to find their compositions (Guerrero-Aconcha, 2009). In indirect methods, the properties of heavy oil-solvent system (i.e. gas pressure, volume of gas dissolved in oil, oil-gas interface position, oil swelling) are measured during diffusion. Some studies (Roman, 2014; Riazi, 1996) indicate that direct methods are relatively expensive, time-consuming and error-prone as sampling alters the system's chemical state.

Among the indirect methods, inferring diffusion coefficient from analyzing gas pressure of a gas-heavy oil system has gained popularity. Such methods are known as Pressure Decay (PD) methods and have been used by Riazi, 1996; Nguyen and Farouq Ali, 1998; Sachs, 1998; Zhang et al., 2000; Dill and Bloomberg, 2003; Creux et al., 2005; Sheikha et al., 2005; Bosse and Bart 2006; Civan and Rusmussen, 2006; Jamialahmadi et al., 2006; Etiminan et al., 2010 and 2011; Zamanian et al., 2012; Roman and Hijazi, 2014; Ratnakar and Dindoruk, 2015.

These researchers considered diffusion coefficient as a constant value. An important shortcoming of these works is their inability to differentiate between various stages of gas diffusion process at high temperatures. Sheikha et al., (2006) were the first to observe three different stages of diffusion process in CH_4-, C_2H_6- and N_2- bitumen systems at 50-90^oC. A similar observation was reported by Tharanivasan (2006) under changing boundary conditions.

Propane is the most common solvent used in solvent-based recovery processes. In spite of this, there is very limited work done in estimating propane's diffusion coefficient in heavy oil. Therefore, it is of great importance to produce additional data for this particular system and to improve the simulation studies. In this study we have chosen propane (C_3) and butane (C_4) as our solvents.

During VAPEX, it is important that the solvent remains in the gas phase as this would greatly reduce the amount of solvent required to fill in the evacuated pore space, therefore, making the VAPEX process more economical (Abdolkarim et al., 2011). At dew point pressure, the solubility of the vaporized solvent become maximum. Therefore, it is suggested to have the injection pressures close to vapor pressures of solvents (Butler et al., 1995) resulting in high rate of diffusion and high density difference between solvent and oil. Therefore, we have set our experimental conditions accordingly.

Propane (C_3) and butane (C_4) are considered the most common VAPEX solvents due to their satisfactory solubility and diffusivity in heavy oil and bitumen (Das, 1995; Das and Butler, 1998). However, injecting pure solvents in a reservoir whose pressure is greater than their dew point pressures may lead to solvent condensation in situ. Compositional simulators used to characterize phase behavior of injected solvent-heavy oil assume that injected solvent and heavy oil in the grid blocks are at equilibrium conditions (Nghiem and Sammon, 1997).

Bayestehparv et al. (2017) developed a non-equilibrium model for expanding solvent steam-assisted gravity drainage accounting for diffusion, dispersion, and heat transfer at the pore scale. The results showed that the assumption of instantaneous phase equilibrium of solvents with heavy oil is not valid. Simulation models cannot account for non-equilibrium interactions i.e. during soaking period. Non-equilibrium phase-behavior data are important to model non-equilibrium interactions. Therefore, it is important to understand the interactions between solvent and heavy oil during the soaking process.

1.3 Objectives of Research

This research has the objectives to;

1. estimate the diffusion coefficient (D) of C_3 and C_4 in heavy oil by analyzing PD data.
2. estimate the solubility of C_3 and C_4 in heavy oil and estimate the resulting viscosity reduction of heavy oil.
3. analyze different stages of the diffusion process.
4. investigate the effect of temperature and type of solvent on D, solubility and equilibration time.
5. visualize the interactions between liquid C_3 and heavy oil during soaking at high temperature and high pressure.

1.4 Structure of Thesis

Chapter 1 presents an overview of the research background, research gap and objectives of this study.

Chapter 2 introduces heavy oil and in-situ recovery techniques. It includes a literature review on diffusion and methods for estimating diffusion coefficient. In addition, it summarizes pressure decline techniques for calculating diffusion coefficient.

Chapter 3 presents the methodology and results of tests conducted to determine diffusion coefficients of propane (C_3) and butane (C_4) at elevated temperatures. This chapter also explains the effect of temperature on diffusion coefficient and investigates different stages of diffusion process.

Chapter 4 gives the results of visualization tests conducted in a high-pressure and high-temperature visual cell for $C_{3(l)}$-heavy oil system. This help us visually explain the mechanisms of solvent-extraction recovery processes during soaking process.

Chapter 5 provides key conclusions from this thesis. References from all chapters are combined and presented after Chapter 5.

Chapter 2: Literature Review

2.1 Heavy Oil Resources

Heavy oil is known for its high viscosity, high specific gravity, low API gravity and low mobility under reservoir conditions. Generally, crude oil with viscosity in the range of 100 to 20,000 cP is considered as heavy oil, whereas crude oil with viscosity higher than 20,000 cP is termed as extra heavy oil or bitumen (Chopra et al., 2010). Heavy oil and bitumen comprise 9,000 billion barrels of original oil in place (OOIP) in the world, of which 72% is in North and South America (British Petroleum Outlook, 2018).

In Northern Alberta, heavy oil reserves are accumulated as three different deposits (Athabasca, Cold Lake and Peace River; as shown in Figure 2-1) with proven heavy oil and bitumen reserves of about 175 x 10^9 barrels (ERCB, 2008). These reserves rank third in the world, after Venezuela and Saudi Arabia (Energy Markets Fact Book-Canada, 2015). Tertiary or enhanced oil recovery (EOR) processes are used to exploit heavy oil resources. Such EOR processes are segregated into in-stu and ex-situ recovery methods. Ex-situ recovery methods involves open-pit mining of oil sands located near the surface, whereas, in-situ methods are used to recover heavy oil and bitumen beneath the surface. The commonly used in-situ recovery methods are summarized in Figure 2-2.

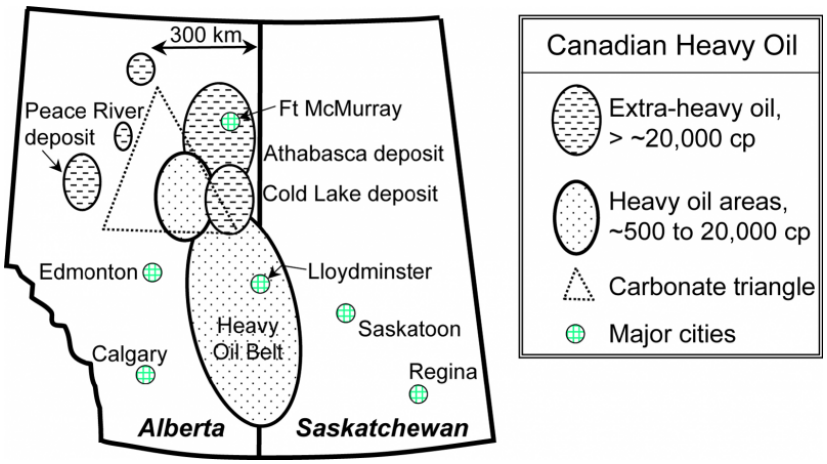

Figure 2-1: Canadian heavy oil reserves (PetroWiki, 2018)

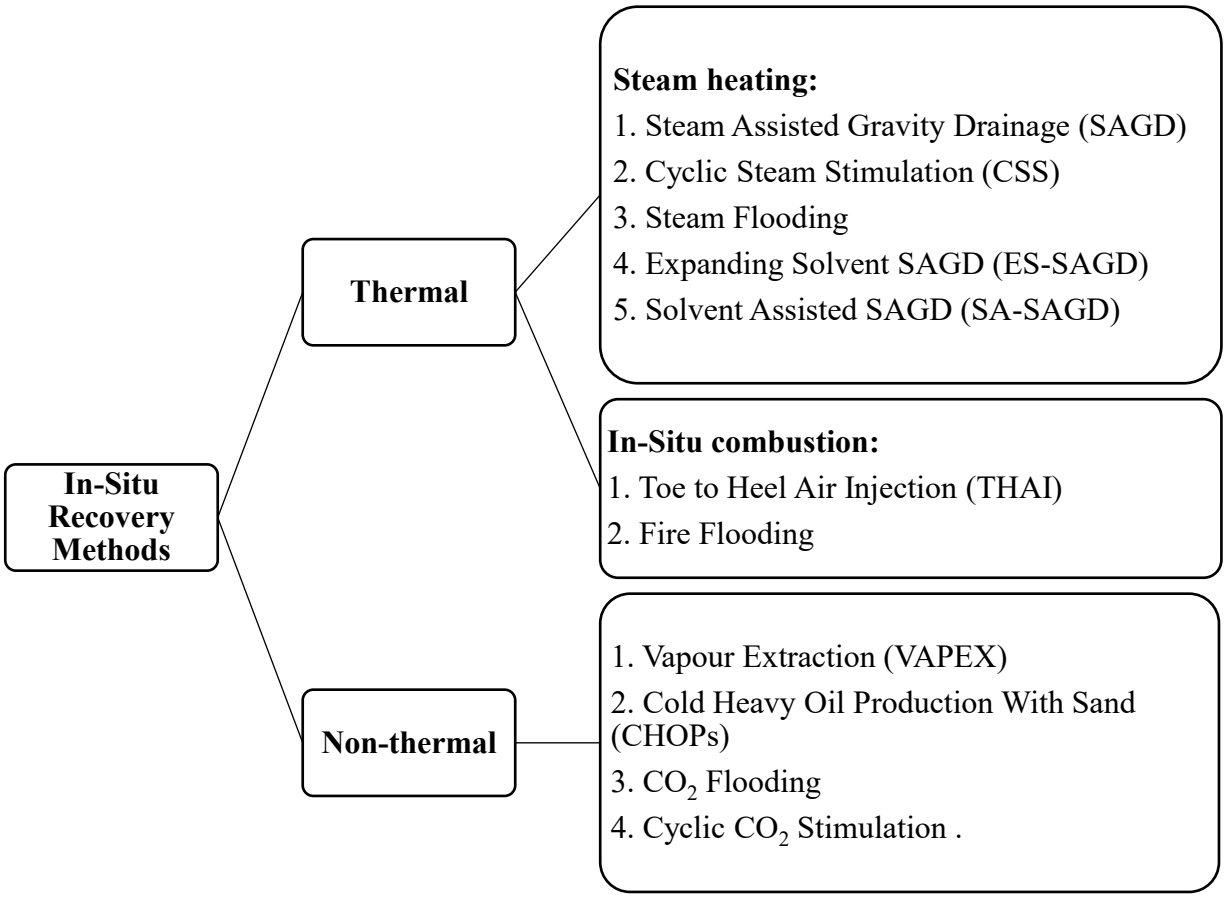

Figure 2-2: In-situ heavy oil recovery methods

2.2 In-Situ Heavy Oil Recovery Methods

Heavy oil is highly viscous and immobile at reservoir conditions (Butler and Mokrys, 1991; Yazdani and Maini, 2005; Roopa and Dowe, 2007). Therefore, the success of in-situ recovery methods depends on significantly reducing heavy oil's in-situ viscosity to improve its mobility. Generally, heavy oil recovery methods fall under two categories: thermal and non-thermal recovery methods.

2.2.1 Thermal Recovery Methods

In thermal recovery processes, the viscosity of heavy oil is reduced by means of introducing heat in the reservoir. Heat is provided by means of steam injection or in-situ combustion (burning in-situ oil) (Roman, 2015; Bannerjee, 2012). Steam based recovery methods include; steam-assisted

gravity drainage (SAGD), cyclic steam stimulation (CSS), expanding solvent SAGD (ES-SAGD) and Steam Flooding. In-situ combustion includes fire flooding and Toe to Heel Air Injection (THAI).

2.2.2 Non-Thermal Recovery Methods

Non-thermal recovery methods include water flooding, immiscible and miscible carbon dioxide flooding, solvent flooding, water-alternating gas injection (WAG), and vapor extraction (VAPEX) (Guo et al., 2016; Shah et al., 2010; Thomas et al., 1999). Among these methods, solvent-based recovery processes have become increasingly attractive (Al-Hadhrami et al., 2014). In such processes, diluents (light hydrocarbons) are injected to reduce the viscosity of heavy oil (Butler et al., 1993).

The concept of heavy oil extraction using miscible gaseous solvents has been known for a relatively long time (Allen et al., 1974). VAPEX was introduced by Butler and Mokrys (1991) as an analogue to Steam Assisted Gravity Drainage (SAGD). It requires drilling a pair of horizontal wells (injection well above and production well below) into the heavy oil zone as shown in Figure 1-1. The solvent is injected in the upper well at a pressure close to the reservoir pressure. Heavy oil is diluted by diffusion of solvent into the heavy oil. The diluted oil flows into the lower well due to gravity drainage.

To develop and understand solvent-based recovery methods, it is important to understand the mass transfer between solvent and oil (Civan et al., 2009), particularly the inter-mass transfer coefficient (k) and the diffusion coefficient (D). These parameters are used to calculate the transfer rates of gas diffusing through the gas/heavy oil interface (Riazi, 1996).

2.3 Diffusion

Diffusion is the process through which mass is transported (flux) from one part of the system to another as a result of random molecular motion and concentration gradients (Crank, 1979). In general, a solvent-based process involves solvent dissolution (transfer of solvent mass into heavy oil) by molecular diffusion and convective dispersion (Yazdani and Maini, 2004). In this study, the concentration gradient is considered as the only means of mass transfer in diffusion i.e. absence

of mixing (convection). Thus, in this study, we focus on solvent mass transfer due to diffusion only. Fick's law is generally used to describe the diffusion process and provides the basis for determining the crucial parameter of mass transfer i.e. diffusion coefficient (*D*). The following sections discuss the factors that influence the diffusion process;

2.3.1 Diffusing Species

Diffusion greatly depends on the material that is diffusing and the material through which it will diffuse. The magnitude of diffusion coefficient, *D*, is an indicator of diffusion rate. Since the value of *D* is fixed for a given element in a given material, the extent of diffusion is decided by the diffusing species itself. At a fixed temperature, all particles have the same average energy. This means that light atoms (such as gas) are more mobile than heavy atoms (such as solids and liquids).Therefore, we observe that rates of gas-gas diffusion > liquid-liquid diffusion > solid-solid diffusion.

2.3.2 Temperature

Temperature is a major factor which affects diffusion. The temperature dependence of the diffusion coefficient was expressed by Arrhenius equation and is given by Eq. 2.1

$$D(T) = D_o exp\left(-\frac{Q}{RT}\right) \tag{2.1}$$

where, D_o is the pre-exponential factor and the Q is the activation energy for diffusion. Increasing the temperature will result in increase in magnitude of *D* i.e. increase in diffusion rate.

2.3.3 Concentration Difference

The rate of diffusion depends on the difference between concentrations of species involved. High concentration difference will result in high diffusion rates. For example, gas diffusion through a thin membrane will occur quickly if there is a high concentration of the gas on one side and none of the gas on the other side of the wall. If there is already an almost equal amount of gas on both sides, diffusion will be much slower.

2.4 Fick's Laws of Diffusion

Fick (1855) was the first to quantitatively describe diffusion by creating an analogy between heat and mass transfer. His theory states that heat transfer by conduction and mass transfer by diffusion (driven by concentration gradient of species) are due to random molecular motions. Therefore, he adopted the mathematical equation of heat conduction derived by Fourier (1822) and developed diffusion equation known as Fick's laws of diffusion. His theory has two approaches; (i) Steady state of diffusion; and (ii) Non-steady state of diffusion.

2.4.1 Steady State of Diffusion

Also known as Fick's first law of diffusion. The mathematical theory of diffusion is based on the hypothesis that the rate of mass transfer through a unit area of cross-section is proportional to the concretion gradient measured normal to the section (Crank, 1979). Eq. 2.2 describes steady state of diffusion where, F is diffusion flux or mass transported per unit time per unit area and dC/dx is the concentration gradient and D is the diffusion coefficient. In steady-state diffusion the diffusion flux is independent of time i.e. we have uniform concentration gradient.

$$F = -D\frac{dC}{dx} \tag{2.2}$$

2.4.2 Non-Steady State of Diffusion

It is also known as Fick's second law of diffusion. It describes the change in concentration with time at a definite location rather than the mass diffusing across a unit area in unit time. In most practical situations, diffusion in non-steady i.e. diffusion flux and concentration gradient vary with time. Eq 2.3 is Fick's second law.

$$\frac{dC}{dt} = D\frac{d^2C}{dx^2} \tag{2.3}$$

2.5 Diffusion Coefficient

The diffusion coefficient or diffusivity is the proportionality constant between the flux and potential (concentration gradient between diffusing species). It is denoted by *D* and has dimensions of $(\text{Length})^2.(\text{Time})^{-1}$. It is an important indicator of diffusion rates. The higher the *D*, the faster the species diffuse into each other.

2.6 Estimating Diffusion Coefficient of Solvents in Heavy Oil

It is difficult to estimate diffusion coefficient (Tyrell, 1964). Estimation of diffusion coefficients of solvents in heavy oil is challenging because heavy oil is opaque, highly viscous and a complex mixture of different components. Also, formation of asphaltenes when solvents contact heavy oil makes the diffusion study more challenging (Ghanvati, 2014). Diffusion coefficients of solvents in heavy oil are extremely low of the order of 10^{-8} to 10^{-10} m^2/s (Zhang et al., 2000; Upreti et al., 2002; Etminan et al., 2010); thus, prolonging the time taken for conducting diffusion experiments.

Diffusion coefficients (*D*) cannot be measured directly but can be calculated by analyzing data obtained through various experimental methods. These can be categorized into two groups, (i) direct methods; and (ii) indirect methods. Direct methods involve sampling heavy oil-solvent mixtures at different times for compositional analysis (Guerrero, 2009). Such methods are expensive, time-consuming and error-prone as sampling alters the experimental conditions (Roman, 2014; Riazi, 1996). Indirect methods involve measuring heavy oil-solvent system properties (i.e. gas pressure, volume of gas dissolved in oil, oil-gas interface position, oil swelling, swelling of pendant drop, changes in Nuclear Magnetic Response (NMR) and density profile of the mixture) during the diffusion process.

Thus, there is no universally recognized technique for measuring diffusion coefficients. Using indirect methods, Das and Butler (1996) developed empirical correlations for estimating diffusion coefficients of propane and butane in Peace River bitumen as a function of the mixture viscosity, concentration of diffusing species and temperature. Yang and Gu (2005 and 2006) developed a dynamic pendant drop volume analysis (DPDVA) method to measure diffusion coefficients and oil swelling factors. Their results show that both the diffusion coefficient and the oil swelling factor of a heavy oil–solvent system increase with increasing pressure at room temperature. Etminan et

al. (2011) conducted three sets of experiments (including Levenberg-Marquardt method, physical sand pack model and a set of PVT measurements) for a system of propane and Athabasca bitumen. and proposed constant-pressure technique. Etminan et al. (2011) kept pressure constant and measured changes in volume due to gas dissolution in liquid phase. Maintaining constant pressure and detecting small changes in volume of dissolved gas are some of the difficulties associated with this technique.

2.7 Pressure Decay Technique

Among all indirect methods, pressure decay (PD) method has attracted more attention due to its simplicity and robustness (Roman, 2014; Etminan, 2010). The PD method was introduced by Riazi (1996) to eliminate the short comings of direct methods. In this technique, solvent (gas) is injected into a high pressure cell (diffusion cell) with heavy oil in the bottom as shown in Figure 2-3. The cell is pressurized by injecting solvent (gas); after which, the cell pressure decays with time and is monitored. The technique is based on measuring pressure decay due to molecular diffusion of solvent vapour into heavy oil. The pressure decay continues as the gas diffuses into the heavy oil. Riazi (1996) also monitored the position of the gas-liquid interface in the diffusion cell. He then applied mass transfer model i.e. mass leaving gas phase is equal to the mass diffusing in the heavy oil, to estimate the diffusion coefficient. The pressure decay method is a simple laboratory technique, but the estimation of diffusion coefficient depends on the mathematical modelling, type of gases and liquid phases (Roman, 2014).

The PD method has become the standard technique for measuring diffusion coefficients. This method has been adopted to estimate diffusion coefficients of solvents (light hydrocarbons) into crude oils. The PD method for determining diffusion coefficients has been applied by Riazi (1996), Nguyen and Farouq Ali(1998), Sachs (1998), Zhang et al. (2000), Dill and Bloomberg (2003) Creux et al. (2005), Sheikha et al. (2005), Bosse and Bart (2006), Civan and Rusmussen (2006), Jamialahmadi et al. (2006) Etiminan et al. (2010 and 2011), Zamanian et al. (2012), Roman and Hijazi (2014), Ratnakar and Dindoruk (2015). Despite its simplicity, the PD method is time consuming and can take weeks to get a single measurement.

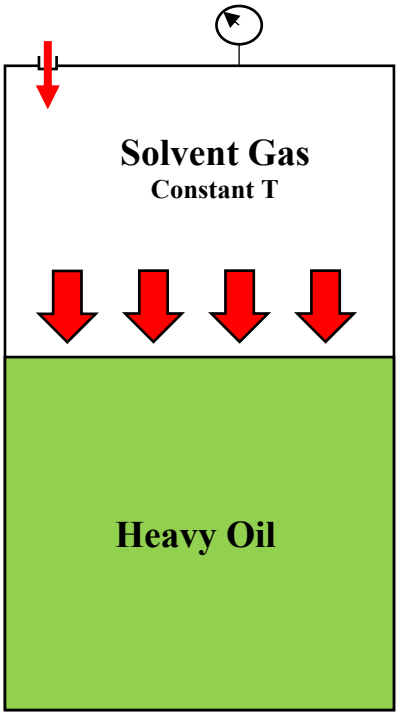

Figure 2-3: Schematic of diffusion cell used by Riazi, 1996.

Zhang et al. (2000) adapted a simplified version of the approach of Riazi (1996) for a gas-heavy oil system and pioneered the graphical technique for estimating diffusion coefficient. They neglected oil swelling and only measured pressure decline in the gas phase. In this study, we have adopted Zhang's model (Zhang et al., 2000) to calculate diffusion coefficients. This method is explained in detail in Section 3.4.1.

2.8 Diffusion Coefficient in Solvent-based Recovery Methods

Diffusion coefficient is used to calculate the transfer rate of gas penetrating into heavy oil (Reid et al., 1985). The higher the *D*, the faster the solvent diffuses into oil. The magnitude of diffusion coefficients affects the time required for the heavy oil to achieve desirable viscosity reduction. Therefore, it is a key factor controlling oil production (Li and Yang, 2016; Okazzawa, 2007; Boustani and Maini, 2001). This makes diffusion coefficient an important parameter in designing solvent-based recovery processes for heavy oil reservoirs.

During a solvent-based recovery process, vaporized solvents gradually dissolve into the heavy oil and significantly reduce its viscosity. This results in improved mobility of the heavy oil. In order

to effectively design and simulate solvent-based oil recovery processes, we need to determine the injection rate and solvent amount required to achieve the desired heavy oil mobility and viscosity reduction (Tharanivasan et al., 2006). To determine these estimation of diffusion coefficients and solubility of a solvent in heavy oil is required within acceptable accuracy.

Chapter 3: Calculating the Diffusion Coefficients of Gaseous Propane and Butane in Heavy Oil

In this chapter, we calculate the diffusion coefficients (D) of propane (C_3) and butane (C_4) in heavy oil at different experimental conditions. We perform four tests on a propane-heavy oil system at temperatures ranging from 65°C to 130°C and one test on a butane-heavy oil system at 130°C. First, the experimental set-up and methodology for these diffusion tests are discussed. The pressure decline technique proposed by Zhang et al. 2000 is used to calculate D. Also, we investigate the effect of temperature on (i) D; (ii) diffusion equilibration time; (iii) diffusion rate; (iv) solubility of the solvent i.e. C_3 and C_4 in heavy oil; and (v) the viscosity of the mixture of heavy oil and solvent.

3.1 Experimental Set-up

Figure 3-1 shows the experimental setup used for C_3-heavy oil and C_4-heavy oil diffusion tests. The visual cell has a cylindrical chamber made of stainless steel having 2.13" and 3.5" inner and outer diameters, respectively. The internal volume of the cell is 590 cm^3. The cell is equipped with a heating jacket that controls temperature with an accuracy of ± 0.02°C. It is connected to a Type-K thermo-couple for monitoring temperature. A digital pressure transducer is also connected to the visual cell for measuring system pressure. A data acquisition system is used for measuring pressure every second with an accuracy of ±2 psig. The cell is equipped with two sight glasses. We place a light source next to the rear sight glass and a camera in front of the front sight glass for observing interface level and interactions between solvent and heavy oil during the test.

We use two accumulators for injecting heavy oil and solvents into the visual cell. The accumulators are connected to a continuous pulse-free pump. The pump can be operated to inject fluids at constant rate or constant pressure. We connect the bottom valve of the visual cell to the accumulator which is filled with heavy oil. The pump injects deionized (DI) water into the lower part of the accumulators at pressure of 2000 psig, resulting in the upward movement of the piston, and pushing heavy oil into the visual cell up to the required volume. During the injection of heavy

oil in the visual cell, the tubes were contantly heated via heat gun to increase the flow rate of heavy oil.

We connect the top valve of the visual cell to the second accumulator filled with gaseous solvent. Similarly, the pump injects DI water into the lower part of the accumulator at 450 psig. The upward movement of piston pushes the pressurized and liquefied solvent into the visual cell. Visual cell is set at high temperature so that liquefied solvent becomes vapor in the visual cell.

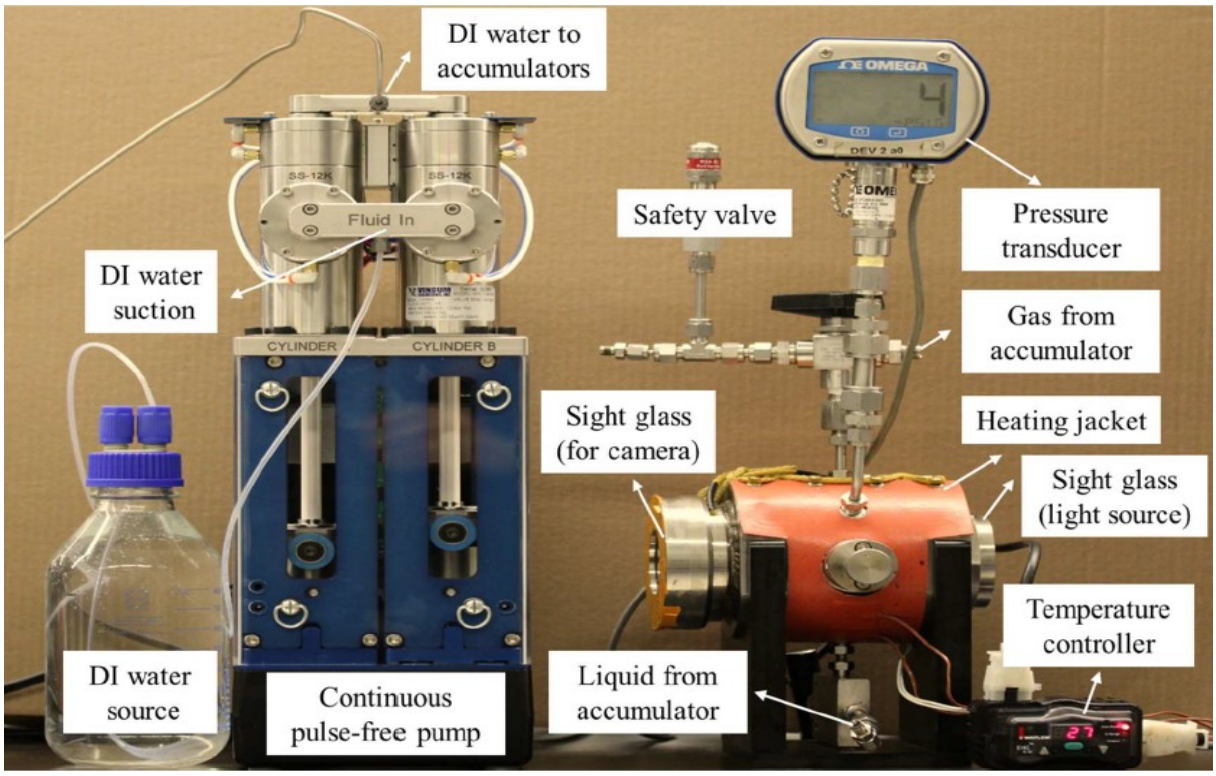

Figure 3-1: Visualization setup used for C_3-heavy oil and C_4-heavy oil diffusion experiments. Accumulators are not shown here (Yassin et al. 2017).

3.2 Materials

The heavy oil sample used in this study is collected from a producing well in Clearwater formation. Its molecular weight is 475 g/gmol, its specific gravity is 1.02 and its viscosity is 60,306 cP at 22°C. Figure 3-2 shows the oil's compositional analysis using a simulated distillation method (Standard D2887-84). The compositional analysis indicates that the oil sample contains more than 19.8wt% of C_{100+}. The heavy oil's molecular weight is measured using freezing point depression method. Figure 3-3 shows the temperature profile of the oil sample's calculated density ($\rho_{heavy\ oil}$)

and viscosity ($\mu_{heavy\ oil}$) at atmospheric pressure. Density and viscosity calculations are based on correlations (Eqs. 3.1 and 3.2) developed by Eghbali and Dehghanpour (2018) for the same heavy oil sample. These are:

$$\rho_{bitumen} = 0.0034T^2 - 3.4852T + 1756.9 \quad (3.1)$$

$$\mu_{bitumen} = \exp\{\exp[20.54 - 3.19\ln(T)]\} \quad (3.2)$$

Propane (C_3) and butane (C_4) of purities 99.9% each, are used as solvents.

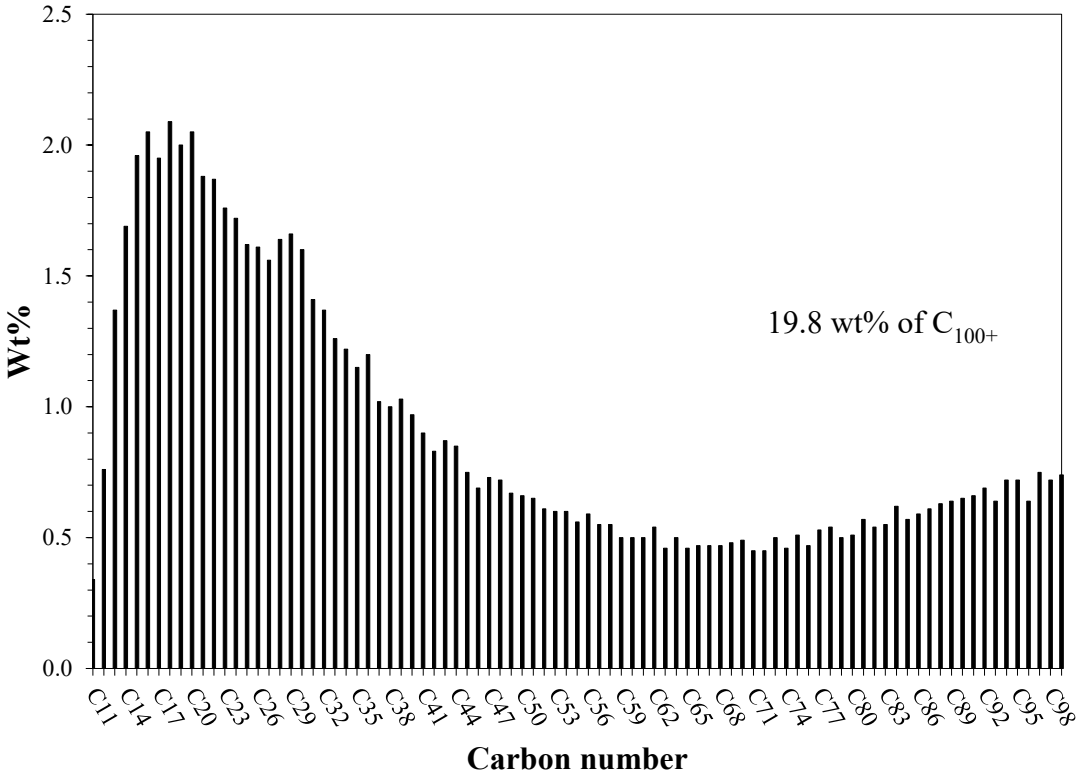

Figure 3-2: Compositional analysis of Clearwater heavy oil sample measure by simulated distillation test (Standard D2887-84)

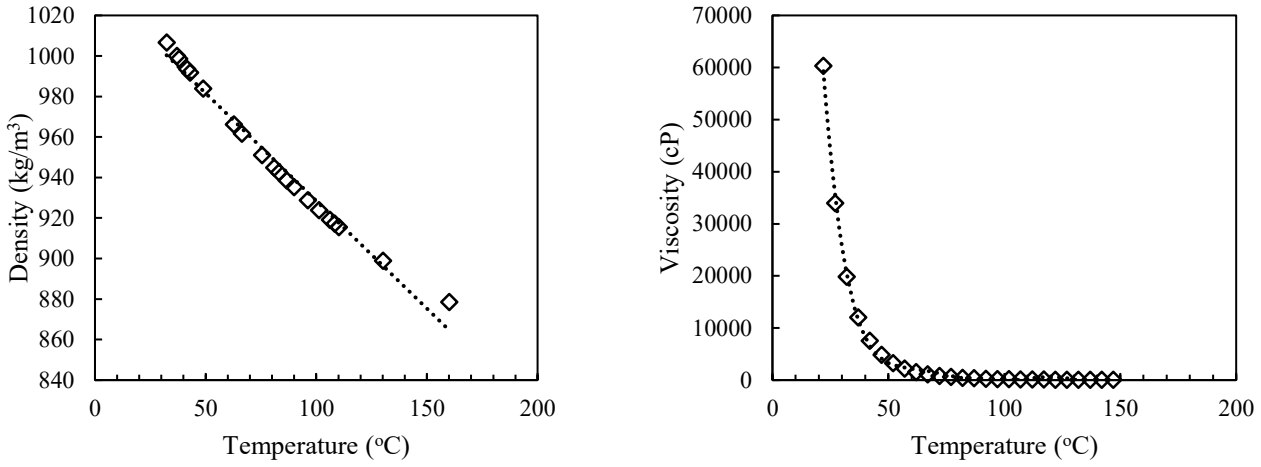

(a) (b)

Figure 3-3: a) Density calculated and b) Viscosity of Clearwater heavy oil as a function of temperature.

3.3 Experiment Methodology

We use following procedure to conduct the pressure decline tests using the visual cell. A similar procedure is adopted for C_3-heavy oil and C_4-heavy oil systems.

- First, the visual cell is checked for any leakages. Then the top flange of visual cell is connected to a vacuum pump. To remove the air in the system, we vacuum the cell and close the top flange.

- The first accumulator is loaded with heavy oil and connected to the bottom valve of the visual cell. We inject heavy oil into the visual cell at constant pressure of 2,000 psig while heating the accumulator and tubes with a heat gun to ensure fast transport of heavy oil into the visual cell. After filling the required volume of the visual cell with heavy oil, the bottom valve is closed. The cell temperature is set at the test temperature (T_{set}) and is left overnight. Experimental conditions for each test are shown in Table 3-1.

- Once the set temperature is reached, we record the heavy oil level before solvent injection and calculate the base volume of heavy oil at P = 0 psig ($V_{\text{heavy oil}}|p_{=0}$). This volume is used to calculate heavy oil expansion factor (EF) defined by Eq. 3.3. $V_{\text{heavy oil}}|p'$is the volume of heavy oil phase at $p' > 0$ psig during the pressure buildup and soaking processes.

$$EF = \frac{V_{heavy\ oil}|p'}{V_{heavy\ oil}|p=0} \quad (3.3)$$

- We inject solvent into the visual cell to reach set pressures (P_{set}) shown in Table 3-1. Solvent remains in vapor state at T_{set} for P_{set} (NIST Webbook).
- The visual-cell pressure declines over time. Pressure gauge of the visual cell is connected to the computer to record pressure versus time every second. The recorded data is then used to estimate the diffusion coefficients. We reach equilibrium conditions once the visual cell pressure is stabilized over time and reaches the equilibrium pressure (P_{eq}).
- A high resolution camera is used to monitor the gas-liquid interactions at the interface.

Table 3-1: Experimental conditions for propane-heavy oil and butane-heavy oil diffusion tests.

Property	***Test 1***	***Test 2***	***Test 3***	***Test 4***	***Test 5***
Solvent	C_3H_8	C_3H_8	C_3H_8	C_3H_8	C_4H_{12}
Temperature (T_{set}), ^{O}C	130.00	100.00	85.00	65.00	130.00
Set pressure (P_{set}), kPa	1867.58	1902.61	1885.51	1643.06	1819.26
Volume of heavy oil injected, cm^3	280.00	295.00	300.00	325.00	310.00
Volume of gas injected, cm^3	310.00	295.00	290.00	265.00	280.00
Equilibrium pressure (P_{eq}), kPa	1055.37	780.20	950.31	630.52	1035.29

3.4 Mathematical Analysis

3.4.1 Diffusion Coefficient Calculation

We used Zhang's model (Zhang et al., 2000) to determine the diffusion coefficient (D) of solvents (C_3 and C_4) into heavy oil at different temperatures. The reason is because of negligible swelling in the heavy oil sample. This model is used to interpret the measured pressure decline data. A range

of simple to very complex solutions can be expected for this problem depending on how the boundary conditions are defined (Moghaddam et al., 2009). Initial and boundary conditions of this model pertaining to our visual cell are shown in Figure 3-4.

The assumptions made for this model are as follows:

a) Heavy oil is non-volatile. Therefore, there is only mass transfer of the gas into the heavy oil through the oil-gas interface located at $z=z_o$.

b) Swelling of the liquid phase (heavy oil) is negligible. It means z_o and cross-sectional area at gas-oil interface remain constant throughout the diffusion process.

c) The gas concentration at the interface is at equilibrium i.e. $C = C_{ee(p)}$. Therefore, the resistance to mass transfer at the interface is negligible.

d) Gas phase is pure (single component) and remains so throughout the test.

e) Temperature remains constant throughout the process.

f) Constant gas compressibility.

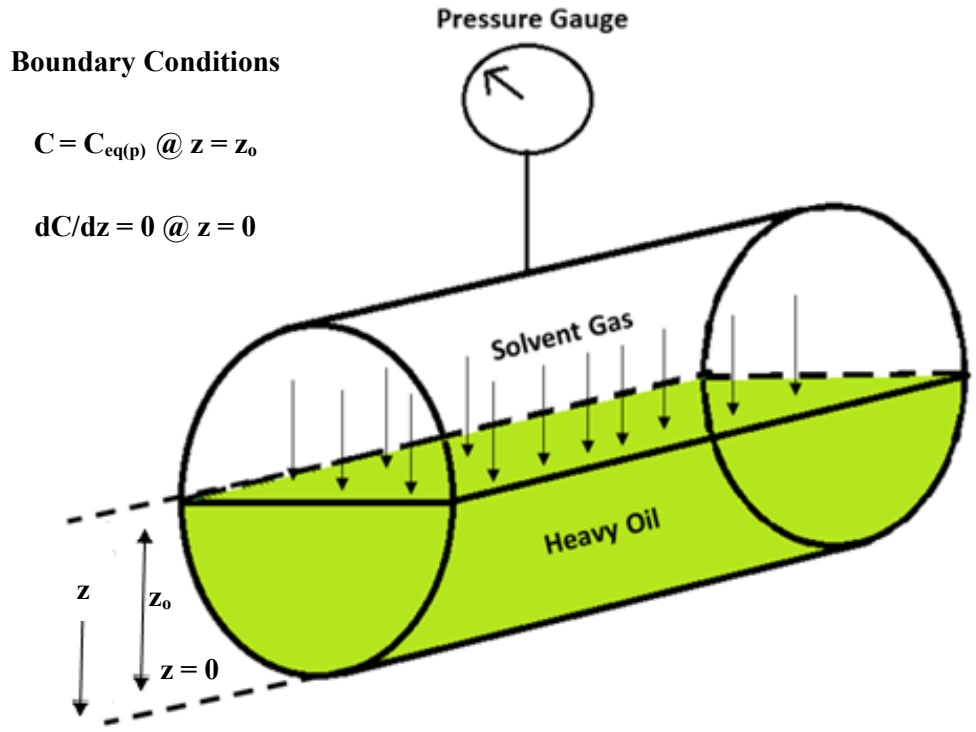

Figure 3-4: Schematic of the visual cell and boundary conditions of the experiment

Diffusion of the solvent gas into the heavy oil occurring in the visual cell as shown in Figure 3-4 can be mathematically expressed in the form of one-dimensional diffusion described by Fick's second law:

$$\frac{d\mathrm{C}}{dt} = D\frac{d^2\mathrm{C}}{dz^2} \tag{3.4}$$

Initial and boundary conditions of the diffusion cell are as follows:

$$0 < z < z_o, t = 0, \mathrm{C} = 0 \tag{3.5}$$

$$z = z_o, t > 0, \mathrm{C} = C_{eq(P)} \tag{3.6}$$

We also apply boundary conditions:

$$z = 0, t > 0, \frac{dC}{dz} = 0 \tag{3.7}$$

The initial molar concentration of gas in heavy oil is assumed zero. $C_{eq(p)}$ is the equilibrium concentration of gas at oil-gas interface. It varies with pressure and temperature. Since the experimental conditions are isothermal, $C_{eq(p)}$ depends only on the pressure decline during the diffusion process. Eq. 3.4 is solved using the initial and boundary conditions to determine the molar concentration as a function of space and time (Crank, 1979):

$$C_{(z,t)} = C_{eq(P)} - \frac{4C_{eq(P)}}{\pi}\sum_{n=0}^{\infty}\frac{(-1)^n}{2n+1}\cos\left(\frac{(2n+1)\pi z}{2z_o}\right)\exp\left(\frac{-(2n+1)^2\pi^2 D}{4z_o^2}t\right) \tag{3.8}$$

A material balance is used to relate pressure decline with mass transfer taking place at the interface due to diffusion (Zhang et al., 2000). The moles of solvent gas removed from the gas phase is equal to the moles of gas transferred across the interface and entering into the liquid phase, based on this following material balance equation can be obtained as

$$\frac{V}{Z_g RT}\frac{dP(t)}{dt} = -DA\left(\frac{dC}{dz}\right)_{z=z_o} \tag{3.9}$$

The volume of the gas, cross-sectional area and the compressibility of the gas are constant. Thus, Eq. 3.9 can be simplified as:

$$\frac{dP(t)}{dt} = -\beta D\left(\frac{dC}{dz}\right)_{z=z_o} \tag{3.10}$$

where,

$$\beta = \frac{Z_g RT}{h} = Constant \tag{3.11}$$

Eq. 3.10 is integrated with respect to time:

$$\int_{P(t)}^{P_{eq}} dP(t) = -\beta D \int_{t}^{\infty} \left(\frac{dC}{dz}\right)_{z=z_o} dt \tag{3.12}$$

Differentiating Eq. 3.8 with respect to z at z = z_o:

$$\left(\frac{dC}{dz}\right)_{z=z_o} = \frac{4C_{eq(P)}}{z_o} \text{ x } \sum_{n=0}^{\infty} \frac{1}{(2n+1)^2} \exp\left(\frac{-(2n+1)^2\pi^2 D}{4z_o^2} t\right) \tag{3.13}$$

Substituting Eq. 3.13 in Eq. 3.12:

$$P(t) - P_{eq} = \frac{8\beta z_o C_{eq(p)}}{\pi^2} \text{ x } \sum_{n=0}^{\infty} \frac{1}{(2n+1)^2} \exp\left(\frac{-(2n+1)^2\pi^2 D}{4z_o^2} t\right) \tag{3.14}$$

At large values of *t,* the infinite series in Eq. 3.14 converges and can be approximated by the first term (Crank, 1979):

$$P(t) - P_{eq} = \frac{8\beta z_o C_{eq(p)}}{\pi^2} \text{ x } \exp\left(-\frac{\pi^2 D}{4z_o^2} t\right) \tag{3.15}$$

Rearranging Eq. 3.15 to give the following relationship between pressure and time:

$$Ln\left(P(t) - P_{eq}\right) = ln\left(\frac{8\beta z_o C_{eq(p)}}{\pi^2}\right) + \left(-\frac{\pi^2 D}{4z_o^2} t\right) \tag{3.16}$$

The pressure decline data obtained from the experiment is plotted in accordance with the above equation. This results in a straight line, slope of the line is given by:

$$\text{slope} = \left(-\frac{\pi^2 D}{4z_o^2}\right) \tag{3.17}$$

From the slope of the resulting line, we calculate diffusion coefficient whereas intercept value can be used to get equilibrium molar concentration at liquid-gas interface.

Visual cell has the radius of 2.99 cm, length of 21 cm and volume of 590 cm^3. Z_0 of oil in visual cell is given by:

$$z_o = \frac{injected\ oil\ volume}{2r * 16.5} \tag{3.18}$$

Where r is the radius of the cell.

3.4.2 Solubility Calculation

In this study, we express solubility as grams of solute in cm^3 of solvent. Researchers (Etminan, 2010; Ramussen et al.,2009; Sheikha et al., 2005; Upreti et al., 2002) have used similar units to express solubility of gas in oil.

We consider the visual cell as a closed system. Therefore, the total volume of the system remains constant. During diffusion, the number of moles leaving gas phase becomes part of the heavy oil mixture. Initial number of moles in gas phase are given by Eq. 3.19. Where, P_i is the gas injection pressure in psig, V_g is volume of gas phase in cm^3, Z_g is the gas compressibility factor at the injection pressure in $psig^{-1}$, R is the universal gas constant and T is temperature in °C. Similarly, final moles of gas in gas phase are calculated, it is given by Eq. 3.20, where subscript "f" is for final (equilibrium) conditions. Difference between n_{gi} and n_{gf} will give the moles (n) of gas that are diffused in heavy oil. We assume that there is only one-way mass transfer i.e. we donot consider extraction or vaporization of light oil components in the gas phase. Eq. 3.21 gives the equation to calculate solubility of solvent in heavy oil, where MW is the molecular weight.

$$n_{gi} = \frac{P_i V_g}{Z_g RT} \tag{3.19}$$

$$n_{gf} = \frac{P_f V_f}{Z_f RT} \tag{3.20}$$

$$\text{solubility } (g/cm^3) = \frac{\left(n_{gi} - n_{gf}\right) MW}{(\mathrm{V}_{oil})_T} \tag{3.21}$$

3.5 Data Clustering Methodology.

In this study, K-means clustering method is used to cluster data generated using Eq. 3.16. It is also known as Lloyd's algorithm and is most popular clustering algorithm used in scientific applications (Berkhin, 2006). This method minimizes the average squared distance between points in the same cluster thus resulting in grouping of data points.

The algorithm begins with "k" centers that are chosen randomly from the data points. This algorithm undergoes two-steps:

1. First step is called as assignment where, each point is assigned to the nearest "k" center.
2. Second step is called center calculation where, each center is recomputed as the center of mass of all points are assigned to it.

These two-steps (assignment and center calculation) are repeated until the process stabilizes. Matlab code for K-means clustering is attached in Appendix D. Code adopts following process sequence:

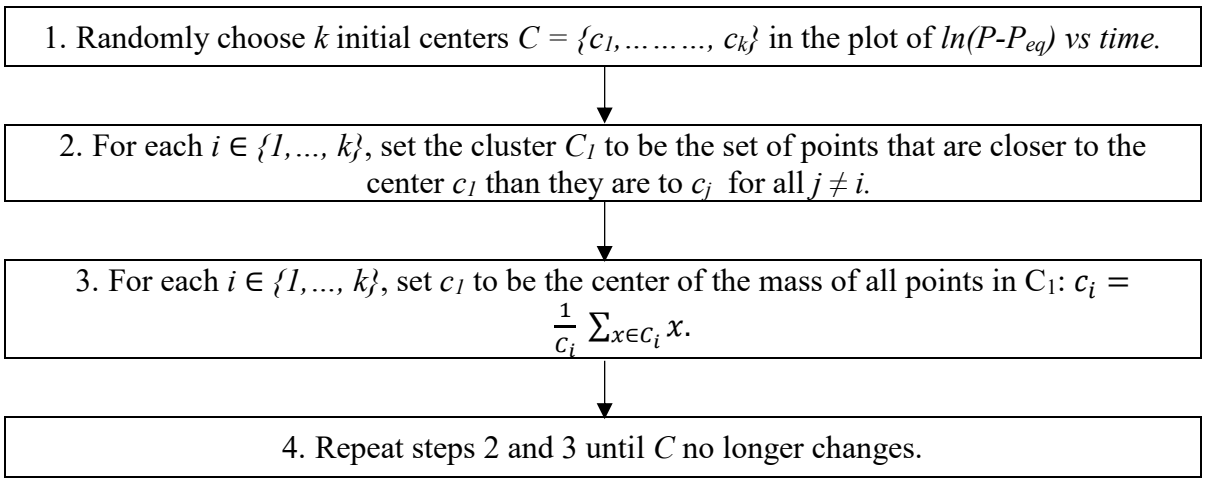

Figure 3-5: Process sequence of k-means clustering used in this study.

3.6 Results

Figure 3-6a to Figure 3-6d show C_3-heavy oil interface at four test conditions: tests 1, 2, 3 and 4, respectively. They are conducted at temperatures of 130ºC, 100ºC, 85ºC and 65ºC, respectively. Figure 3-6e shows C_4-heavy oil interface at 130ºC referred as test 5. The initial and equilibrium pressures are mentioned in Table 3-1. The results show that the heavy oil sample has negligible expansion as a result of solvent diffusion into it. Thus, Zhang's model can be applied to calculate *D*. Zhang's proposed model assumed constant diffusion coefficient, on-way mass transfer (gas to oil), constant gas compressibility, isothermal conditions, no chemical reaction between gas and oil, negligible swelling of oil, and no resistance to mass transfer at the gas/heavy oil interface. To quantify the heavy oil expansion, we define the expansion factor (EF) as the volume of heavy oil after solvent injection divided by the volume of heavy oil before solvent injection into the cell at the test temperature.

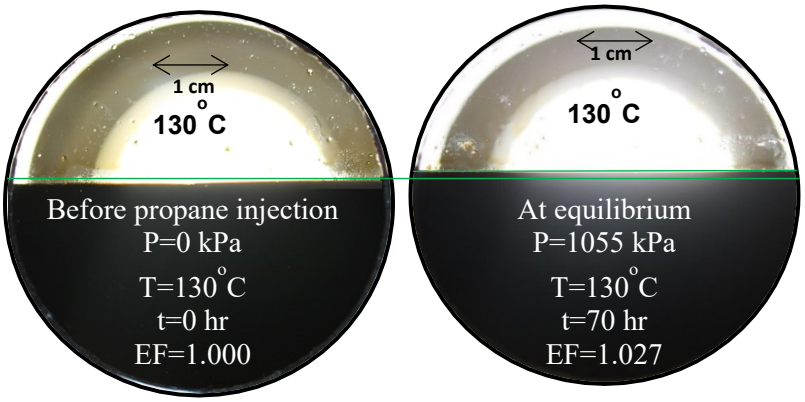

(a)

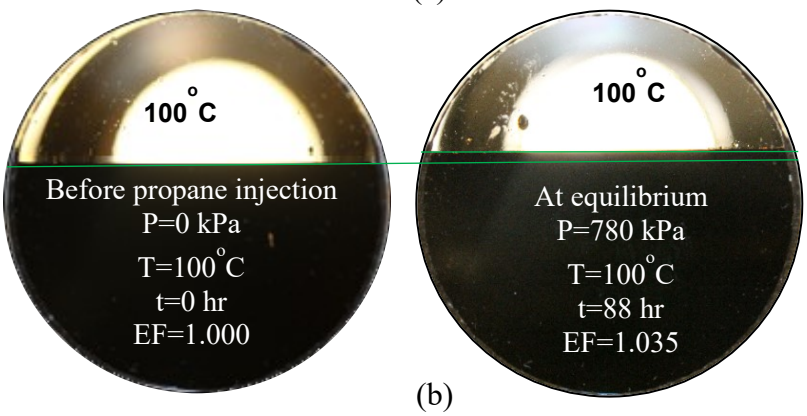

(b)

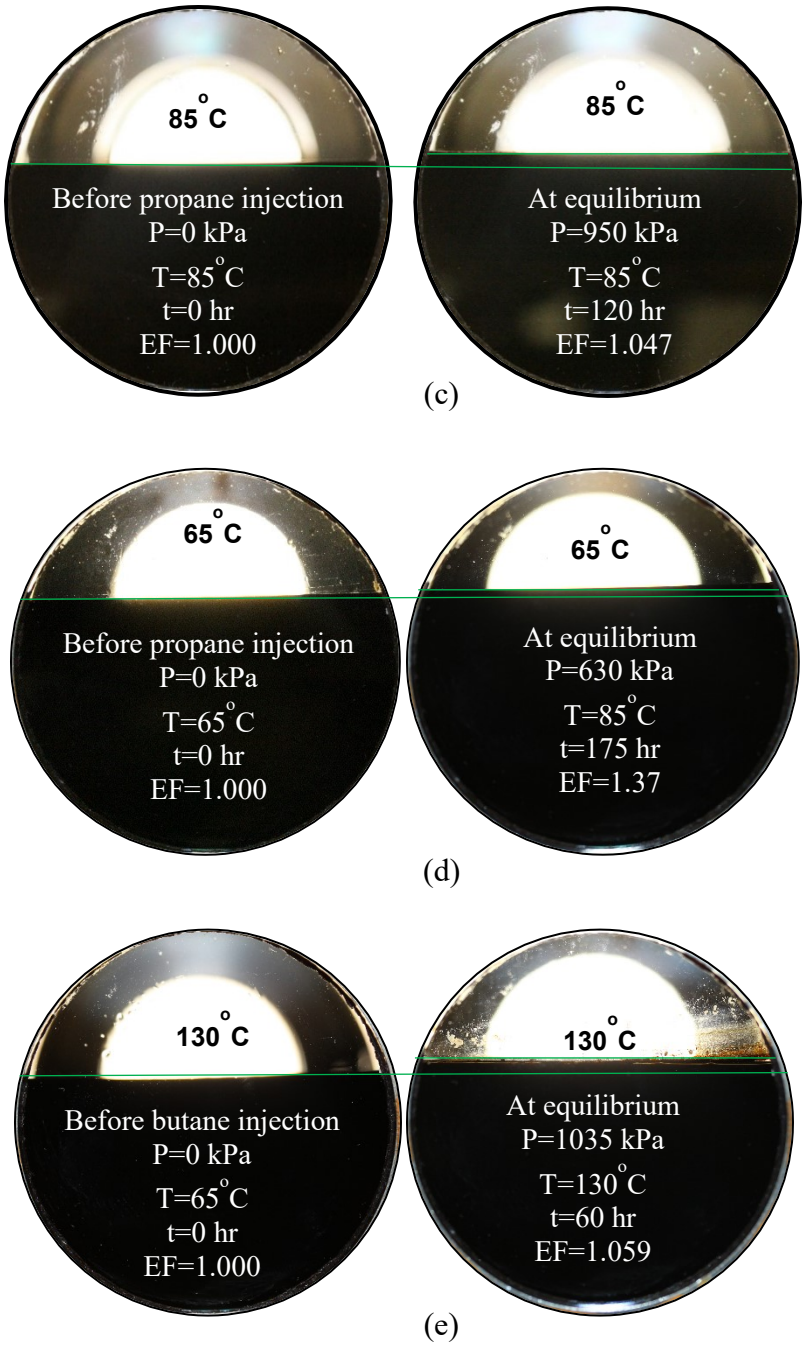

Figure 3-6: 2D view of visual cell's sight glass showing solvent-heavy oil interface at initial and equilibrium conditions. (a), (b), (c), (d) are the tests of C_3-heavy oil system conducted at temperatures of 130°C, 100°C, 85°C and 65°C, respectively. (e) shows interface of C_4-heavy oil at 130°C.

3.6.1 Pressure Decline Data

Figure 3-7 and Figure 3-8 show pressure decline data for C_3-heavy oil (at different temperatures) and C_4-heavy oil system, respectively. We observe fluctuations (i.e. increasing and decreasing of

pressure) in the pressure profiles of both systems. These fluctuations can be due to the extraction of lighter hydrocarbon components from heavy oil to gas phase which violates the model's assumption of one-way diffusion (i.e. from gas to oil). System pressure is equal to the sum of partial pressures of the gas phase components. Initially after C_3 injection, we have pure gas (single component) hence $P_{system} = P_{solvent}$. The extracted hydrocarbon molecules which are now part of the gas phase contribute to P_{system} (i.e., $P_{system} = P_{solvent} + P_{HC}$). The pressure fluctuations can also be attributed to fluctuations in temperature (i.e., ±0.5°C) even though the cell was provided with a heating jacket.

3.6.1.1 C_3-Heavy Oil System

Figure 3-7a to Figure 3-7d shows the measured pressure profiles of C_3- heavy oil system for tests 1, 2, 3 and 4 after closing the injection valve. The immediate decline in pressure after injecting C_3 into the system suggests gas diffusion into the heavy oil. Since, the system monitors gas pressure, this pressure decline indicates molecular diffusion of C_3 from bulk phase to heavy oil.

C_3 concentration at the C_3-heavy oil interface is higher than that at the bottom of the visual cell and this results in a concentration gradient. Therefore, C_3 moves from region of higher C_3 concentration to lower C_3 concentration (from C_3 bulk phase to heavy oil) based on Fick's first law of diffusion. Diffusion of C_3 into the heavy oil phase leads to pressure decline.

The pressure decline curves shown in Figure 3-7a to Figure 3-7d can be divided into two parts. Part (A) is the **rapid decline period** during which we observe a sharp decline in pressure with respect to time. Part (B) is the **equilibrium period** during which we observe pressure fluctuations of ±0.1 kPa/hr to ±1.2 kPa/hr.

For tests 1, 2, 3 and 4, the rapid decline period ends after 20, 33, 55 and 140 hrs respecively. High concentration gradient between C_3 bulk phase and heavy oil at the beginning of test leads to this rapid pressure drop i.e. faster diffusion of C_3 into heavy oil. The duration of this rapid decline period decreases with increasing temperature. After the end of rapid decline period, the pressure fluctuations of ±0.2 kPa/hr, ±1.2 kPa/hr, ±0.13 kPa/hr and ±0.2 kPa/hr are observed in test 1, 2, 3 and 4, respectively. We define this period as the equilibrium period. Table 3-2 summarizes the durations of the rapid decline period and equilibrium period. In rapid decline period, we observe

larger percentage of pressure reduction.Table 3-2 summarizes the durations and pressure drops (in percentages) of the rapid decline period and equilibrium period.

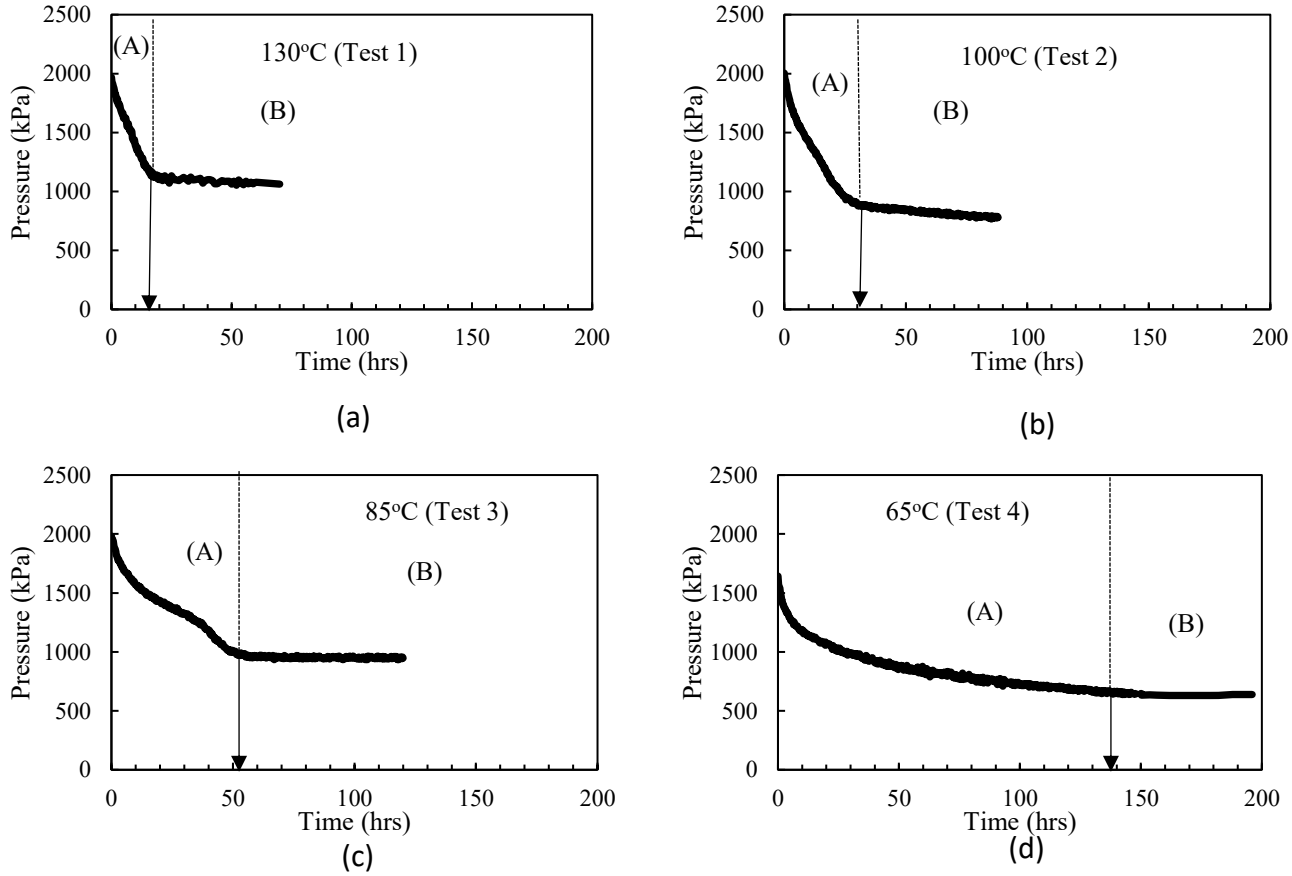

Figure 3-7: Pressure profile of C_3-heavy oil mixture for (a) Test 1; (b) Test 2, (c) Test 2 and (d) Test 4. In all the tests, we observe two regions; (A) rapid decline period; and (B) equilibrium period.

Table 3-2: Duration and pressure drops in percentage of rapid decline and equilibrium period for tests 1-4.

Test Name	Temperature (°C)	Pi (kPa)	Rapid Decline Period		Equilibrium Period	
			ΔP (%)	Δt (hrs)	ΔP (%)	Δt (hrs)
Test 1	130	1867.58	98.6	20	1.4	50
Test 2	100	1902.61	92.2	33	7.8	54
Test 3	85	1885.51	97.9	55	2.1	70
Test 4	65	1643.06	98.9	140	1.1	55

3.6.1.2 C_4-Heavy Oil System

Figure 3-8 shows the pressure decline of C_4-heavy oil system referred as test 5. Similar to the curves of C_3-heavy oil system, pressure declines due to diffusion of C_4 in the heavy oil. We immediately observe a pressure decline after injecting C_4 into the system.

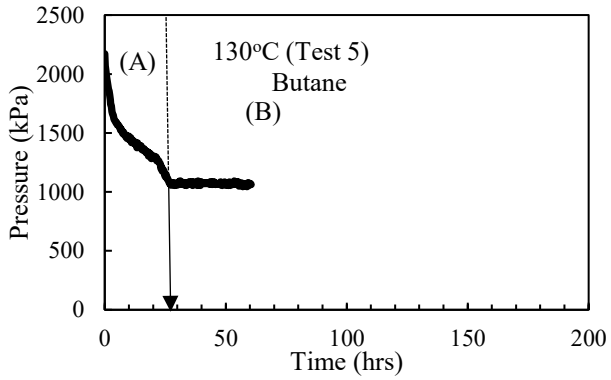

Figure 3-8: Pressure profile of C_4-heavy oil mixture. We observe two regions; (A) rapid decline period; and (B) equilibrium region.

This pressure decline is due to of diffusion of C_4 moles in heavy oil. We observe two distinct regions in the pressure decline curve; (A) rapid decline period; and (B) equilibrium period. For test 5, after rapid decline period ends after 29 hrs, the pressure fluctuations of ±0.1 kPa/hr are observed.

3.6.2 Three Different Regions Identified

In previous studies (Fengshang Du, 2016, Sheikha *et al.,* 2005; 2006; Nguyen, 1997), three different zones of diffusion process are reported. Figure 3-9 shows experimental data of $\ln[P(t) - P_{eq}]$ vs. Time for CO_2 – light crude oil system by Fengshang Du (2016). The plot shows three distinct CO_2 dissolution periods. The best fit straight line for the first period (I) has a much larger slope than that for second period (II), with a transition period in between. He concluded that a constant diffusion coefficient cannot quantify the entire dissolution process. According to him period I, is the convection dominated period and period II is the diffusion dominated period. Therefore, diffusion coefficient estimated using period II is the "molecular diffusion coefficient".

A graphical method to calculate diffusion coefficient is proposed by Sheikha et al. (2006). They reported three different zones of diffusion. Figure 3-10 shows a plot of $\text{erfc}^{-1}(P_t/P_i)$ vs $t^{0.5}$ indicating

different zones reported by Sheikha et al., 2006 for CH_4 – bitumen system at 50ºC. The data corresponding to early and late time periods show a departure from straight line, the slopes of these lines were excluded in the calculation of diffusion coefficients.

The zones were reported as; (i) **first zone**, the early time period identified by a lower slope, (ii) **second zone,** the intermediate region starting from the time when slope changes to the time when the diffusive front reaches to the physical boundary of the diffusion cell, and (iii) **third zone,** covers the time region after the diffusive front has reached to the physical boundary of the diffusive cell. According to Sheikha et al. diffusion coefficient calculated using second zone translated to the molecular diffusion coefficient.

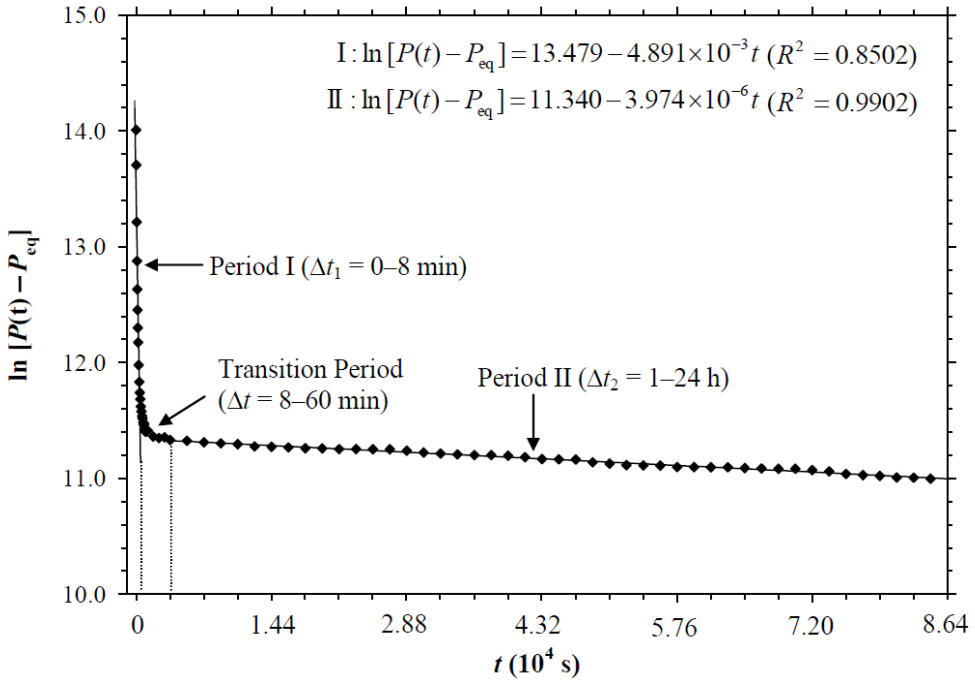

Figure 3-9: Experimental data of ln[P(t) – P_{eq}] vs. Time for CO_2-light oil systems at T=56ºC showing three distinct dissolution periods. (Fengshang Du, 2016)

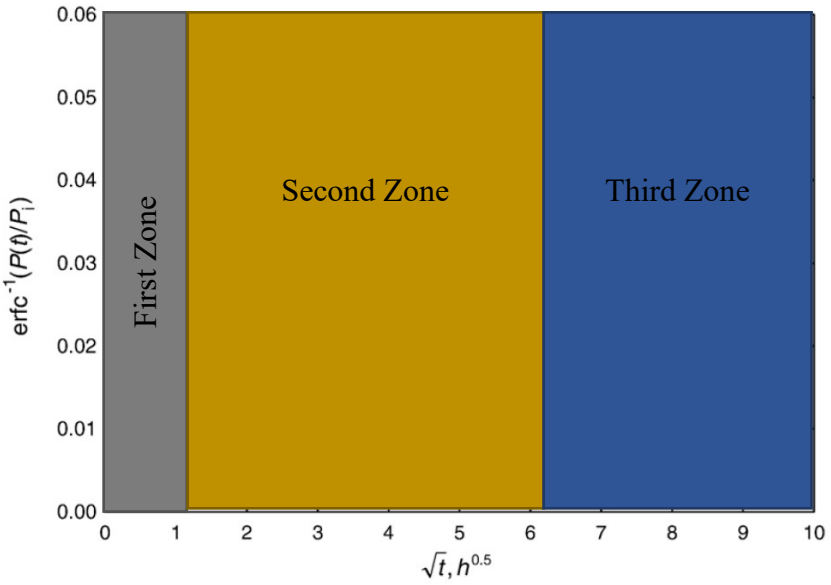

Figure 3-10: Estimation of diffusion coefficient using Graphical Metihod for CH_4 in Athabasca bitumen at 50°C. (modified from Sheikha et al., 2006)

Therefore, in this thesis *k*-means data clustering technique is used to identify beginning and the end times of each period. Since previous studies showed existence of three diffusion periods, *k* was set to 3 for data clustering. As a result of data clustering the beginning and end times of the regions, were found. These regions were termed as early region, transition region and late time region.

Figure 3-11 shows plot of Ln(P-P_{eq}) vs Time for Test 1 i.e. C_3-heavy oil system at 130°C. Green, blue and red color represents early, transition and late time region. Data of late-time regions is scattered, therefore, only early and transition region is used for the estimation of the diffusion coefficient. For test 1 (see Figure 3-11), the early and transition region have the duration of 10 and 12 hrs, respectively. Similar analysis was performed on other tests. See Appendix E for the plots generated for other tests. Table 3-3 summarized the duration of early and transition regions for all the tests.

The early region is affected by the interfacial effects and diffusion resistance offered by oil to gas (Sheikha et al, 2006), transition region is the difusion-dominated region (Fengshuang, 2016) and diffusive front reaches the physical boundary of diffusion cell in late-time region. Researchers (Guerrero, 2009; Sheikha et al., 2005; 2006) neglected early-time and late-time data for estimating diffusion coefficient.

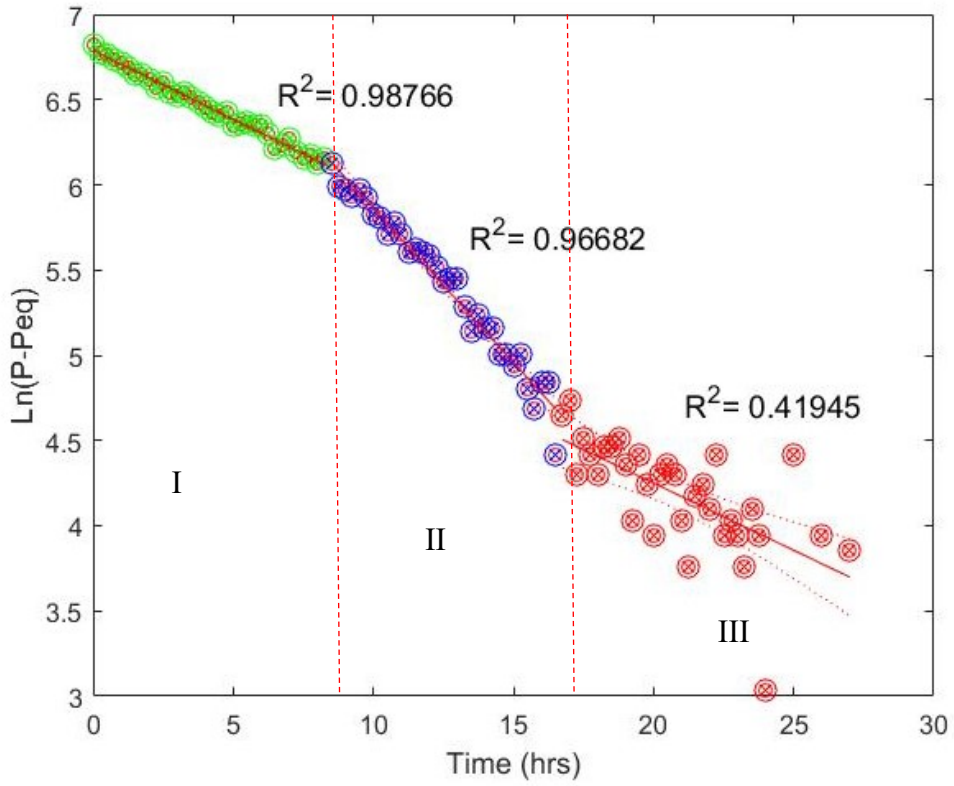

Figure 3-11: Plot of Ln(P-P_{eq}) vs time for C_3-heavy oil system at 130°C. Green, blue and red color represents early, transition and late time region.

Table 3-3: Duration and diffusion coeficients for all tests.

Test Conditions	***Regions***	***Duration, hrs***
C_3, T=130°C	Early Transition	8 9
C_3, T=100°C	Early Transition	14.25 15.75
C_3, T=85°C	Early Transition	40 20
C_3, T=65°C	Early Transition	6.75 145
C_4, T=130°C	Early Transition	16.75 9

3.6.3 Diffusion Coefficients

The calculation of the diffusion coefficients (D) is divided into two parts; i) D for C_3-heavy oil system at high temperatures of 65ºC, 85ºC, 100ºC and 130ºC; and ii) D for C_4-heavy oil system at 130ºC. We use the model proposed by Zhang et al. (2000) to calculate D. Plots are developed between $\ln(P-P_{eq})$ and time using Eq. 3.16.

3.6.3.1 Diffusion Coefficients for C_3-Heavy Oil System

Figure 3-12a to Figure 3-12d shows plots of $\ln(P-P_{eq})$ vs time for tests conducted at 130ºC, 100ºC, 85ºC and 65ºC respectively. They are referred as test 1, 2, 3 and 4, respectively. As a result of data clustering we identify beginning and end points of three different regions: early region (region 1), transition region (region 2) and late time region (region 3). In late-time region the data is scatterred therefore, we calculate the diffusion coefficients for early and transition region, and solubility of C_3 in the heavy oil and viscosity of mixture of C_3 and heavy oil at the equilibrium conditions.

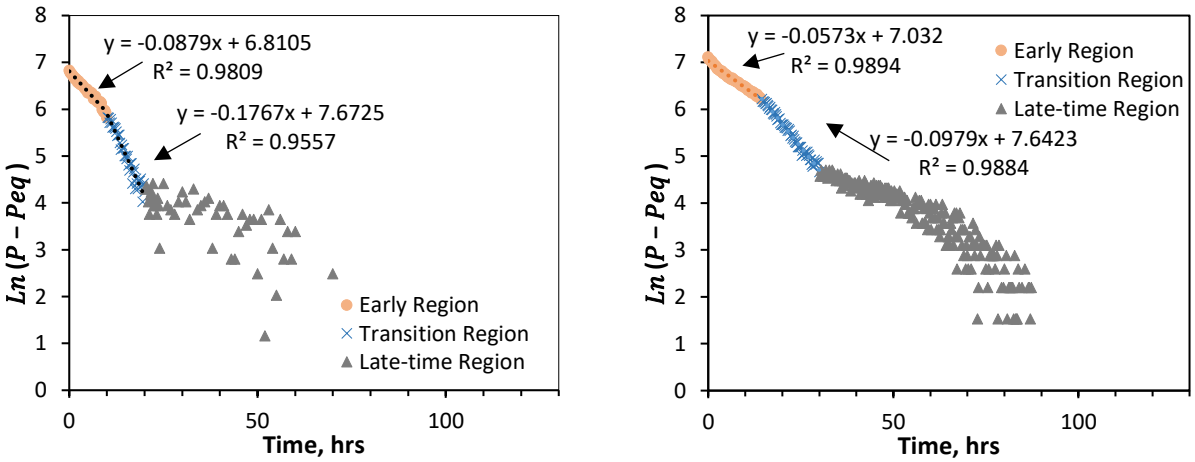

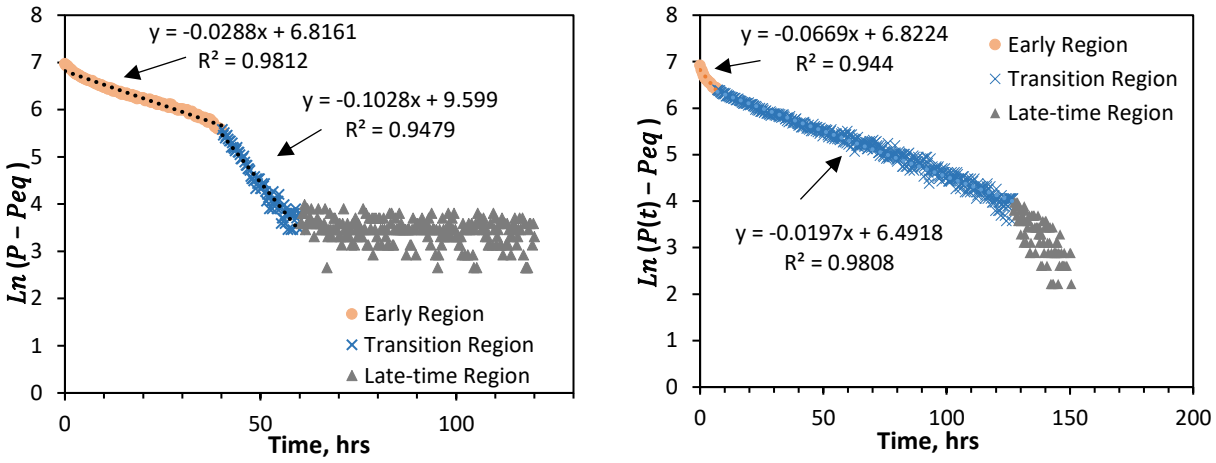

Figure 3-12: Plot of Ln(P-P_{eq}) vs Time for C_3-heavy oil system at (a) 130°C, (b) 100°C, (c) 85°C, and (d) 65°C.

For test 1 (see Figure 3-12a), the early and transition region have the duration of 10 and 7 hrs, respectively. We calculate the diffusion coefficient (D) using the slopes of the lines of best fit. For test 1's early region, D is 0.561 x 10^{-9} m^2/s. For its transition region, D is 1.128 x 10^{-9} m^2/s (which is twice the value for the early region). We observe high value of D in transition region. A similar trend is observed for tests 2, 3 and 4 (see Figure 3-12b and Figure 3-12d).

3.6.3.2 Diffusion Coefficient for C_4-Heavy Oil System

Figure 3-13 shows a plot between ln(P-P_{eq}) vs time for C_4-heavy oil system, where P_{eq} is 1035 kPa and T=65°C. Similar to the observations made for C_3-heavy oil system at high temperatures, we observe profile of different regions. Beginning and end of each region was determined using k means clustering method.

Data from early and transition region is used to calculate the diffusion coefficient. Data points in late-time regions are scattered. D for early and late-time region is 0.207 x 10^{-9} m^2/s and 2.63 x 10^{-9} m^2/s, respectively. Again, we observe high value of D for transition region. D for all tests is summarized in Table 3-4.

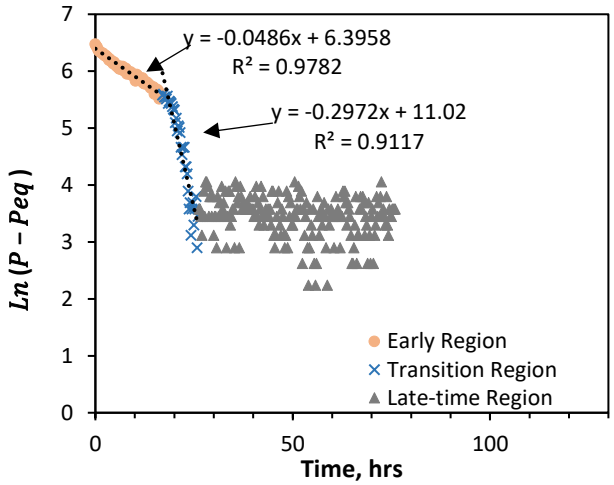

Figure 3-13: Plot of Ln(P-P_{eq}) vs Time for C_4-heavy oil system at 130°C.

Table 3-4: Summary of diffusion coefficients of early and transition region for all tests.

Test Conditions	***Regions***	***D, 10^{-9} m^2/s***
C_3, T=130°C	Early Transition	0.561 1.128
C_3, T=100°C	Early Transition	0.261 0.404
C_3, T=85°C	Early Transition	0.048 0.345
C_3, T=65°C	Early Transition	0.006 0.010
C_4, T=130°C	Early Transition	0.207 2.363

3.6.4 Solubility of Solvent Diffused in Solvent-Heavy Oil System

3.6.4.1 Solubility of C_3 in the C_3-Heavy Oil System

Table 3-5 shows the solubility of C_3 in C_3-heavy oil system vs time for all the tests. Highest solubility is achieved for test 2 i.e. at 100°C. Solubility of gas in oil is directly proportional to the partial pressure of that gas as predicted by Henry's law (Caroll, 1991). Pressure of the visual cell is the partial pressure of the solvent (gas). The temperature derivative of the solubility by Gibbs-Helmholtz is;

$$\frac{\partial lnx}{\partial 1/T} = \frac{\Delta s}{R} \tag{3.22}$$

Where, x is the mole fraction of gaseous solute (reciprocal to 'solvent' in this paper) at saturation, T is the temperature, s is the entropy of gas at system temperature and pressures and R is the universal gas constant. If $\Delta s > 0$, the solubility of gas in liquid will increase with increasing temperature. If $\Delta s < 0$, the solubility will decrease with increasing temperature. In this study variations in experimental conditions (initial and equilibrium pressures) resulted in varying solubilities of C_3 in heavy oil. The calculated solubilities of C_3 in heavy oil are summarized in Table 3-5 and are found to be close to values reported in literature.

Table 3-5: Solubility of C_3 in heavy oil at different temperatures calculated in this study and previous studies

System	Temperature (°C)	Solubility (g/cm^3)	Solubility (wt%)	Reference
C_3 – heavy oil	65	0.0184	N/A	This study
	85	0.0208	N/A	
	100	0.0237	N/A	
	130	0.0201	N/A	
CO_2 – bitumen	75	0.0328	N/A	Upreti et al., 2000
	50	0.0393	N/A	Etminan et al., 2010
	120	N/A	2.5	Eghbali and Dehghanpour, 2017
CH_4 – Dodecane	65	0.0110	N/A	Etminan et al., 2010
C_3 – bitumen	120	N/A	14.9	Eghbali and Dehghanpour, 2017
C_4 – bitumen	120	N/A	12.5	Eghbali and Dehghanpour, 2017
C_4 – heavy oil	130	0.0204	N/A	This study

3.6.4.2 Solubility of C_4 in the C_4-Heavy Oil System

Solubility of C_4 in C_4-heavy oil system vs time at 130°C is 0.0204 g/cm^3. The solubility is determined in a similar way as that of C_3-heavy oil system.

3.6.5 Viscosity of Heavy Oil after Diffusion of Solvent

Initial viscosity of heavy oil at T_{set} was calculated using Eq. 3.2, whereas, the viscosity of the mixture (C_3 + heavy oil) is calculated using the models proposed by Eghbali and Dehghanpour (2018). They employed non-linear viscosity modelling, given by Eq. 3.23.

$$\ln \mu_L = \sum_{i=k\ and\ nk} N_i x_i ln\mu_{iL} \tag{3.23}$$

Where, N_k is modifed weighing factor of the key component, N_{nk} is modified weighing factor of the non-key parameter x_i is mole fraction and μ_{iL} is viscosity of liquid.

Table 3-6: Summary of viscosity of heavy oil before and after diffusion of solvent in heavy oil

System	Test	Temperature (ºC)	Initial Viscosity Before Solvent Diffusion (cP)	Final Viscosity After Solvent Diffusion (cP)
C_3 – heavy oil	Test 1	130	52.99	23.85
	Test 2	100	161.16	66.08
	Test 3	85	328.33	121.48
	Test 4	65	1054.93	337.58
C_4 – heavy oil	Test 5	130	52.99	18.50

Table 3-6 shows the viscosity of heavy oil before and after solvent diffusion for each test. It is gotten by subtracting final mixture viscosities from initial oil viscosities at T_{set}. It can be observed that viscosity reduction decreases with increasing temperature. This reduction is highest (68%) for 65ºC (test 4) and lowest for 130 ºC (test 1 and test 5). This trend shows that the effect of solvent on viscosity reduction is more significant at lower temperatures.

3.7 Discussion

3.7.1 High Value of *D* in Transition Region

Figure 3-14 shows that D for test 1's early and transition regions is 0.561 x 10^{-9} m^2/s and 1.128 x 10^{-9} m^2/s, respectively. D for transition region is more than twice the D for early region. A similar trend is observed for tests 2, 3 and 4 as shown in Figure 3-14.

The early region is affected by interfacial effects and diffusion resistance (Sheikha et al, 2006), transition region is difusion-dominated region (Fengshuang, 2016) and diffusive front reaches the physical boundary of diffusion cell in late-time region. Therefore, it is not recommended to use early-time and late-time data for estimating diffusion coefficient (Guerrero, 2009; Sheikha et al, 2005, 2006).

The techniques presented by Sheikha et al (2005, 2006) to calculate diffusion coefficients isolated early and late time region for estimating diffusion coefficient. The resistance provided to gas at the interface during early region results in lower D value (Civan Ramussen 2006; 2009). The existence of this film-resistance delays transfer of gas through two phases. This prevents instantaneous thermodynamic equilibrium at the gas-heavy oil interface (Etminan, 2014). Therefore, it is not ideal to use early time data without quantifying the film resistance (Roman, 2015; Nguyen. 1997). Rasmussen et al. (2009) considered resistance to mass transfer at interface in their calculation of diffusion coefficients. Later, Etminan et al. 2013 proposed following model considering inter-mass transfer resistance at the interface:

$$-D\frac{\partial C}{\partial z} = k\,[C_s(t) - C(z,t)] \tag{3.24}$$

Where, D is diffusion coefficient, k is mass-transfer coefficient, $C_s(t)$ is time independent interface concentration and C(z,t) is the concentration at the gas-oil interface. Etminan et al. (2013) concluded there is no mass transfer in the system if k=0, hence there in no decay in pressure. When k becomes large, i.e. $k \to \infty$, there is no resistance to mass transfer which is acceptable at late times (Roman, 2015; Tharanivasan et al., 2004). After the end of early region, the resistance at the interface diminishes. This results in smooth transfer of mass from gas to liquid. Thus, we observe higher D in the transition region.

When the system moves from transition region to late-time region, the pressure has declined significantly; therefore, number of moles of gas phase has been reduced which results in reduction of the concentration gradient. As reported by Henry's law, pressure of gas in gas-liquid systems, is controlled by the number of the moles of gas phase. There is no significant change in pressure as we move from transition region to late-time region (see Figure 3-8). This translates into a lower value of D in late time region.

Figure 3-14 shows *D* for C_3-heavy oil system. *D* values are highest for transition regions in all tests. Also, *D* values for transitions regions increases with temperature.

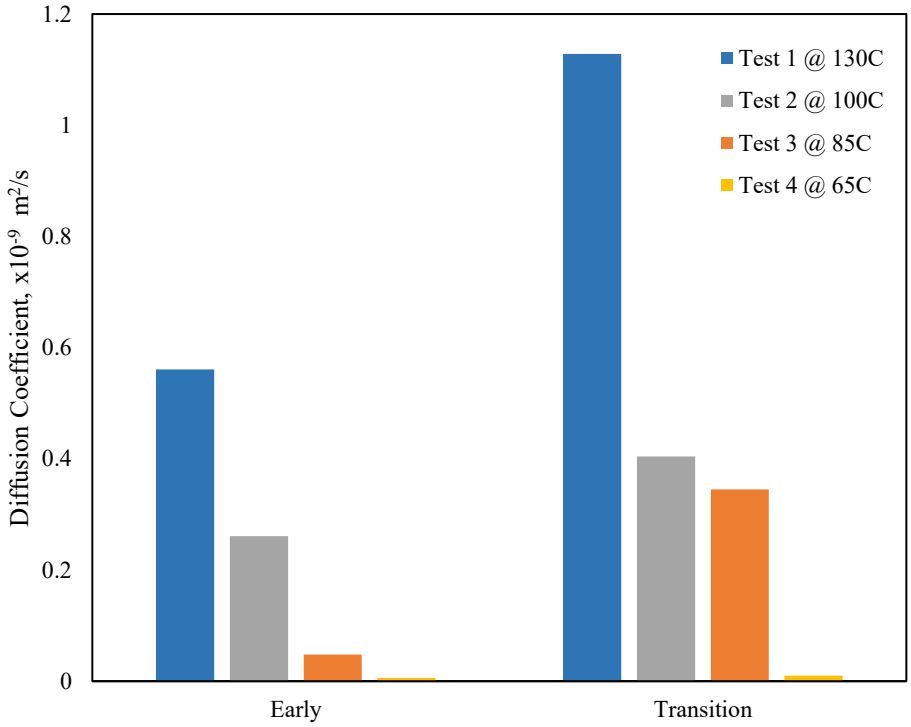

Figure 3-14: Diffusion coefficients for test C_3-heavy oil system. Transition region for each test has the highest value.

Table 3-7 compares the values of *D* for the transition region for tests 1, 2, 3 and 4 with C_3 diffusion values in literature at different temperatures. The values calculated in this study are similar to the values reported in literature for same system.

Table 3-7: C_3 diffusion coefficients in different oils (Modified from Li and Yang, 2016)

Gas	Reference	Heavy Oil	Viscosity (cP)	Pressure (kPa)	Temperature (K)	Diffusion Coefficient (10^{-9} m²/s)
C_3H_8	Luo et al. 2007	Bitumen Lloydminster	24137 @ 297.05 K	200-800	297.05	0.053 – 0.490
	Yang and Gu 2006b	Heavy Oil Lloydminster	23000 @ 297.05 K	400-900	297.05	0.090 – 0.680

	Ganapathi 2009		13144 @ 290 K	400-600	298.00	0.110 – 0.180
	This study	Heavy Oil Cold Lake	52.99 @ 403.15 K	1050-1969	403.15	0.043 – 1.128
			161.16 @ 373.15 K	950-1986	373.15	0.038 – 0.404
			328.33 @ 358.15 K	700-1902	358.15	0.005 – 0.345
			1054.93 @ 338.15 K	1643-630	338.15	0.006 – 0.010
C_4H_{12}	This study	Heavy Oil Cold Lake	52.99 @ 403.15 K	1050-1969	403.15	0.008 – 2.363

3.7.2 Effect of Temperature on *D*

For C_3-heavy oil system, the tests were conducted at constant temperatures of 130ºC, 100ºC, 85ºC and 65ºC. When we investigate the transitions regions, test 1 (130ºC) has the highest value of *D*. As shown in and Figure 3-15, diffusion coefficient increases with increasing temperature.

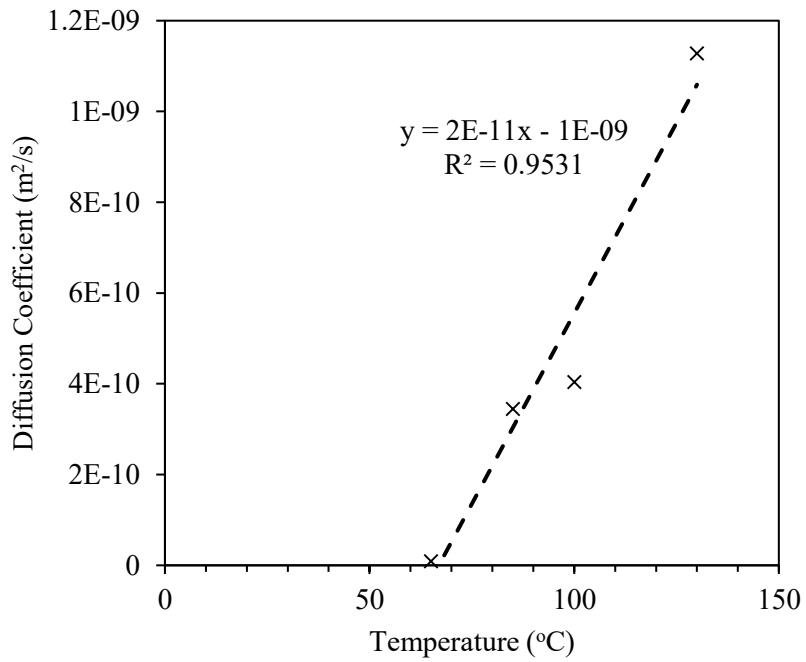

Figure 3-15: Plot of Diffusion Coefficient (D) vs T. Positive slope indicates that with increasing temperature, D decreases.

In the diffusion process, solvent (C_3) molecules under concentration gradient has to overcome the resistance against the molecules of heavy oil (Etminan, 2010). At low temperatures, density and viscosity of heavy oil is high. Thus, the molecules are densely packed and are strongly affected by fields of neighboring molecules. As a result, the diffusion coefficients in denser liquid is lower than less dense liquid. Therefore, it can be said that higher the temperature and less viscous the heavy oil, higher the diffusion coefficient will be.

One of the earliest equations for determining diffusion coefficient of gas in liquid is the Stokes-Einstein equation (Einstein, 1906):

$$D = \frac{R}{6N_A \pi \eta_a} T \tag{3.25}$$

Eq. 3.25 shows that D is directly proportional to absolute temperature. Temperature affects the diffusion process in two ways:

1) At higher temperatures, the average kinetic energy of gas molecules increases, which in turn, increases the velocity of gas molecules. The increased velocity means that there is

greater chance of collision between molecules, resulting in an increased rate of diffusion. Therefore, at higher temperatures, we have higher values of *D* compared to that at lower temperatures.

2) Increasing the temperature, decreases the viscosity of heavy oil, which in turn increases the diffusion coefficient. At higher temperatures, the resistance provided by heavy oil against diffusion of C_3 is less compared to the one at lower temperatures. At room temperature, the viscosity of heavy oil is 60306 cP. At 130ºC, before the injection of C_3, the viscosity of heavy oil is already reduced to 53cP. Whereas at 85ºC, the heavy oil has a viscosity of 378 cP. Higher viscosity of heavy oil at 85ºC results in lesser D than at higher temperatures. Figure 3-16a shows that viscosity of heavy oil decreases with increasing temperature. Figure 3-16b shows that *D* increases as oil viscosity decreases. Therfore, we can say that increase in temperature results in viscosity reduction of heavy oil, which causes increase in *D*.

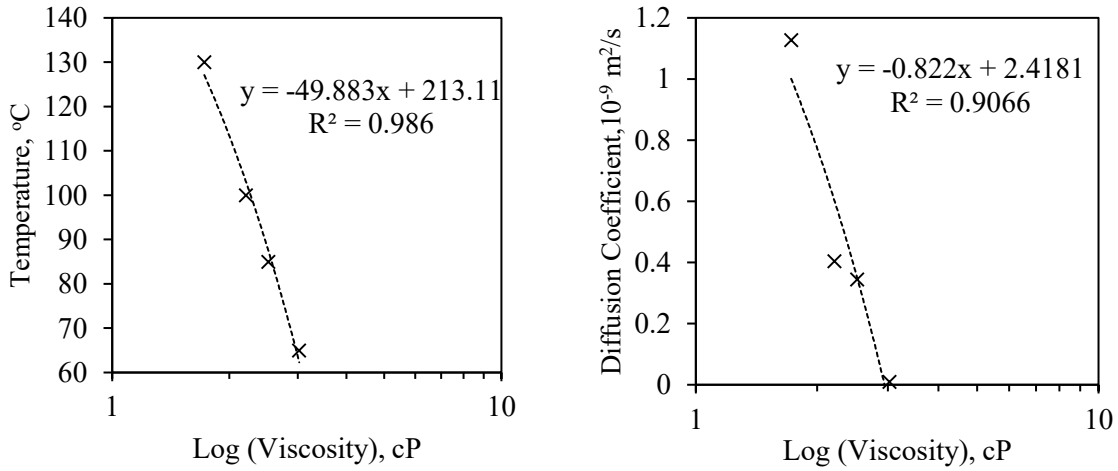

Figure 3-16: a) Plot of Temperature vs Log (Viscosity). With increase in temperature viscosity reduces. (b) Diffusion coefficients of transition region vs Log (Viscosity) at different temperatures. Negative slopes indicated that with increase in viscosity *D* decreases

3.7.3 Viscosity Reduction of Heavy Oil by C_3 vs C_4

We calculate viscosity of solvent-heavy oil mixture at equilibrium pressures using the viscosity model developed by Eghbali and Dehghanpour (2017). Table 3-8 shows initial viscosity of heavy oil at the test temperatures and final viscosities of solvent-heavy oil mixtures. Using C_4 as solvent results in 65% of viscosity reduction of heavy oil in comparison to 55% reduction by C_3. This is because solubility and *D* of C_4 in heavy oil is higher than of C_3. Similar observation is reported by Zhao et al., 2018. Therefore, we can say that butane performs better than propane.

Table 3-8: Comparison between C_3- and C_4-heavy oil systems.

Solvent	Temperature (°C)	Initial viscosity of heavy oil (cP)	Solubility of solvent in heavy oil (g/cm^3)	Final viscosity of solvent-heavy oil mixture (cP)	Viscosity reduction (%)	$D_{transition}$ (10^{-9} m^2/s)
C_3	130	52.99	0.0201	24.10	55	1.13
C_4	130	52.99	0.0204	18.5	65	2.36

3.8 Sources of Errors

Diffusion coefficient values calculated are subject to the following errors:

1) We used material balance law to calculate the injected moles of solvent. During solvent injection in the visual cell, pressure buildup in the accumulator results in solvents' liquefaction. Thus, there are some uncertainties in the calculation of the injected mole values.

2) Swelling of heavy oil is not considered in the model. Also varying gas compressibility with pressure is ignored. Due to these simplifying assumptions, the diffusion coefficient values obtained are expected to be underestimated.

3) We used images taken during the experiments to obtain the EF by analyzing solvent-heavy oil interface. However, there are some solid particles on the glass, which can cause errors in finding the accurate interface. Therefore, the presented EF values may not be accurate. EF determination is also affected by temperature fluctuation during pressure buildup process.

4) We identified starting and ending points of regions using data clustering technique. Inaccurate selection of end points might lead to error in the calculation of diffusion coefficients.

5) To pressurize the visual cell, we use a pulse-free pump with maximum flow rate of 29 cm^3/min. It takes 10-25 minutes to reach the set pressure. Diffusion may occur during this period of pressure build-up and can result in underestimation of *D* for early region.

3.9 Summary

In this chapter, we discussed the experimental methodology of determining diffusion coefficients (*D*) for C_3- and C_4- heavy oil systems at different temperatures. We also calculated the solubility of solvents into heavy and the resulted viscosity reduction. Key observations from this study can be summarized as follows;

1) Diffusion starts immediately after pressure buildup (gas injection), resulting in sharp (rapid) pressure decline during first few hours of soaking.

2) The pressure decline curves for C_3- and C_4- heavy oil system temperatures can be divided in to two parts: (i) rapid decline period and (ii) equilibrium period. Sharp pressure decline is observed in rapid decline period because of faster diffusion of solvent into heavy oil. This is due to presence of large concentration gradient between solvent and heavy oil.

3) Diffusion process of C_3- and C_4- heavy oil system undergoes three different stages i.e. early region, transition region, and late time region. Early region is affected by the ressitance offered by oil film to solvent diffusion, transition region is transition region is difusion-dominated region, whereas, in late-time region the diffusive front has reached the physical boundary of the cell.

4) As temperature increases, the diffusion coefficient also increases. Plot of D vs Temperature resulted in a straight line thus indicating that diffusion is directly proportional to the temperature. Since, viscosity is temperature dependent, therefore, it is hard to assess the effect of temperature on diffusion coefficient without being influenced by viscosity change.

Chapter 4: Interactions between Liquid Propane and Heavy Oil during Soaking Process

In this chapter, we investigate and visualize interactions between heavy oil and liquid propane (C_3H_8) during soaking process. We conduct tests to investigate the effect of (i) temperature and pressure and (ii) mass of $C_{3(l)}$ injected on C_3-heavy oil interactions. The physical properties (i.e. compositional analysis, density and viscosity) of the heavy oil are explained Section 3.2.

4.1 Methodology

To visualize and investigate C_3-heavy oil interactions, we use the visual cell setup shown in Figure 3-1. We use accumulators and pulse-free pump to inject the heavy oil and solvent into the visual cell. The visual cell's specifications are explained in detail in Section 3.1. First, we conduct a base test at conditions shown in Table 4-1. For test 2 (high-temperature case) and test 3 (low mixing ratio case), we change the temperature and mixing ratio, respectively, compared with the base case. For test 1 and test 2, we change the temperature but keep the mixing ratio same. Whereas, for test 3, we reduce the mixing ratio while keeping the temperature same as of test 1.

In this study, we define mixing ratio as ratio of C_3 moles at set pressures (P_{set}) and test temperatures (t_{set}) to moles of oil (before C_3 injection i.e. at P=0 psig). Mixing ratios given by Eq. 4.1 are reported in Table 4-1.

$$Mixing\ Ratio = \frac{Moles\ of\ C_3|P_{set}, T_{set}}{Moles\ of\ oil|P_{=0}, T_{set}} \tag{4.1}$$

Table 4-1: Experimental conditions for investigation of C_3/heavy oil interactions

Property	**Test 1** (Base Case)	**Test 2** (High Temperature Case)	**Test 3** (Low Mixing Ratio Case)
Temperature, ^oC	55	75	55
Moles of heavy oil injected, mol	0.67	0.64	0.68
$C_{3(l)}$ moles, mol	0.60	0.44	0.27
$C_{3(g)}$ moles, mol	0.20	0.38	0.21
Mixing ratio	1.19	1.28	0.70
Set pressure (P_{set}), psig	283	385	288

The following procedure is followed for the tests:

1. First, the visual cell is checked for any leakages. Then, the top flange of the visual cell is connected to a vacuum pump to remove the air in the system.

2. The first accumulator is loaded with oil and is connected to the bottom valve of the visual cell. We inject oil into the visual cell at constant pressure of 2,000 psig while heating the accumulator and tubes with a heat gun to ensure fast transport of oil into the visual cell. After filling the visual cell with oil to required volume, the bottom valve is closed.

3. The cell temperature is set at the test temperature (T_{set}) and is left overnight. Experimental conditions of test 1 (base case) are listed in Table 4-1 . The following variations were made for test 2 and 3;

    i. In test 2 (high temperature case), we increased the temperature from 55°C (base case) to 75°C (test 2) to observe the effect of temperature on the interactions. The mixing ratios for both tests are kept almost similar.

    ii. In test 3 (low mixing ratio case), we decreased the mixing ratio by from 1.19 (base case) to 0.70 (test 3) by decreasing the mass of $C_{3(l)}$ injected. The temperature of test 3 is same as of base case i.e. 55°C.

4. Once set temperature is reached, we record heavy oil level before C_3 injection and calculate the base volume of heavy oil at P = 0 psig ($V_{\text{heavy oil}}|p_{=0}$). This volume is used to calculate heavy oil expansion factor (EF) defined by Eq. 3.. $V_{\text{heavy oil}}|p'$is the volume of heavy oil phase at $p' > 0$ psig during the pressure buildup and soaking processes.

5. We inject $C_{3(l)}$ into the visual cell to reach the set pressures (P_{set}). P_{set} is the saturation pressure of pure C_3 at test temperatures and are obtained from NIST Webbook. Pressure buildup continues till we reach desired mixing ratio in visual cell as shown in Table 4-1. We do not completely fill the visual cell with $C_{3(l)}$. Therefore, at the top of visual cell, there is still $C_{3(g)}$ phase in equilibrium with $C_{3(l)}$ phase, as schematically shown in Figure 4-1. By doing this, we can visualize the $C_{(l)}$ level during the soaking process.

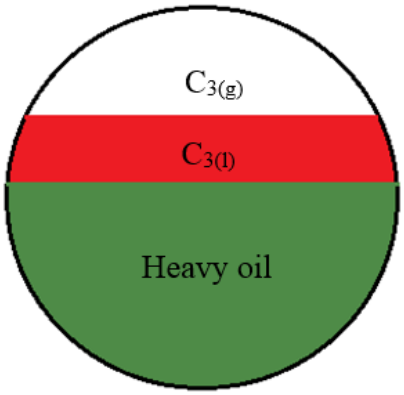

Figure 4-1: Schematic of different phases at the end of the pressure buildup process. Heavy oil is at the bottom of cell with liquid propane ($C_{3(l)}$) in the middle and gaseous propane ($C_{3(g)}$) at the top.

6. The visual-cell pressure is recorded by the data-acquisition system which is later used to plot versus time. We visualize the interfaces of $C_{3(l)}$-heavy oil and $C_{3(l)}$-$C_{3(g)}$ during this soaking process. We consider final conditions once we observe that a homogenous mixture between C_3 and heavy oil is developed.

4.2 Results and Discussions

We divide this section into three parts. First, we present and discuss the results of test 1 (base case). Second, we compare the results of test 2 with test 1 to evaluate the effects of temperature on $C_{3(l)}$-oil interactions. Finally, we compare the results of test 3 with test 1 to evaluate the effects of mixing ratio on $C_{3(l)}$-oil interactions.

4.2.1 Test 1: Base Case, T = 55°C, Mixing Ratio = 1.19

Figure 4-2 shows the heavy oil and C_3 levels corresponding to: (a) initial test conditions used to determine the base volume of oil before C_3 injection; (b) end of pressure buildup process (P_{set}), and (c) end of soaking process at P_f. respectively. Initially, there is 0.67 mol of heavy oil in the visual cell at 0 psig (Figure 4-2a). We start C_3 injection and increase the pressure from 0 to P_{set} = 283 psig in 0.58 hours (Figure 4-2b). We did not completely fill the visual cell with $C_{3(l)}$ so that we can visualize the $C_{3(l)}$-$C_{3(g)}$ interface. Therefore, there is $C_{3(g)}$ phase in equilibrium with $C_{3(l)}$ phase at the top of the visual cell. According to Figure 4-2b, oil EF is 1.03 after injection of 0.80 mol of C_3 that consists of 0.60 mol of $C_{3(l)}$ and 0.20 mol of $C_{3(g)}$. Mixing ratio of 1.19 is achieved after the end of pressure buildup.

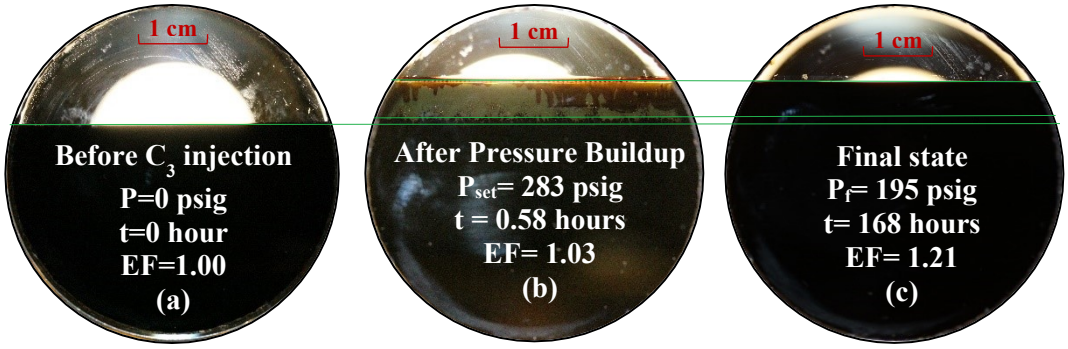

Figure 4-2: Images of heavy oil and C_3 levels at T_{set} = 55°C. The pictures correspond to (a) initial conditions of the test for determination of the base oil volume; (b) end of buildup process (P_{set}), and (c) end of soaking process at final conditions (P_f). The diameter of the sight glass is 4.8 cm. Green lines show the level of oil during different stages of soaking process till final conditions.

After the pressure buildup process, the soaking process begins, during which oil EF increases from 1.03 to 1.21 (Figure 4-2c). The visual-cell pressure declines and reaches to P_f = 195 psig after approximately 168 hours. The pressure of visual cell is controlled by the partial pressure of $C_{3(g)}$, therefore this decline in pressure is due to the diffusion of $C_{3(g)}$ in to liquid phase (Habibi et al., 2017). Comparing Figure 4-2b with Figure 4-2c shows that the colorless $C_{3(l)}$ at P_{set} appears to be black color at P_f. Figure 4-3 presents the pressure decline vs. time during the soaking process.

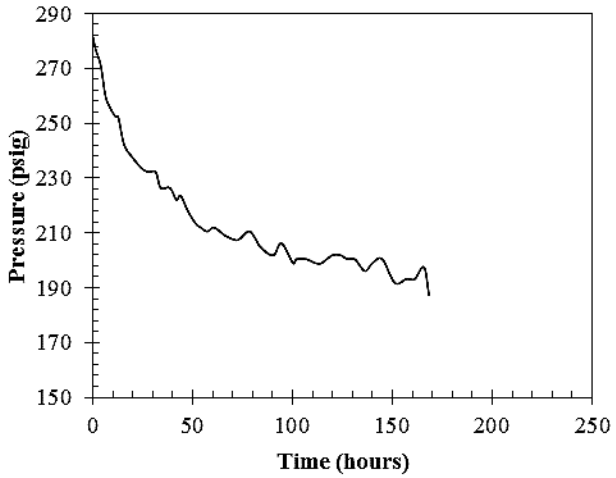

Figure 4-3: Pressure decline vs. time during the soaking process at T_{set} = 55°C

Figure 4-4 shows a closer view of $C_{3(l)}$-heavy oil and $C_{3(l)}$-$C_{3(g)}$ interfaces at different times during the soaking process. Figure 4-4d shows an image taken at final conditions, after 168 hours of soaking. At final conditions, we observe that $C_{3(l)}$ changes from colorless to black, indicating the

mixing of heavy oil components into $C_{3(l)}$. To investigate the mixing mechanisms, we look into $C_{3(l)}$-heavy oil and $C_{3(l)}$-$C_{3(g)}$ interfaces during the soaking process (Figure 4-4b and Figure 4-4c).

4.2.1.1 Formation of Two Distinct Layers: Layer 1 (L_1) and Layer 2 (L_2)

Figure 4-4a is an image taken immediately after the end of pressure buildup and this marks the start of soaking process. We can observe that extraction of heavy oil components (red arrows in Figure 4-4a) from oil to $C_{3(l)}$ starts instantly after the end of pressure buildup. The color change of $C_{3(l)}$ occurs in two stages. Initially, we observe that around one-third of $C_{3(l)}$ layer becomes darker, and is labelled Layer 1 (L_1) in Figure 4-4b. This transformation continues for approximately 15 hours till the pressure reaches 251 psig. Once L_1 is completely black, the remaining $C_{3(l)}$ becomes light brown and is labelled as Layer 2 (L_2) Figure 4-4b. The original $C_{3(l)}$ is now divided into L_1 and L_2 as shown in Figure 4-4b. Since $C_{3(l)}$ is colorless, the change in color is attributed to the extraction of hydrocarbon components from heavy oil as shown in Figure 4-4b. Since heavier components tend to absorb more light than lighter components, light color indicates presence of lighter components and black color indicates presence of heavier components. Therefore, as the concentration of hydrocarbon components or extraction of heavier hydrocarbon components from oil in $C_{3(l)}$ increases, the color of $C_{3(l)}$ becomes darker. In the next two subsections, we further investigate the images of L_1 and L_2 during the soaking process and explain the flow patterns that led to the transformation of colorless $C_{3(l)}$ into black.

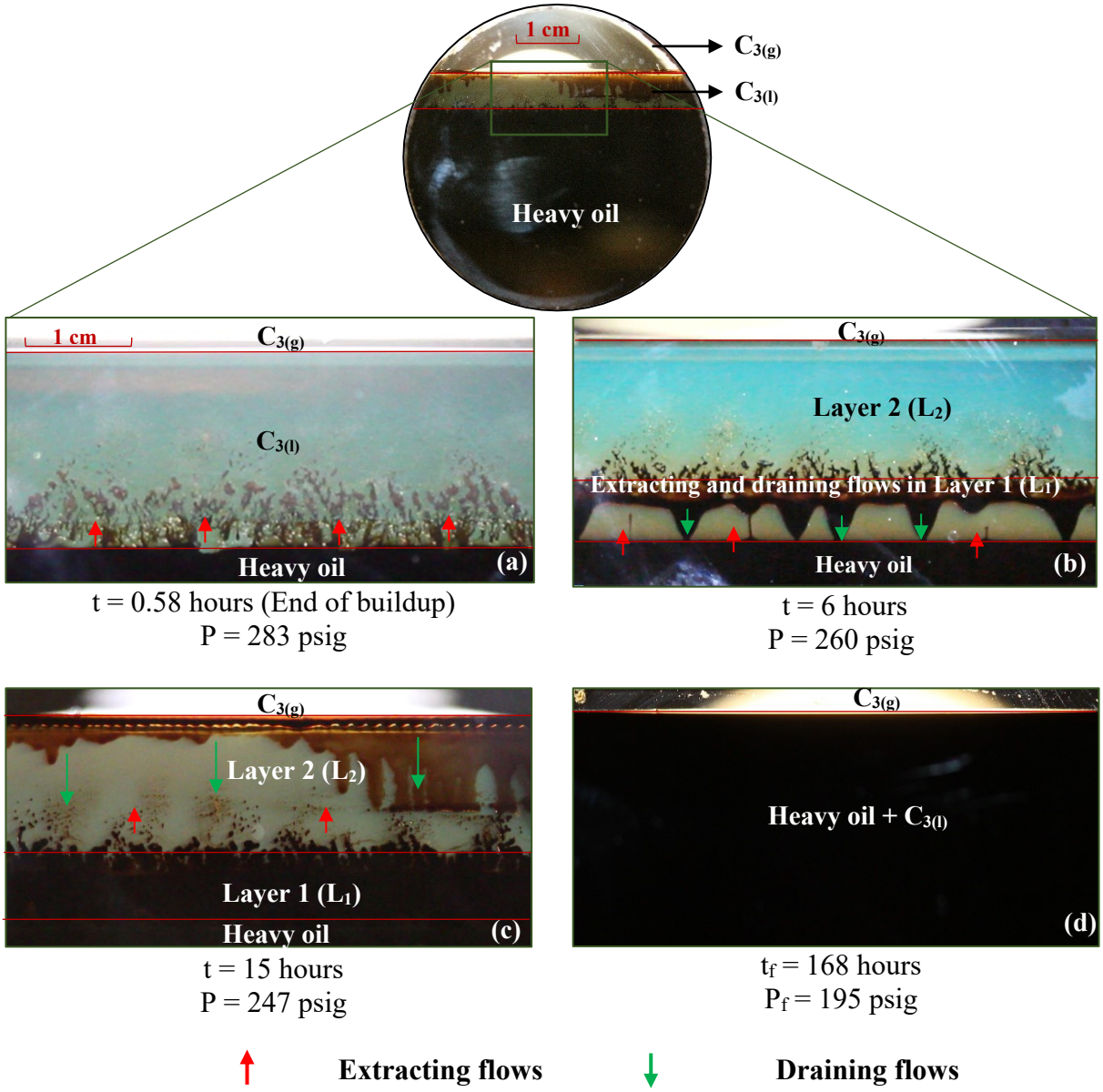

Figure 4-4: Magnified images of oil-$C_{3(l)}$ and $C_{3(l)}$-$C_{3(g)}$ interfaces at different times. (a) Image taken at the end of the pressure buildup (P_{set} = 283 psig). Upward red arrows indicates immediate extraction of oil components in $C_{3(l)}$ (b) Extracting (upward red arrows) and draining (green arrows) flows in Layer 1 (L_1) at P = 260 psig and t = 6 hours. (c) The color of L_1 is completely changed to black color. Extracting and draining flows in Layer (L_2) at P = 247 psig and t = 15 hours. (d) At final conditions (P_f = 195 psig) L_1 and L_2 turn into black color. The color becomes darker as the concentration of heavier components increases.

4.2.1.2 Extracting and Draining Flows in Layer 1 (L_1)

Figure 4-4b is an image taken after 6 hours of the soaking process. It shows two distinct upward (extracting) and downward (draining) flows in L_1. Extracting flows start immediately after the

pressure buildup process as shown in Figure 4-4a. We do not observe such flows in the upper part of $C_{3(l)}$ (L_2 layer) until L_1 is turned completely into black color.

Figure 4-5a through Figure 4-5c shows the development of extracting/draining flows in L_1, leading to formation of a single homogenous phase in L_1. The time lapse between Figure 4-5a and Figure 4-5c is approximately 13 hours. Extracting flows illustrated in Figure 4-5b are attributed to upward movement of heavy oil components driven by the concentration gradient into the $C_{3(l)}$ phase. The extracted oil components accumulate at the upper part of L_1 and form a heavier/denser layer. As the size this heavy layer increases, it drains downward towards the $C_{3(l)}$-oil interface by gravity force (downward green arrows in Figure 4-5b). As pressure declines, the extracting and draining flows become less pronounce and color of L_1 changes into black (Figure 4-5c). This results in counter-current flow of oil components and acts as natural mixing in $C_{3(l)}$. Meanwhile, L_2 color gradually changes into light brown (Figure 4-5c) due to extraction of lighter heavy oil components from L_1 into L_2.

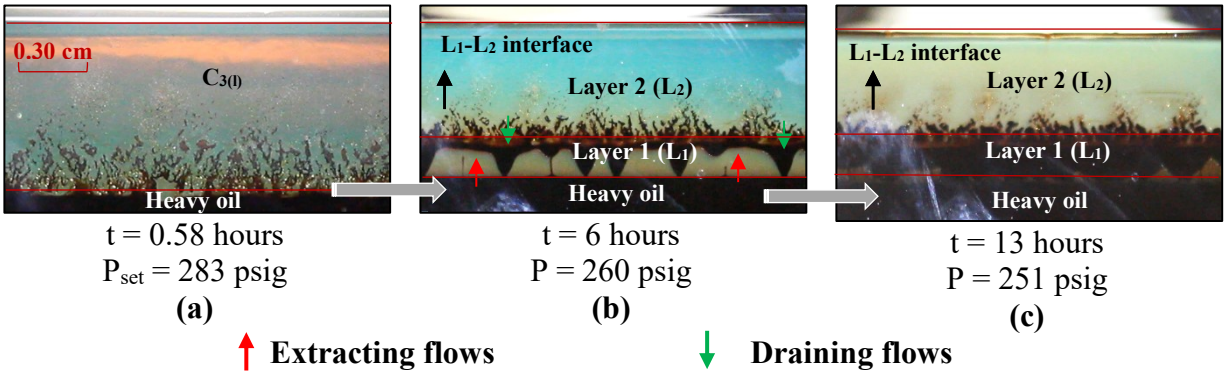

Figure 4-5: Magnified images showing the interactions within L_1 and L_2 layers (a) $C_{3(l)}$ was injected into the cell and it took 35 minutes to reach P_{set}. At the end of pressure build-up process, $C_{3(l)}$ is at the top of heavy oil. Upward red arrows indicates immediate extraction of oil components in $C_{3(l)}$ and form L_1. (b) Upward red arrows show extraction of oil components that are accumulated at the L_1/L_2 interface and form a denser layer. Green arrows show the draining flows of these accumulations toward the $C_{3(l)}$-oil interface. (c) After 13 hours, L_1 is turned into black color whereas L_2 is turned into light brown color.

4.2.1.3 Extracting and Draining Flows in Layer 2 (L_2)

Figure 4-6a is taken after 15 hours of soaking process which shows that L_1 has completely turned into dark brown and we start to observe extracting (red arrows) and draining (green arrows) flows in L_2. First, the components of oil rise and accumulate at the interface of L_2-$C_{3(g)}$, as shown in Figure 4-6a and Figure 4-6b, forming a heavier/denser phase at the top of L_2 (represented by dark

brown color). As the size of this heavier phase increases, it drains downward toward the L_1-L_2 interface. Eventually, the color of L_2 turns into black at final conditions (Figure 4-6c, P_f = 195 psig), suggesting the complete mixing of oil with $C_{3(l)}$ in L_2.

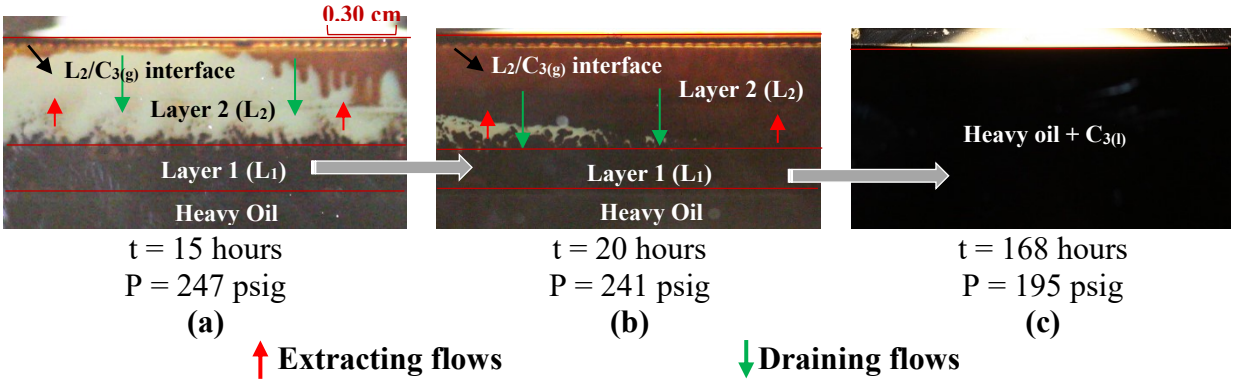

Figure 4-6: Magnified images show the extracting and draining flows in L_2. (a) L_1 color is changed into black. Green arrows show draining flows from L_2-$C_{3(g)}$ interface. (b) Color of the draining flows in L_2 becomes darker due to further extraction of heavy oil components from L_1 into L_2. (c) After 168 hours of soaking between heavy oil and $C_{3(l)}$, a single homogenous phase is formed.

4.2.2 Test 2: High Temperature Case, T = 75ºC, Mixing Ratio = 1.28

The objective of this test is to investigate the effects of temperature on C_3-oil interactions by keeping similar mixing ratios. Therefore, we conduct this test at 75ºC and compare the results with those of the base case (test 1) conducted at 55ºC. We kept the mixing ratio for test 1 and test 2 almost similar. Due to the increase in temperature, the saturation pressure (P_{sat}) of C_3 increases to 410 psia. At 55 ºC, P_{sat} is 285 psia, based on the data from NIST Webbook, as shown in Figure 4-7. The experimental procedure for test 2 is same as of test 1 and is explained in detail in Section 4.1.

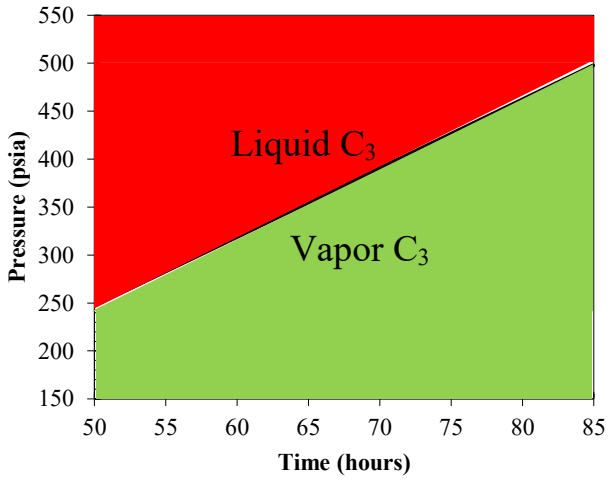

Figure 4-7: Saturation curve of C_3. Saturation pressure of C_3 at 55°C and 75°C are 285 psia and 410 psia respectively. (NIST Webbook)

Figure 4-8 shows the oil and C_3 levels corresponding to (a) initial test conditions used to determine the base volume, (b) end of pressure buildup process (P_{set}), and (c) at final conditions P_f. We continue injecting C_3 in the system until pressure reaches to P_{set} = 385 psig in 0.87 hrs (see Figure 4-8b).

After buildup process, the C_3-heavy oil system contains 0.44 mol of $C_{3(l)}$, 0.38 mol of $C_{3(g)}$ and 0.64 mol of heavy oil. Immediately after pressure buildup, we observe pressure decline as shown in Figure 4-9, narking the start of soaking process which continues until reaching P_f = 250 psig after 237 hrs. Figure 4-8c shows that at the final state heavy oil has has reached EF of 1.18. Comparing Figure 4-8b with Figure 4-8c shows that the colorless $C_{3(l)}$ at P_{set} is completely transformed into black color at P_f. This change in color indicates the mixing of heavy oil components into $C_{3(l)}$.

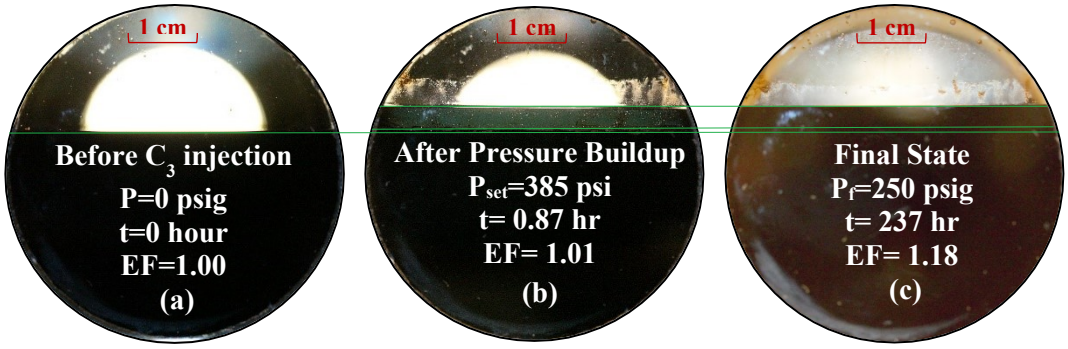

Figure 4-8: Images of heavy oil and C_3 levels at T_{set} = 75°C. The pictures correspond to (a) initial conditions of the test for determination of the base oil volume; (b) end of buildup process (P_{set}), and (c) end of soaking process at final conditions (P_f). The diameter of the sight glass is 4.8 cm.

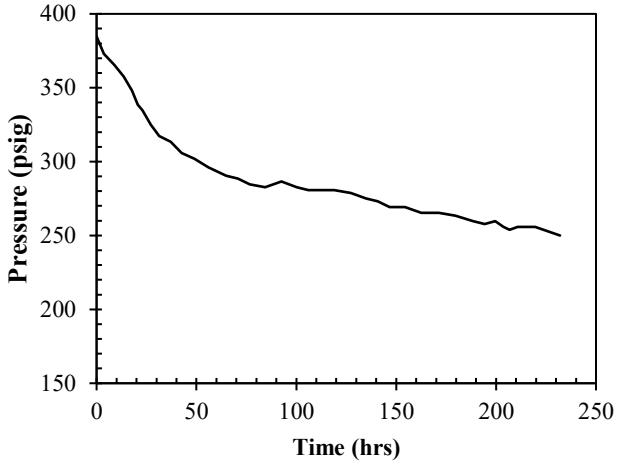

Figure 4-9: Pressure decline vs. time during the soaking process at T_{set} = 75°C

4.2.2.1 Formation of Two Distinct Layers: Layer 1 (L_1) and Layer 2 (L_2)

Similar to the test 1, we observe formation of two distinct layers during the soaking process; Layer 1 (L_1) and Layer 2 (L_2). Figure 4-10 shows a closer view of $C_{3(l)}$-heavy oil and $C_{3(l)}$-$C_{3(g)}$ interfaces at different times during the soaking process.

As explained for test 1 (base case), the color change of $C_{3(l)}$ occurs in two stages. Initially, we observe that one-third of $C_{3(l)}$ becomes darker (called as L_1). When colorless L_1 becomes black, the rest of $C_{3(l)}$ (called as L_2) starts getting darker, suggesting the extraction of heavy oil components.

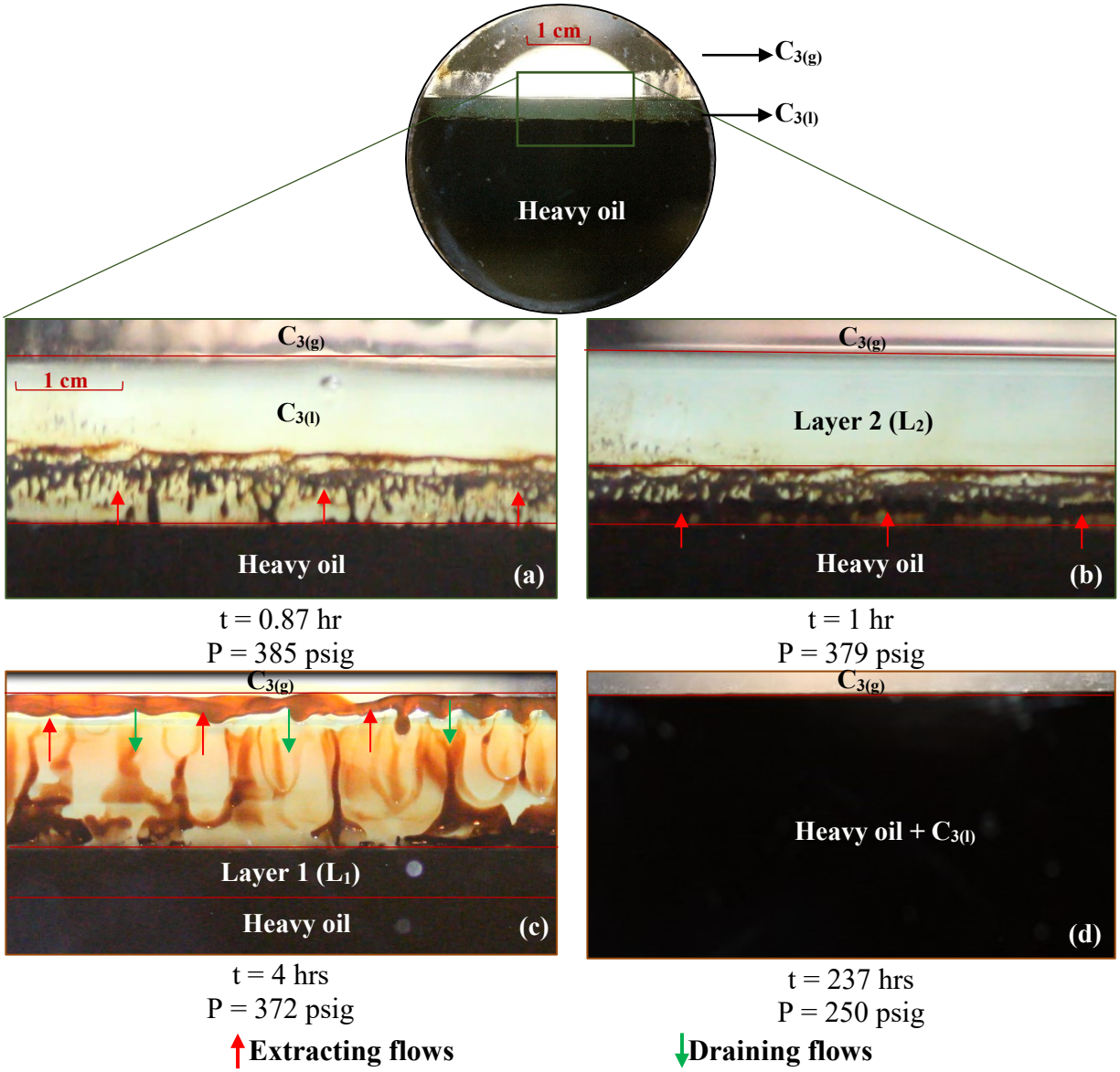

Figure 4-10: Magnified images of heavy oil-$C_{3(l)}$ and $C_{3(l)}$-$C_{3(g)}$ interfaces at different times for test 2. (a) Image is taken after the pressure buildup (P=385 psig). Extraction flows start immediately after pressure buildup. (b) Extracting and draining flows in layer 1 (L_1) at P = 379 psig and t= 1 hr. (c) Extracting and draining flows in L_2 at P = 372 psig and t= 4 hrs. (d) At final conditions L_1 and L_2 turn into black color. The color becomes darker as the concentration of heavier components increases.

4.2.2.2 Extracting Flows in Layer 1 (L_1)

Figure 4-10a and Figure 4-10b show the extraction flows (red arrows) in L_1, which start immediately after the end of pressure buildup. Meanwhile, we do not observe such flows in the upper part of $C_{3(l)}$ (L_2 layer). Figure 4-11a, Figure 4-11b, and Figure 4-11c show the extracting

flows which make the color of L_1 darker and more uniform. The time lapse between Figure 4-11a to Figure 4-11c is approximately 17 minutes. Pressure at the end of the transformation reaches to 378 psig from P_{set} = 385 psig.

Extracting flows (red arrows) in Figure 4-11b are attributed to the upward movement of oil components driven by the concentration gradient between oil and $C_{3(l)}$ phases, forming L_1-L_2 interface. At L_1-L_2 interface, the concentration of extracted hydrocarbon components increases, resulting in a denser mixture (oil+C_3) and it starts draining towards heavy oil.

Figure 4-11b and Figure 4-11c show that extracting flows of oil components continue in L_1 till it becomes black or becomes homogenous with oil beneath it. Dark color indicates the presence of heavier components or it darken as result of increase in concentration of hydrocarbon components. Meanwhile, L_2 remains transparent which indicates insignificant diffusion of oil components into it.

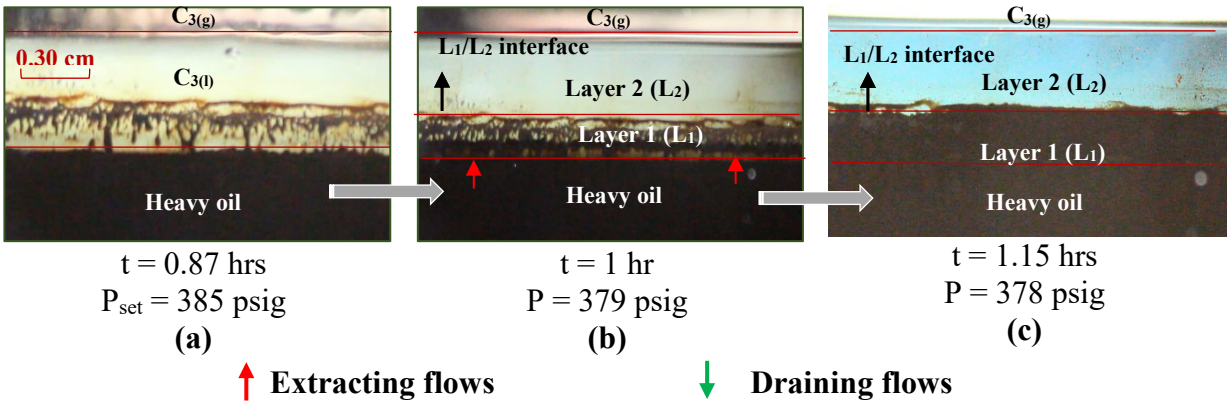

Figure 4-11: The sequence of events which lead to the mixing the heavy oil sample and the lower part of $C_{3(l)}$ (Layer 1). (a) Extraction currents at the end of buildup process. (b) and (c) hydrocarbon extraction in L_1 continues for 0.15 hrs till the color of L_1 is completely transformed to black. Dark color indicates presence of higher concentration of extracted hydrocarbon components.

4.2.2.3 Extracting and Draining Flows in Layer 2 (L_2)

Figure 4-12a, taken after 1.5 hrs of soaking process, shows that L_1 is completely black and we observe extracting flows (red arrows) in L_2. First (Figure 4-12a), the hydrocarbon components are extracted from L_1-L_2 interface. Light brown extraction flows are due to low concentration of extracted oil components or it may also be due to presence of oil components of low molecular weight.

Extracted hydrocarbon components are collected at the interface of L_2-$C_{3(g)}$, as shown in Figure 4-12a and Figure 4-12b, forming a heavier/denser phase at the top of L_2 (represented by dark brown color in Figure 4-12b). As this phase become heavier, it drains towards L_1-L_2 interface. Eventually, the color of L_2 turns into black at final conditions (Figure 4-12c, P_f = 250 psig), suggesting the mixing of oil with $C_{3(l)}$ in L_2. Thus, initially the diffusive flux of oil components is dominant within $C_{3(l)}$, later as the density of the extracted phase increases, gravity drainage become dominant. The natural mixing due to counter-current flow of the oil components accelerate the dissolution of the extracted oil components in $C_{3(l)}$.

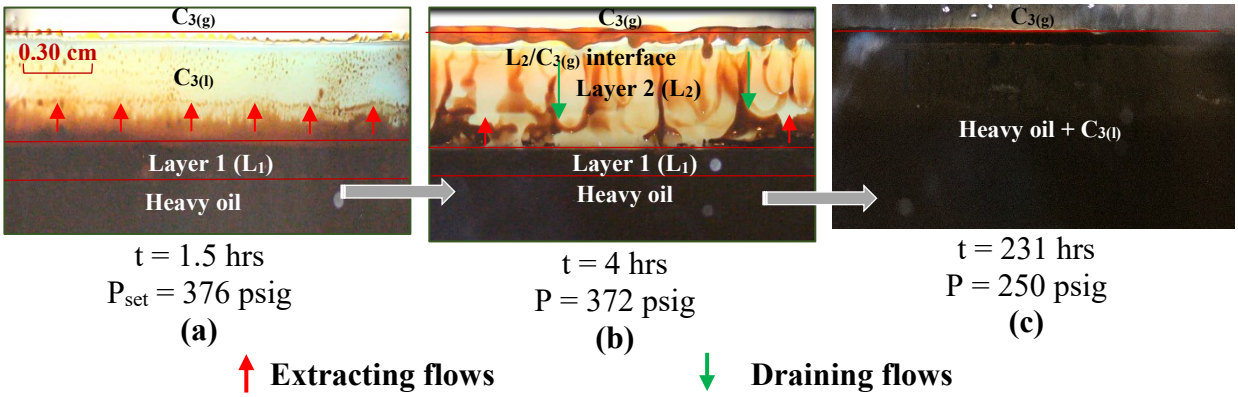

Figure 4-12: The sequence of events which lead to the mixing of $C_{3(l)}$ and the extracted oil components. (a) Extraction of light components from L_1 at t = 1.5 hrs. Light brown color reflects lower concentration of heavy oil components or presence of oil components of low molecular weight (b) Extracting and draining flows observed in L_2 at t = 4 hrs. (c) At final conditions, L_2 looks completely black.

4.2.2.4 Effect of Temperature on the Interactions

Here, we compare the results of test 1 and test 2, conducted at 55°C and 75°C, respectively, to investigate the effects of temperature on the interactions. In both tests, the sequence of events is following: (i) L_1 and L_2 layers are formed in $C_{3(l)}$; (ii) colorless L_1 becomes black or dark brown while L_2 remains colorless or light brown; and (iii) L_2 turns into black color at final conditions suggesting the mixing of extracted oil components with $C_{3(l)}$.

It is observed that temperature affects the duration of these events. Transformation of L_1 from colorless to black for tests 1 and 2 takes 13 hrs (see Figure 4-5) and 0.28 hrs (see Figure 4-11), respectively. This is because increasing temperature decreases the viscosity of oil as it is a strong function of temperature (Eghbali and Dehghanpour, 2017; Pathak et al., 2012). This reduction in viscosity lowers intermolecular attraction or cohesive forces between the liquid molecules. Hence,

the faster liquid (heavy oil) molecules results in faster extracting and draining flows for test 2 than the test 1.

4.2.3 Test 3: Low Mixing Ratio Case, Mixing Ratio = 0.70

Test 3 is conducted to investigate the effect of mixing ratio (solvent to oil) on $C_{3(l)}$-oil interactions. In test 3 we reduced the mixing ratio in comparison to test 1 from 1.19 to 0.70 while maintaining same temperatures. Since, the temperatures of both tests are same, therefore the saturation pressures (shown in Figure 4-7) are also same. Thus, P_{set} is almost same for both tests. In test 3, we inject 0.27 mol (11.88 g) of $C_{3(l)}$ in the system compared to 0.60 mol (26.4 g) of $C_{3(l)}$ in test 1. Table 4-1 shows the experimental conditions of base test and test 3. The experimental procedure for test 3 is same as of test 1 and is explained in Section 4.1.

Figure 4-13 shows the oil and C_3 levels corresponding to (a) initial test conditions used to determine the base volume; (b) end of pressure buildup process (P_{set}), and (c) end of soaking process at P_f. We continue injecting C_3 in the system until pressure reaches to P_{set} = 288 psig in 0.33 hrs as shown in Figure 4-13b.

Figure 4-14 shows pressure decline of C_3-heavy oil system for test 3. Immediately we observe pressure decline when starting the soaking process, which continues until the pressure reaches to P_f = 170 psig after 118 hrs. Figure 4-13c shows that at the final conditions oil has reached EF up to 1.09. Figure 4-13c shows C_3-oil system at final conditions, we observe that the colorless $C_{3(l)}$ has transformed into black color. This change in color indicates the mixing of oil components with $C_{3(l)}$.

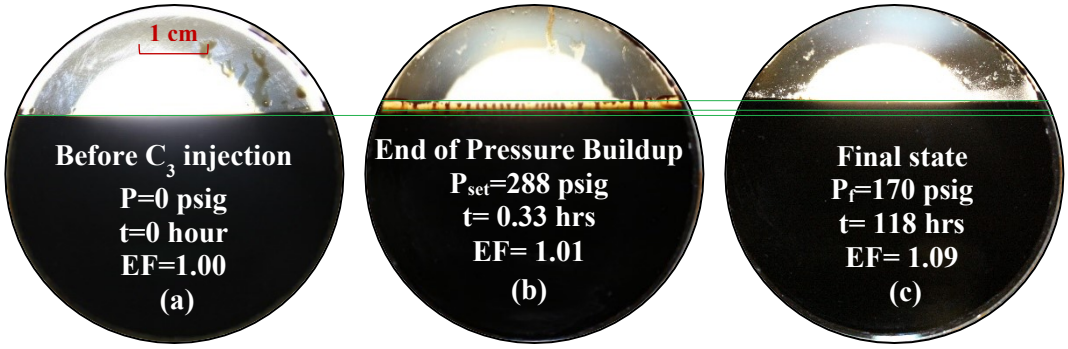

Figure 4-13: Images of heavy oil and C_3 levels at T_{set} = 55ºC (test 3). The pictures correspond to (a) initial conditions of the test for determining the base oil volume; (b) end of buildup process (P_{set}), and (c) end of soaking process at final conditions (P_f). The diameter of the sight glass is 4.8 cm. Green lines indicate levels of oil at different time of soaking process.

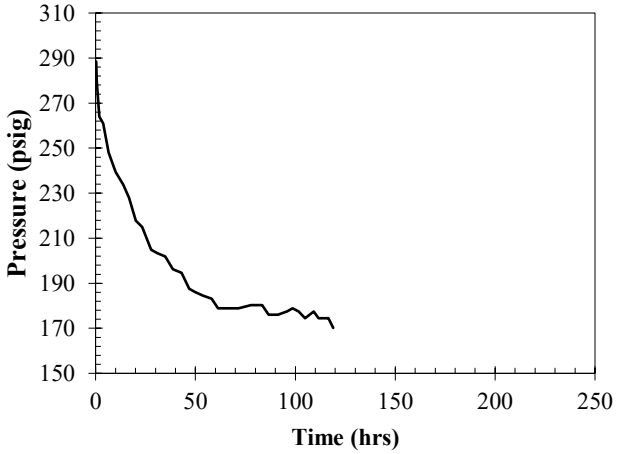

Figure 4-14: Pressure decline for test 3.

4.2.3.1 Extracting and Draining Flows in $C_{3(l)}$

Figure 4-15 shows a closer view of $C_{3(l)}$-oil and $C_{3(l)}$-$C_{3(g)}$ interfaces at different times during the soaking process. The extracting and draining flows observed in Figure 4-15b to Figure 4-15d lead to the mixing of extracted oil components with $C_{3(l)}$. Figure 4-15c, taken after 4 hrs of soaking process, shows the drainage of the accumulated oil components towards $C_{3(l)}$-oil interface. The extracting and draining flows continue till $C_{3(l)}$ turns into black at final conditions (P_f = 170 psig).

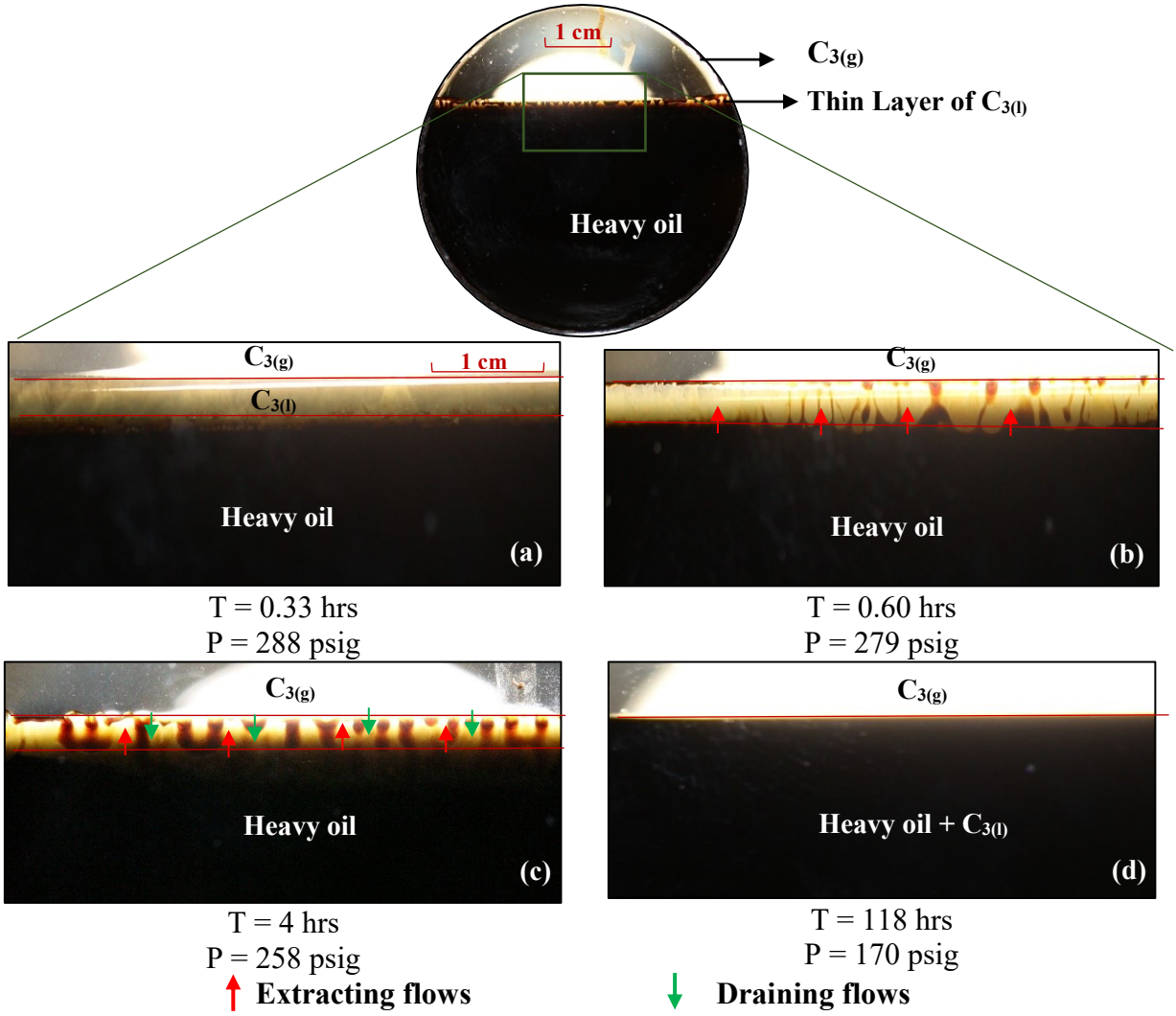

Figure 4-15: Magnified images of heavy oil-$C_{3(l)}$ and $C_{3(l)}$-$C_{3(g)}$ interfaces at different times for test 3. (a) Formation of a thin colorless $C_{3(l)}$ layer at the top of heavy oil after the pressure buildup (P=288 psig). (b) Extracting flows in layer 1 (L_1) at P = 279 psig and T= 0.60 hrs. (c) Extracting and condensing flows in $C_{3(l)}$ at P = 258 psig and t= 4 hrs. (d) At final conditions, $C_{3(l)}$ is turned into black color, suggesting the mixing of extracted oil components with $C_{3(l)}$.

4.2.3.2 Effect of Solvent Mass on the Interactions

In test 3, we reduce the mixing ratio in comparison to test 1. In test we had mixing ratio of 1.19, whereas in test 3 it is 0.70. Lower mixing ratio is achieved by reducing mass of injected C_3. In test 3, we inject 0.27 mol (11.88 g) of $C_{3(l)}$ in the system compared to 0.60 mol (26.4 g) of $C_{3(l)}$ in test 1. In both cases, we observed transformation of colorless $C_{3(l)}$ to black color suggesting extraction of heavy oil components. The sequence of the events is different for the two tests. For test 1, following sequence was observed:

i. Formation of L_1 and L_2 layers in $C_{3(l)}$.
ii. Extracting and draining flows occur within L_1 changing its color to black.
iii. When L_1 is black, extracting and draining flows occur within L_2 changing its color to black.

For test 3, $C_{3(l)}$ undergoes extracting and draining flows until the formation of a homogenous phase at final conditions. Since $C_{3(l)}$ is relatively short, we do not observe formation of two distinct layers (Layer 1 and Layer 2) in test 3 (see see Figure 4-15) as it was observed in test 1 (see Figure 4-4). Therefore, by reducing the mixing ratio, homogeneous phase between $C_{3(l)}$ and oil develops in only one stage rather than going through to two stages.

4.2.4 Foamy Oil Production during Pressure Depletion

For evacuating the cell of its contents, the top valve of the visual cell is connected to the vent of the laboratory for rapid evacuation i.e. fast depletion rate. During pressure depletion, we observed foamy oil formation in the visual cell. Foamy oil is considered as a mixture of heavy oil with entrapped gas bubbles (Smith 1988; Maini et al., 2010).

Figure 4-16a and Figure 4-16 show images of the visual cell before and during pressure depletion for test 1 respectively. The bubbles forming in the oil during pressure depletion led to complete filling of the visual cell as shown by Figure 4-16b. Similar observation is made for test 2, shown in Figure 4-16c and Figure 4-16d. Foamy oil behavior of C_3-heavy oil system was also reported by Zhou, 2016. We assumed that that at the test temperatures and pressures heavy oil components are not vaporized. Therefore, these gas bubbles are of C_3 that are being liberated from the C_3-oil mixture. Figure 4-16e shows foamy oil collected at the end of test 3 at room conditions.

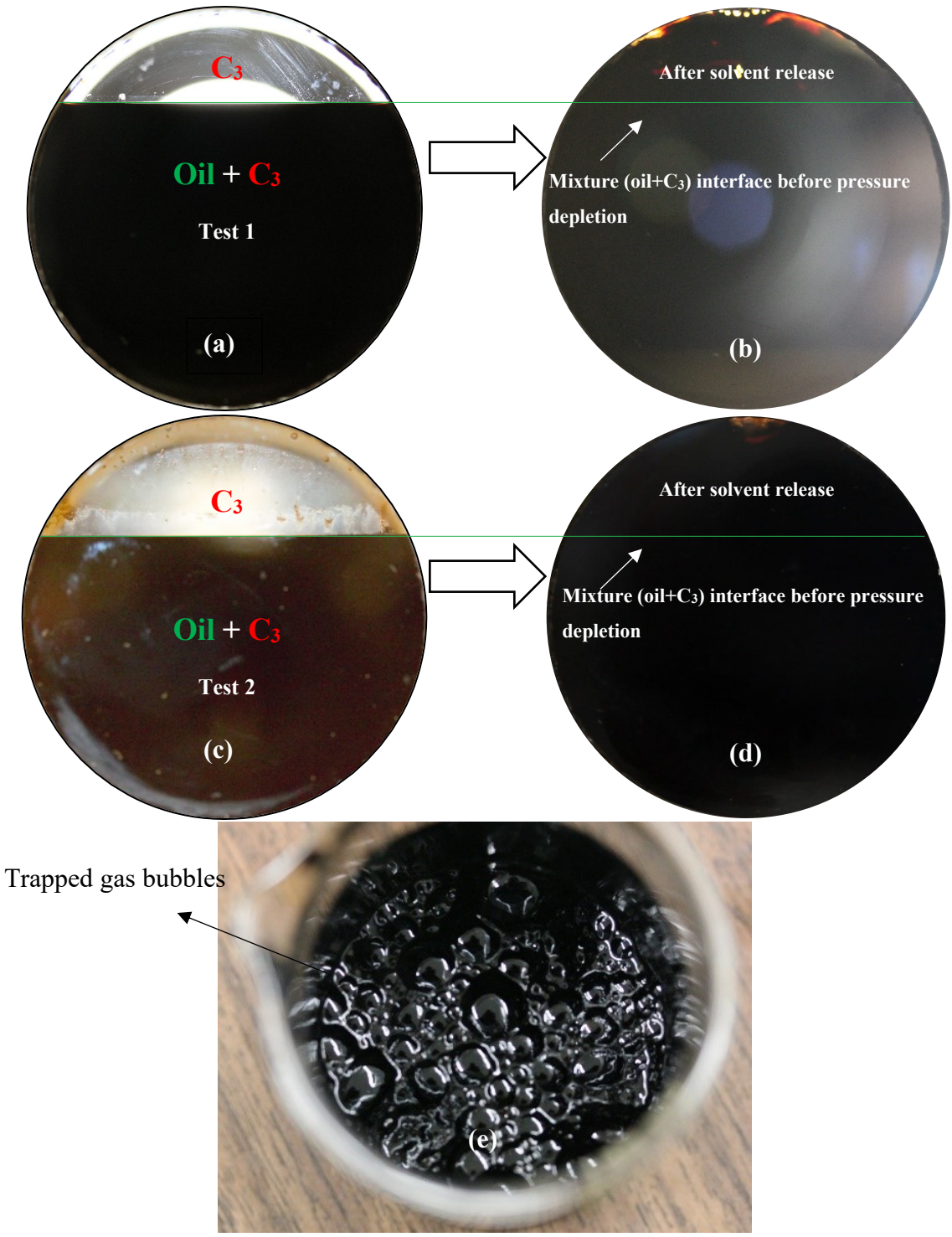

Figure 4-16: Images showing production of foamy oil during rapid pressure depletion. Green line shows level of mixture of C_3 and oil before rapid pressure depletion. (a) Image for test 1 before releasing solvent or depleting pressure. (b) Image for test 1, after pressure depletion bubbles start forming and fills the visual cell completely. (c) Image for test 2, before pressure depletion. (d) after releasing solvent, bubbles start forming resulting in swelling of oil that fill the visual cell completely. (e) Foamy oil collected at room conditions for test 3.

4.3 Summary

In this chapter, we performed three tests to investigate the interactions between $C_{3(l)}$ and heavy oil during soaking process. Test 1 was the base case. Test 2 was conducted at high temperature. Test 3 was conducted with low mass of $C_{3(l)}$. Key observations from this study can be summarized as follows;

1) At equilibrium conditions in all the tests, it was observed that colorless $C_{3(l)}$ completely turns black. This indicates the presence of higher concentration of heavy oil components.

2) During soaking process, large mass of $C_{3(l)}$ (test 1 and test 2) resulted in two stage transformation process i.e. extracting and draining flows in Layer 1 (L_1) are followed by extracting and draining flows Layer 2 (L_2). This continues till the formation of homogenous mixture between C_3 and heavy oil. Whereas, with less mass of $C_{3(l)}$ (test 3), transformation occurs in only one stage.

3) It was also observed that at high temperatures, the transformation of $C_{3(l)}$ from colorless to black occurs at faster rate than at low temperatures.

4) Production of foamy oil is observed during rapid pressure depletion.

Chapter 5: Conclusions and Recommendations

5.1 Conclusions

In this study, diffusion coefficient of propane and butane in heavy oil was measured. Also, a visualization study of interactions between propane and heavy oil during soaking process was done. The following are conclusions from the studies described in this work.

- The pressure decay (PD) technique along with simplified assumption is convenient indirect method to determine diffusion coefficients of gaseous solvents in heavy oil at high temperatures. In addition to this, it can help us identify different stages of diffusion process at high temperatures. Diffusion of gaseous solvents in to heavy oil undergoes three different stages; early region, transition region and late time region at high temperatures. Diffusion coefficients (D) calculated using transition region represents true value of D, therefore, it is important to isolate early and late time region data. Whereas PD technique does not identify stages of diffusion process at low temperatures.

- In early region, heavy oil offers resistance to mass transfer resulting in low diffusion coefficient. In transition region, the resistance offered by heavy oil to solvent diminishes thus resulting in highest diffusion coefficient. Whereas, in late time region the solvent interface has reached the bottom of diffusion cell, this causes low concentration gradient and results in lowest diffusion coefficient.

- As temperature decreases, D decreases and equilibration time increases. This indicates a low diffusion rate of solvent in heavy oil. However, viscosity reduction due to diffusion of solvent is dominant at low temperatures.

- Butane has faster diffusion rate into heavy oil than propane. Butane outperformed propane in terms of heavy oil viscosity reduction and solvent's solubility in heavy oil as well.

- Extraction of heavy oil starts immediately after the injection of liquid propane. This continues till liquid propane and heavy oil develops a uniform phase.

- In liquid propane, diffusivity and gravity control the extracting and draining flows, respectively. As heavy oil extraction starts, heavy oil components rise upwards in liquid propane under the influence of diffusive forces due to concentration gradient. After reaching a certain level in liquid propane, extracted components start accumulating until they are heavy enough to drain downwards under the influence of gravity. The competition between extracting and draining flows continues till the formation of a homogenous phase. The process expedites at high temperatures.

- Mixture of liquid propane and heavy oil results in formation of foamy oil during pressure depletion. Foamy oil production increases the flow rates.

5.2 Recommendations

In this study, we used Zhang's model (Zhang et al., 2000) model to estimate diffusion coefficient. Each assumption in Zhang's model have some effect(s) on the estimated diffusion coefficient. It is important to identify these effects and quantify the error caused by each assumption.

A visual cell is prone to gas leakage. This leakage can be so small and undetectable by gas leak detectors. Developing a mathematical technique to quantify errors due to gas leakage will improve data accuracy from the visual cell.

In this study, we tested bulk diffusion of solvent vapors into oil in the absence of porous systems. Therefore, it is important to develop a mathematical technique to relate diffusion in porous system with diffusion in bulk system.

It is important to compare the results of similar experiments on gas mixtures and pure gases. The effects of asphaltene precipitation on diffusion coefficient is another interesting area to investigate.

The performance of similar visualization study of interactions between heavy oil and solvents (other than liquid propane) is important to determine optimal choice of solvents for hydrocarbon recovery.

Bibliography

Al-Hadhrami, M. (2014). Investigations into Heavy Oil Recovery by Vapour Extraction (VAPEX)

Allen, J.C. 1974. Gaseous solvent heavy oil recovery, Canadian Patent No. 446874, February 28, 1974.

Badamchi Zadeh, A. (2013). Use of CO2 in VAPEX, Experimental and Modeling Study (PhD Dissertation, University of Calgary).

Banerjee, D. K. (2012). Oil sands, heavy oil & bitumen: from recovery to refinery. PennWell Books.

Bayat, A. E., Junin, R., Kharrat, R., & Hejri, S. (2015). Evaluation of vapour extraction process and its prospect as an enhanced oil recovery method. International Journal of Oil, Gas and Coal Technology, 9(4), 394-421.

Bayestehparvin, B., Abedi, J., & Farouq Ali, S. M. (2017, February). Development of a Non-Equilibrium Pore Scale Reservoir Simulator. In SPE Canada Heavy Oil Technical Conference. Society of Petroleum Engineers.

Berkhin, P. (2006). A survey of clustering data mining techniques. In Grouping multidimensional data (pp. 25-71). Springer, Berlin, Heidelberg.

Bosse, D., & Bart, H. J. (2006). Prediction of diffusion coefficients in liquid systems. Industrial & engineering chemistry research, 45(5), 1822-1828.

Boustani, A., Maini, B.B., 2001. The role of diffusion and convective dispersion in vapour extraction process. J. Can. Pet. Technol. 40 (4), 68–77

British Petroleum Statistical Review of World Energy. British Petroleum Corporate Communications Services, London. (2018).

Butler, R. M., & Mokrys, I. J. (1989). Solvent Analog Model of Steam-Assisted.

Butler, R. M. (1991). Thermal recovery of oil and bitumen (Vol. 46). Englewood Cliffs, NJ: Prentice Hall.

Butler, R. M., & Mokrys, I. J. (1991). A new process (VAPEX) for recovering heavy oils using hot water and hydrocarbon vapour. Journal of Canadian Petroleum Technology, 30(01).

Butler, R. M., Mokrys, I. J., & Das, S. K. (1995, January). The solvent requirements for Vapex recovery. In SPE International Heavy Oil Symposium. Society of Petroleum Engineers.

Butler, R. M., & Jiang, Q. (2000). Improved recovery of heavy oil by VAPEX with widely spaced horizontal injectors and producers. Journal of Canadian Petroleum Technology, 39(01).

Chopra, S., Lines, L., Schmitt, D. R., & Batzle, M. (2010). Heavy-Oil Reservoirs: Their Characterization and Production. In Heavy Oils: Reservoir Characterization and Production Monitoring (pp. 1-69). Society of Exploration Geophysicists.

Civan, F., & Rasmussen, M. L. (2001, January). Accurate Measurement of Gas Diffusivity in Oil and Brine under Reservoir Conditions. In SPE production and operations symposium. Society of Petroleum Engineers.

Civan, F. & Rasmussen, M. L. (2006). Determination of Gas Diffusion and Interface-Mass Transfer Coefficients for Quiescent Reservoir Liquids. SPE Journal, 11(01), 71-79.

Crank, J. (1979). The Mathematics of Diffusion. Oxford university press.

Creux, P., Meyer, V., Cordelier, P. R., Franco, F., & Montel, F. (2005, January). Diffusivity in heavy oils. In SPE International Thermal Operations and Heavy Oil Symposium. Society of Petroleum Engineers.

Das, S. (2005). Diffusion and Dispersion in the Simulation of VAPEX Process. Paper SPE 97924 presented at the SPE. PS-CIM/CHOA International Thermal Operations and Heavy Oil Symposium, Calgary, 1-3 November. doi: 10.2118/97924-MS.

Das, S. K., & Butler, R. M. (1995, January). Extraction of heavy oil and bitumen using solvents at reservoir pressure. In Technical meeting/petroleum conference of the South Saskatchewan section. Petroleum Society of Canada.

Das, S. K. & Butler, R. M. (1996, January). Countercurrent Extraction of Heavy Oil and Bitumen. In International Conference on Horizontal Well Technology. Society of Petroleum Engineers.

Das, S. K., & Butler, R. M. (1998). Mechanism of the vapor extraction process for heavy oil and bitumen. Journal of Petroleum Science and Engineering, 21(1-2), 43-59.

Dill, K., & Bromberg, S. (2003). Molecular driving forces: statistical thermodynamics in biology, chemistry, physics, and nanoscience. Garland Science.

Du, F. (2016). An Experimental Study of Carbon Dioxide Dissolution into a Light Crude Oil (Doctoral dissertation, Faculty of Graduate Studies and Research, University of Regina).

Eghbali, S. & Dehghanpour, H. (2017, October). An Experimental and Modeling Study of Solvent-Bitumen Phase Behavior at Elevated Temperatures Using Cold Lake Bitumen. In SPE Annual Technical Conference and Exhibition. Society of Petroleum Engineers.

Eghbali, S., Dehghanpour, H., Dragani, J., Zhang, X., (2018, March). Phase Behaviour and Viscosity of Bitumen-CO2/Light Hydrocarbon Mixtures at Elevated Temperatures: A Cold Lake Case Study, In SPE Canada Heavy Oil Technical Conference. Society of Petroleum Engineers.

Einstein, A. (1905). On the motion of small particles suspended in liquids at rest required by the molecular-kinetic theory of heat. Annalen der physik, 17, 549-560.

Etminan, S. R., Maini, B. B., Hassanzadeh, H., & Chen, Z. J. (2009, January). Determination of Concentration Dependent Diffusivity Coefficient in Solvent Gas Heavy Oil Systems. In SPE Annual Technical Conference and Exhibition. Society of Petroleum Engineers.

Etminan, S. R., Maini, B. B., Chen, Z., & Hassanzadeh, H. (2010). Constant-pressure technique for gas diffusivity and solubility measurements in heavy oil and bitumen. Energy & Fuels, 24(1), 533-549.

Etminan, S. R., Haghighat, P., Maini, B. B., & Chen, Z. J. (2011, January). Molecular diffusion and dispersion coefficient in a propane-bitumen system: case of vapour extraction (VAPEX) process. In SPE Europec/EAGE annual conference and exhibition. Society of Petroleum Engineers.

Etminan, S. R., Javadpour, F., Maini, B. B., & Chen, Z. (2014). Measurement of gas storage processes in shale and of the molecular diffusion coefficient in kerogen. International Journal of Coal Geology, 123, 10-19.

Energy Resources Conservation Board. (2009). Alberta's energy reserves 2008 and supply/demand outlook 2009–2018. Energy Resources Conservation Board, Statistical Series, ST98–2009.

Fick, A. (1855). Ueber diffusion. Annalen der Physik, 170(1), 59-86.

Fourier, J. (1822). Theorie analytique de la chaleur, par M. Fourier. Chez Firmin Didot, père et fils.

Ghanavati, M., Hassanzadeh, H., & Abedi, J. (2014). Application of taylor dispersion technique to measure mutual diffusion coefficient in hexane+ bitumen system. AIChE Journal, 60(7), 2670-2682.

Guerrero Aconcha, U. E., & Kantzas, A. (2009, January). Diffusion of Hydrocarbon Gases in Heavy Oil and Bitumen. In Latin American and Caribbean Petroleum Engineering Conference. Society of Petroleum Engineers.

Gu, Y. P. Measurement of Solvent Diffusivity in Heavy Oil and Evaluation of Solvent-Based Recovery Processes.

Guo, K., Li, H., & Yu, Z. (2016). In-situ heavy and extra-heavy oil recovery: A review. Fuel, 185, 886-902.

Hart, A. (2014). Advanced studies of catalytic upgrading of heavy oils (Doctoral dissertation, University of Birmingham).

Hartley, G. S., & Crank, J. (1949). Some Fundamental Definitions and Concepts in Diffusion Processes. Transactions of the Faraday Society, 45, 801-818.

Handy, L. L. (1959). An Evaluation of Diffusion Effects in Miscible Displacement. Journal of Petroleum Technology, 11(03), 61-63.

Henry, W. (1803). "Experiments on the quantity of gases absorbed by water, at different temperatures, and under different pressures". Phil. Trans. R. Soc. Lond. 93: 29–274.

Hosseini Pour, A., Azin, R., & Yunan, M. (2011, January). Comprehensive study to determine optimum solvent composition for VAPEX in a heavy oil reservoir. In SPE Enhanced Oil Recovery Conference. Society of Petroleum Engineers.

Jamialahmadi, M., Emadi, M., & Müller-Steinhagen, H. (2006). Diffusion coefficients of methane in liquid hydrocarbons at high pressure and temperature. Journal of Petroleum Science and Engineering, 53(1-2), 47-60.

Jiang, T., Zeng, F., Jia, X., & Gu, Y. (2014). A new solvent-based enhanced heavy oil recovery method: Cyclic production with continuous solvent injection. Fuel, 115, 426-433.

Karmaker, K., & Maini, B. B. (2003, January). Applicability of vapor extraction process to problematic viscous oil reservoirs. In SPE Annual Technical Conference and Exhibition. Society of Petroleum Engineers.

Kok, M. V., & Acar, C. (2007). Feasibility study of heavy oil field. Energy Sources, Part A: Recovery, Utilization, and Environmental Effects, 30(3), 189-199.

Luhning, R. W., Das, S. K., Fisher, L. J., Bakker, J., Grabowski, J., Engleman, J. R., ... & Boyle, H. A. (2003). Full scale VAPEX process-climate change advantage and economic consequences A. Journal of Canadian Petroleum Technology, 42(02).

Maini, B. B., & Busahmin, B. (2010, May). Foamy oil flow and its role in heavy oil production. In AIP Conference Proceedings (Vol. 1254, No. 1, pp. 103-108). AIP.

Mehrotra, A. K., & Svrcek, W. Y. (1986). Viscosity of Compressed Athabasca Bitumen. The Canadian Journal of Chemical Engineering, 64(5), 844-847.

Moghadam, S., Nobakht, M., & Gu, Y. (2009). Theoretical and physical modeling of a solvent vapour extraction (VAPEX) process for heavy oil recovery. Journal of Petroleum Science and Engineering, 65(1-2), 93-104.

Mokrys, I. J., & Butler, R. M. (1993). The rise of interfering solvent chambers: solvent analog model of steam-assisted gravity drainage. Journal of Canadian Petroleum Technology, 32(03).

Nguyen, T. A., & Ali, S. M. (1998). Effect of nitrogen on the solubility and diffusivity of carbon dioxide into oil and oil recovery by the immiscible WAG process. Journal of Canadian Petroleum Technology, 37(02).

Okazawa, T., 2007. Impacts of concentration dependence of diffusion coefficient on VAPEX drainage rates. The 8th Canadian International Petroleum Conference. Calgary, Alberta. Paper No. 2007–170.

Pathak, V., Babadagli, T., & Edmunds, N. (2012). Mechanics of heavy-oil and bitumen recovery by hot solvent injection. SPE Reservoir Evaluation & Engineering, 15(02), 182-194.

Pacheco-Roman, F. J., & Hejazi, S. H. (2015). Estimation of Solubility and Diffusivity of Gases in Heavy Oils by Use of Late-Time Pressure-Decay Data: An Analytical/Graphical Approach. SPE Journal.

Pourabdollah, K., & Mokhtari, B. (2013). The VAPEX process, from beginning up to date. Fuel, 107, 1-33.

Rasmussen, M. L., & Civan, F. (2009). Parameters of Gas Dissolution in Liquids Obtained by Isothermal Pressure Decay. AIChE journal, 55(1), 9-23.

Ramakrishnan, V. (2003). In-situ recovery of heavy oil by VAPEX using propane (Doctoral dissertation, University of Waterloo).

Ratnakar, R. R., & Dindoruk, B. (2015). Measurement of gas diffusivity in heavy oils and bitumens by use of pressure-decay test and establishment of minimum time criteria for experiments. SPE Journal, 20(05), 1-167.

Riazi, M. R. (1996). A new method for experimental measurement of diffusion coefficients in reservoir fluids. Journal of Petroleum Science and Engineering, 14(3-4), 235-250.

Riazi, M. R., & Whitson, C. H. (1993). Estimating diffusion coefficients of dense fluids. Industrial & engineering chemistry research, 32(12), 3081-3088.

Roman, P., Javier, F., & Hejazi, S. H. (2014, October). Graphical Determination of the Henry's Constant and the Diffusion Coefficient of Gases in Heavy Oils Using Late-Time Pressure-Decay Data. In SPE Annual Technical Conference and Exhibition. Society of Petroleum Engineers.

Roman, P., & Javier, F. (2015). Estimation of Mass Transfer Parameters of Gaseous Solvents in Heavy Oils Using the Pressure-Decay Technique (Doctoral dissertation, University of Calgary).

Roopa, I., & Dawe, R. A. (2007). VAPEX—Gravity-assisted film drainage for heavy oil recovery. Petroleum science and technology, 25(5), 645-658

Sachs, W. (1998). The diffusional transport of methane in liquid water: method and result of experimental investigation at elevated pressure. Journal of Petroleum Science and Engineering, 21(3), 153-164.

Schmidt, T. (1989). Mass transfer by diffusion. AOSTRA Handbook on Oil Sands, Bitumens and Heavy Oils.

Shah A, Fishwick R, Wood J, Leeke G, Rigby S, Greaves M. A review of novel techniques for heavy oil and bitumen extraction and upgrading. Energy Environ. Sci. 2010;3(6):700–14.

Sheikha, H., Pooladi-Darvish, M., & Mehrotra, A. K. (2005). Development of graphical methods for estimating the diffusivity coefficient of gases in bitumen from pressure-decay data. Energy & fuels, 19(5), 2041-2049.

Sheikha, H., Mehrotra, A. K., & Pooladi-Darvish, M. (2006). An inverse solution methodology for estimating the diffusion coefficient of gases in Athabasca bitumen from pressure-decay data. Journal of Petroleum Science and Engineering, 53(3-4), 189-202.

Shuler, P. J., Tang, Y., & Tang, H. (2010, January). Heavy oil production enhancement by viscosity reduction. In SPE Western Regional Meeting. Society of Petroleum Engineers.

Singhal, A. K., Das, S. K., Leggitt, S. M., Kasraie, M., & Ito, Y. (1996). Screening of Reservoirs For Exploitation by Application of Steam Assisted Gravity Drainage/Vapex Processes. Paper SPE 37144 presented at the International Conference on Horizontal Well Technology, Calgary, 18-20November.

Tyrrell, H. J. V. (1964). The origin and present status of Fick's diffusion law. Journal of chemical education, 41(7), 397.

Tharanivasan, A. K., Yang, C., & Gu, Y. (2006). Measurements of Molecular Diffusion Coefficients of Carbon Dioxide, Methane, and Propane in Heavy Oil under Reservoir Conditions. Energy & Fuels, 20(6), 2509-2517.

Thomas S, Farouq Ali SM. Status and assessment of chemical oil recovery methods. Energy Sources 1999;21(1–2):177–89.

Upreti, S. R., & Mehrotra, A. K. (2000). Experimental measurement of gas diffusivity in bitumen: results for carbon dioxide. Industrial & engineering chemistry research, 39(4), 1080-1087.

Upreti, S. R., & Mehrotra, A. K. (2002). Diffusivity of CO2, CH4, C2H6 and N2 in Athabasca bitumen. The Canadian Journal of Chemical Engineering, 80(1), 116-125.

Vargas-Vasquez, S. M., & Romero-Zeron, L. B. (2007). The vapor extraction process. Petroleum Science and Technology, 25(11), 1447-1463.

World Economic Outlook, 2017

Yang, C., & Gu, Y. (2005). New experimental method for measuring gas diffusivity in heavy oil by the dynamic pendant drop volume analysis (DPDVA). Industrial & engineering chemistry research, 44(12), 4474-4483.

Yang, C., & Gu, Y. (2006). A new method for measuring solvent diffusivity in heavy oil by dynamic pendant drop shape analysis (DPDSA). SPE journal, 11(01), 48-57.

Yazdani, A., & Maini, B. B. (2005). Effect of height and grain size on the production rates in the VAPEX process: experimental study. SPE Reservoir Evaluation & Engineering, 8(03), 205-213.

Yazdani, A., & Maini, B. B. (2007, January). Measurements and Modelling of Phase Behaviour and Viscosity of a Heavy Oil-Butane System. In Canadian International Petroleum Conference. Petroleum Society of Canada.

Yazdani, A., & Maini, B. (2009). The effective diffusion/dispersion coefficient in vapor extraction of heavy oil. Petroleum Science and Technology, 27(8), 817-835.

Zainal, S., Hon, V. Y., Saaid, I. M., & Jelani, J. (2009, January). An Evaluation of Gas Diffusivity Measurement in Reservoir Fluid from Low to High Pressure Systems for Oil Recovery Applications. In International Petroleum Technology Conference. International Petroleum Technology Conference.

Zamanian, E., Hemmati, M., & Beiranvand, M. S. (2012). Determination of gas-diffusion and interface-mass-transfer coefficients in fracture-heavy oil saturated porous matrix system. Nafta, 63

Zhang, Y. P., Hyndman, C. L., & Maini, B. B. (2000). Measurement of Gas Diffusivity in Heavy Oils. Journal of Petroleum Science and Engineering, 25(1), 37-47.

Zhou, X., Zeng, F., Zhang, L., & Wang, H. (2016). Foamy oil flow in heavy oil–solvent systems tested by pressure depletion in a sand pack. Fuel, 171, 210-223.

Appendix A: Pressure Decline Data

Pressure Decline Data
T = 130°C, $C_{3(g)}$-heavy oil

Time (s)	Time (hr)	Time (Corrected)	P (psig)
1153	0.320278	0	270.8733
2053	0.570278	0.25	264.4876
2953	0.820278	0.5	263.2105
3853	1.070278	0.75	260.0176
4753	1.320278	1	257.4634
5653	1.570278	1.25	253.6319
6553	1.820278	1.5	249.162
7453	2.070278	1.75	249.8005
8353	2.320278	2	246.6077
9253	2.570278	2.25	241.4991
10153	2.820278	2.5	244.0534
11053	3.070278	2.75	238.3063
11953	3.320278	3	236.3906
12853	3.570278	3.25	237.6677
13753	3.820278	3.5	235.1135
14653	4.070278	3.75	232.5592
15553	4.320278	4	230.0049
16453	4.570278	4.25	227.4506
17353	4.820278	4.5	225.5349
18253	5.070278	4.75	226.8121
19153	5.320278	5	220.4264
20053	5.570278	5.25	221.0649
20953	5.820278	5.5	221.7035
21853	6.070278	5.75	220.4264
22753	6.320278	6	220.4264
23653	6.570278	6.25	216.595
24553	6.820278	6.5	210.2093
25453	7.070278	6.75	211.4864
26353	7.320278	7	214.0407
27253	7.570278	7.25	208.2936
28153	7.820278	7.5	205.7393
29053	8.070278	7.75	207.0164
29953	8.320278	8	203.8236
30853	8.570278	8.25	205.7393
31753	8.820278	8.5	203.8236
32653	9.070278	8.75	195.5222
33553	9.320278	9	194.2451
34453	9.570278	9.25	192.3294
35353	9.820278	9.5	194.2451
36253	10.07028	9.75	191.6908
37153	10.32028	10	186.5822
38053	10.57028	10.25	185.9437
38953	10.82028	10.5	181.4737
39853	11.07028	10.75	184.6665
40753	11.32028	11	181.4737
41653	11.57028	11.25	177.0037
42553	11.82028	11.5	177.6423
43453	12.07028	11.75	177.0037
44353	12.32028	12	176.3651
45253	12.57028	12.25	173.8109
46153	12.82028	12.5	170.618
47053	13.07028	12.75	171.2566
47953	13.32028	13	171.2566
48853	13.57028	13.25	166.148
49753	13.82028	13.5	162.3166
50653	14.07028	13.75	164.8709
51553	14.32028	14	162.9552
52453	14.57028	14.25	162.9552
53353	14.82028	14.5	159.1238
54253	15.07028	14.75	159.1238
55153	15.32028	15	157.8467
56053	15.57028	15.25	159.1238
56953	15.82028	15.5	155.2924
57853	16.07028	15.75	153.3767
58753	16.32028	16	155.9309
59653	16.57028	16.25	155.9309
60553	16.82028	16.5	149.5453
61453	17.07028	16.75	152.7381
62353	17.32028	17	154.0152
63253	17.57028	17.25	148.2681

Time (s)	Time (hr)	Time (Corrected)	P (psig)
64153	17.82028	17.5	150.8224
65053	18.07028	17.75	149.5453
65953	18.32028	18	148.2681
66853	18.57028	18.25	150.1838
67753	18.82028	18.5	150.1838
68653	19.07028	18.75	150.8224
69553	19.32028	19	148.9067
70453	19.57028	19.25	145.7138
71353	19.82028	19.5	149.5453
72253	20.07028	19.75	147.6296
73153	20.32028	20	145.0753
74053	20.57028	20.25	148.2681
74953	20.82028	20.5	148.9067
75853	21.07028	20.75	148.2681
76753	21.32028	21	145.7138
77653	21.57028	21.25	143.7981
78553	21.82028	21.5	146.991
79453	22.07028	21.75	147.6296
80353	22.32028	22	146.3524
81253	22.57028	22.25	149.5453
82153	22.82028	22.5	145.0753
83053	23.07028	22.75	145.7138
83953	23.32028	23	145.0753
84853	23.57028	23.25	143.7981
85753	23.82028	23.5	146.3524
86653	24.07028	23.75	145.0753
87553	24.32028	24	140.6053
91153	25.32028	25	149.5453
94753	26.32028	26	145.0753
98353	27.32028	27	144.4367
101953	28.32028	28	143.7981

Time (s)	Time (hr)	Time (Corrected)	P (psig)
105553	29.32028	29	145.7138
109153	30.32028	30	147.6296
112753	31.32028	31	145.7138
116353	32.32028	32	143.1596
119953	33.32028	33	148.2681
123553	34.32028	34	144.4367
127153	35.32028	35	145.0753
130753	36.32028	36	145.7138
134353	37.32028	37	146.3524
137953	38.32028	38	140.6053
141553	39.32028	39	143.7981
145153	40.32028	40	145.0753
148753	41.32028	41	145.0753
152353	42.32028	42	143.7981
155953	43.32028	43	139.9667
159553	44.32028	44	139.9667
163153	45.32028	45	141.8824
166753	46.32028	46	143.7981
170353	47.32028	47	142.521
173953	48.32028	48	143.1596
177553	49.32028	49	143.1596
181153	50.32028	50	139.3282
184753	51.32028	51	143.1596
188353	52.32028	52	138.051
191953	53.32028	53	144.4367
195553	54.32028	54	140.6053
199153	55.32028	55	138.6896
202753	56.32028	56	143.1596
206353	57.32028	57	139.9667
209953	58.32028	58	141.8824
213553	59.32028	59	139.9667
217153	60.32028	60	141.8824
253153	70.32028	70	139.3282

Pressure Decline Data
T = 100°C, $C_{3(g)}$-heavy oil

Time (s)	Time (hr)	Time (Corrected)	P (psig)
799	0.221944	0	275.9818
1699	0.471944	0.25	268.319
2599	0.721944	0.5	266.4033
3499	0.971944	0.75	262.5719
4399	1.221944	1	261.2948
5299	1.471944	1.25	253.6319
6199	1.721944	1.5	251.7162
7099	1.971944	1.75	248.5234
7999	2.221944	2	245.3306
8899	2.471944	2.25	242.7763
9799	2.721944	2.5	237.0292
10699	2.971944	2.75	237.0292
11599	3.221944	3	233.1977
12499	3.471944	3.25	231.282
13399	3.721944	3.5	229.3663
14299	3.971944	3.75	230.0049
15199	4.221944	4	224.2578
16099	4.471944	4.25	224.2578
16999	4.721944	4.5	222.9806
17899	4.971944	4.75	219.7878
18799	5.221944	5	219.7878
19699	5.471944	5.25	214.6793
20599	5.721944	5.5	215.3178
21499	5.971944	5.75	212.125
22399	6.221944	6	211.4864
23299	6.471944	6.25	208.9321
24199	6.721944	6.5	211.4864
25099	6.971944	6.75	207.0164
25999	7.221944	7	207.655
26899	7.471944	7.25	205.7393
27799	7.721944	7.5	204.4622
28699	7.971944	7.75	202.5465
29599	8.221944	8	201.9079
30499	8.471944	8.25	201.2693
31399	8.721944	8.5	198.715
32299	8.971944	8.75	196.1608
33199	9.221944	9	196.1608
34099	9.471944	9.25	194.2451
34999	9.721944	9.5	194.8836
35899	9.971944	9.75	194.2451
36799	10.22194	10	191.0522
37699	10.47194	10.25	191.6908
38599	10.72194	10.5	189.7751
39499	10.97194	10.75	185.9437
40399	11.22194	11	186.5822
41299	11.47194	11.25	184.6665
42199	11.72194	11.5	184.6665
43099	11.97194	11.75	181.4737
43999	12.22194	12	182.7508
44899	12.47194	12.25	182.1123
45799	12.72194	12.5	179.558
46699	12.97194	12.75	178.9194
47599	13.22194	13	175.7266
48499	13.47194	13.25	178.2808
49399	13.72194	13.5	174.4494
50299	13.97194	13.75	173.8109
51199	14.22194	14	173.8109
52099	14.47194	14.25	171.2566
52999	14.72194	14.5	171.2566
53899	14.97194	14.75	167.4252
54799	15.22194	15	167.4252
55699	15.47194	15.25	166.148
56599	15.72194	15.5	164.2323
57499	15.97194	15.75	164.8709
58399	16.22194	16	162.3166
59299	16.47194	16.25	161.0395
60199	16.72194	16.5	157.8467
61099	16.97194	16.75	159.7624
61999	17.22194	17	156.5695
62899	17.47194	17.25	155.9309
63799	17.72194	17.5	152.0995
64699	17.97194	17.75	150.8224
65599	18.22194	18	153.3767
66499	18.47194	18.25	150.8224
67399	18.72194	18.5	148.9067
68299	18.97194	18.75	145.0753
69199	19.22194	19	145.7138

Time (s)	Time (hr)	Time (Corrected)	P (psig)
70099	19.47194	19.25	146.3524
70999	19.72194	19.5	141.8824
71899	19.97194	19.75	140.6053
72799	20.22194	20	140.6053
73699	20.47194	20.25	140.6053
74599	20.72194	20.5	139.3282
75499	20.97194	20.75	138.051
76399	21.22194	21	138.051
77299	21.47194	21.25	137.4125
78199	21.72194	21.5	135.4968
79099	21.97194	21.75	136.7739
79999	22.22194	22	135.4968
80899	22.47194	22.25	131.6653
81799	22.72194	22.5	132.3039
82699	22.97194	22.75	129.7496
83599	23.22194	23	131.6653
84499	23.47194	23.25	129.1111
85399	23.72194	23.5	127.8339
86299	23.97194	23.75	127.1954
87199	24.22194	24	127.1954
88099	24.47194	24.25	124.6411
88999	24.72194	24.5	124.6411
89899	24.97194	24.75	124.6411
90799	25.22194	25	124.6411
91699	25.47194	25.25	120.1711
92599	25.72194	25.5	122.7254
93499	25.97194	25.75	120.8097
94399	26.22194	26	121.4482
95299	26.47194	26.25	122.0868
96199	26.72194	26.5	120.1711
97099	26.97194	26.75	122.0868
97999	27.22194	27	120.8097
98899	27.47194	27.25	120.1711
99799	27.72194	27.5	118.2554
100699	27.97194	27.75	118.2554
101599	28.22194	28	116.3397
102499	28.47194	28.25	115.7011
103399	28.72194	28.5	116.9783
104299	28.97194	28.75	118.2554
105199	29.22194	29	116.3397
106099	29.47194	29.25	117.6168

Time (s)	Time (hr)	Time (Corrected)	P (psig)
106999	29.72194	29.5	116.9783
107899	29.97194	29.75	116.9783
108799	30.22194	30	113.7854
109699	30.47194	30.25	112.5083
110599	30.72194	30.5	114.424
111499	30.97194	30.75	113.1468
112399	31.22194	31	112.5083
113299	31.47194	31.25	112.5083
114199	31.72194	31.5	112.5083
115099	31.97194	31.75	114.424
115999	32.22194	32	112.5083
116899	32.47194	32.25	111.8697
117799	32.72194	32.5	112.5083
118699	32.97194	32.75	114.424
119599	33.22194	33	112.5083
120499	33.47194	33.25	112.5083
121399	33.72194	33.5	114.424
122299	33.97194	33.75	113.7854
123199	34.22194	34	112.5083
124099	34.47194	34.25	112.5083
124999	34.72194	34.5	111.2311
125899	34.97194	34.75	112.5083
126799	35.22194	35	113.1468
127699	35.47194	35.25	111.8697
128599	35.72194	35.5	111.2311
129499	35.97194	35.75	113.1468
130399	36.22194	36	109.3154
131299	36.47194	36.25	111.2311
132199	36.72194	36.5	109.954
133099	36.97194	36.75	111.2311
133999	37.22194	37	111.8697
134899	37.47194	37.25	111.8697
135799	37.72194	37.5	111.8697
136699	37.97194	37.75	111.2311
137599	38.22194	38	111.2311
138499	38.47194	38.25	111.2311
139399	38.72194	38.5	108.6769
140299	38.97194	38.75	110.5926
141199	39.22194	39	109.954
142099	39.47194	39.25	109.954
142999	39.72194	39.5	110.5926

Time (s)	Time (hr)	Time (Corrected)	P (psig)
143899	39.97194	39.75	110.5926
144799	40.22194	40	109.954
145699	40.47194	40.25	109.3154
146599	40.72194	40.5	110.5926
147499	40.97194	40.75	111.2311
148399	41.22194	41	108.0383
149299	41.47194	41.25	109.954
150199	41.72194	41.5	108.0383
151099	41.97194	41.75	109.954
151999	42.22194	42	109.3154
152899	42.47194	42.25	111.2311
153799	42.72194	42.5	110.5926
154699	42.97194	42.75	108.0383
155599	43.22194	43	108.6769
156499	43.47194	43.25	106.7612
157399	43.72194	43.5	108.6769
158299	43.97194	43.75	109.3154
159199	44.22194	44	109.954
160099	44.47194	44.25	108.0383
160999	44.72194	44.5	108.6769
161899	44.97194	44.75	110.5926
162799	45.22194	45	107.3997
163699	45.47194	45.25	109.3154
164599	45.72194	45.5	109.954
165499	45.97194	45.75	108.0383
166399	46.22194	46	109.954
167299	46.47194	46.25	108.0383
168199	46.72194	46.5	109.954
169099	46.97194	46.75	108.0383
169999	47.22194	47	109.3154
170899	47.47194	47.25	108.0383
171799	47.72194	47.5	107.3997
172699	47.97194	47.75	109.3154
173599	48.22194	48	108.0383
174499	48.47194	48.25	109.3154
175399	48.72194	48.5	107.3997
176299	48.97194	48.75	109.3154
177199	49.22194	49	107.3997
178099	49.47194	49.25	106.7612
178999	49.72194	49.5	108.6769
179899	49.97194	49.75	106.7612
180799	50.22194	50	107.3997
181699	50.47194	50.25	108.6769
182599	50.72194	50.5	107.3997
183499	50.97194	50.75	108.0383
184399	51.22194	51	108.0383
185299	51.47194	51.25	107.3997
186199	51.72194	51.5	107.3997
187099	51.97194	51.75	108.6769
187999	52.22194	52	104.8455
188899	52.47194	52.25	106.7612
189799	52.72194	52.5	107.3997
190699	52.97194	52.75	106.7612
191599	53.22194	53	107.3997
192499	53.47194	53.25	106.1226
193399	53.72194	53.5	106.7612
194299	53.97194	53.75	106.7612
195199	54.22194	54	104.8455
196099	54.47194	54.25	104.8455
196999	54.72194	54.5	104.8455
197899	54.97194	54.75	104.8455
198799	55.22194	55	104.2069
199699	55.47194	55.25	105.484
200599	55.72194	55.5	105.484
201499	55.97194	55.75	105.484
202399	56.22194	56	107.3997
203299	56.47194	56.25	103.5683
204199	56.72194	56.5	106.1226
205099	56.97194	56.75	106.1226
205999	57.22194	57	106.7612
206899	57.47194	57.25	106.1226
207799	57.72194	57.5	106.7612
208699	57.97194	57.75	103.5683
209599	58.22194	58	103.5683
210499	58.47194	58.25	105.484
211399	58.72194	58.5	103.5683
212299	58.97194	58.75	103.5683
213199	59.22194	59	105.484
214099	59.47194	59.25	102.9298
214999	59.72194	59.5	106.1226
215899	59.97194	59.75	104.8455
216799	60.22194	60	106.1226

Time (s)	Time (hr)	Time (Corrected)	P (psig)
217699	60.47194	60.25	102.9298
218599	60.72194	60.5	104.2069
219499	60.97194	60.75	105.484
220399	61.22194	61	105.484
221299	61.47194	61.25	104.2069
222199	61.72194	61.5	106.1226
223099	61.97194	61.75	102.9298
223999	62.22194	62	104.2069
224899	62.47194	62.25	102.9298
225799	62.72194	62.5	102.2912
226699	62.97194	62.75	102.9298
227599	63.22194	63	104.8455
228499	63.47194	63.25	106.1226
229399	63.72194	63.5	103.5683
230299	63.97194	63.75	103.5683
231199	64.22194	64	104.8455
232099	64.47194	64.25	101.6526
232999	64.72194	64.5	101.6526
233899	64.97194	64.75	102.2912
234799	65.22194	65	102.2912
235699	65.47194	65.25	101.6526
236599	65.72194	65.5	103.5683
237499	65.97194	65.75	102.9298
238399	66.22194	66	104.2069
239299	66.47194	66.25	101.6526
240199	66.72194	66.5	104.8455
241099	66.97194	66.75	102.2912
241999	67.22194	67	104.8455
242899	67.47194	67.25	100.3755
243799	67.72194	67.5	102.2912
244699	67.97194	67.75	104.2069
245599	68.22194	68	104.8455
246499	68.47194	68.25	102.9298
247399	68.72194	68.5	101.6526
248299	68.97194	68.75	102.9298
249199	69.22194	69	101.014
250099	69.47194	69.25	102.9298
250999	69.72194	69.5	100.3755
251899	69.97194	69.75	101.6526
252799	70.22194	70	101.014
253699	70.47194	70.25	100.3755
254599	70.72194	70.5	102.2912
255499	70.97194	70.75	102.2912
256399	71.22194	71	100.3755
257299	71.47194	71.25	101.6526
258199	71.72194	71.5	103.5683
259099	71.97194	71.75	101.6526
259999	72.22194	72	101.014
260899	72.47194	72.25	102.9298
261799	72.72194	72.5	101.6526
262699	72.97194	72.75	99.09834
263599	73.22194	73	99.73691
264499	73.47194	73.25	102.2912
265399	73.72194	73.5	101.014
266299	73.97194	73.75	101.6526
267199	74.22194	74	101.6526
268099	74.47194	74.25	101.6526
268999	74.72194	74.5	101.6526
269899	74.97194	74.75	101.6526
270799	75.22194	75	100.3755
271699	75.47194	75.25	101.6526
272599	75.72194	75.5	99.73691
273499	75.97194	75.75	100.3755
274399	76.22194	76	101.014
276199	76.72194	76.5	101.014
277099	76.97194	76.75	101.014
277999	77.22194	77	101.014
278899	77.47194	77.25	101.014
279799	77.72194	77.5	100.3755
280699	77.97194	77.75	101.6526
281599	78.22194	78	101.014
282499	78.47194	78.25	99.09834
283399	78.72194	78.5	101.6526
286099	79.47194	79.25	99.73691
287899	79.97194	79.75	99.73691
288799	80.22194	80	100.3755
290599	80.72194	80.5	101.014
291499	80.97194	80.75	99.09834
293299	81.47194	81.25	99.73691
294199	81.72194	81.5	99.73691
295099	81.97194	81.75	99.73691
295999	82.22194	82	99.73691

Time (s)	Time (hr)	Time (Corrected)	P (psig)
296899	82.47194	82.25	99.73691
297799	82.72194	82.5	99.09834
298699	82.97194	82.75	101.014
299599	83.22194	83	99.09834
300499	83.47194	83.25	99.09834
301399	83.72194	83.5	99.09834
302299	83.97194	83.75	100.3755
303199	84.22194	84	99.73691
305899	84.97194	84.75	99.73691
308599	85.72194	85.5	100.3755
312199	86.72194	86.5	99.73691
313099	86.97194	86.75	99.73691
313999	87.22194	87	99.09834
314899	87.47194	87.25	99.73691

Pressure Decline Data
T = 85°C, $C_{3(g)}$-heavy oil

Time (s)	Time (hr)	Time (Corrected)	P (psig)
1616	0.448889	0	287.4761
2516	0.698889	0.25	282.3675
3416	0.948889	0.5	283.0061
4316	1.198889	0.75	281.0904
5216	1.448889	1	275.3433
6116	1.698889	1.25	272.789
7016	1.948889	1.5	271.5119
7916	2.198889	1.75	268.319
8816	2.448889	2	264.4876
9716	2.698889	2.25	263.2105
10616	2.948889	2.5	260.6562
11516	3.198889	2.75	257.4634
12416	3.448889	3	258.7405
13316	3.698889	3.25	256.1862
14216	3.948889	3.5	254.2705
15116	4.198889	3.75	254.2705
16016	4.448889	4	251.0777
16916	4.698889	4.25	249.8005
17816	4.948889	4.5	249.162
18716	5.198889	4.75	249.162
19616	5.448889	5	245.3306
20516	5.698889	5.25	245.3306
21416	5.948889	5.5	244.692
22316	6.198889	5.75	242.7763
23216	6.448889	6	242.7763
24116	6.698889	6.25	242.1377
25016	6.948889	6.5	241.4991
25916	7.198889	6.75	239.5834
26816	7.448889	7	240.8606
27716	7.698889	7.25	237.6677
28616	7.948889	7.5	237.0292
29516	8.198889	7.75	235.752
30416	8.448889	8	233.8363
31316	8.698889	8.25	235.1135
32216	8.948889	8.5	234.4749
33116	9.198889	8.75	231.282
34016	9.448889	9	230.6435
34916	9.698889	9.25	231.9206
35816	9.948889	9.5	231.282
36716	10.19889	9.75	228.0892
37616	10.44889	10	227.4506
38516	10.69889	10.25	227.4506
39416	10.94889	10.5	227.4506
40316	11.19889	10.75	224.8964
41216	11.44889	11	223.6192
42116	11.69889	11.25	226.1735
43016	11.94889	11.5	224.2578
43916	12.19889	11.75	224.8964
44816	12.44889	12	224.8964
45716	12.69889	12.25	220.4264
46616	12.94889	12.5	221.0649
47516	13.19889	12.75	221.7035
48416	13.44889	13	219.7878
49316	13.69889	13.25	219.7878
50216	13.94889	13.5	219.7878
51116	14.19889	13.75	217.8721
52016	14.44889	14	216.595
52916	14.69889	14.25	219.1492
53816	14.94889	14.5	214.6793
54716	15.19889	14.75	216.595
55616	15.44889	15	215.9564
56516	15.69889	15.25	214.6793
57416	15.94889	15.5	214.6793
58316	16.19889	15.75	215.9564
59216	16.44889	16	212.125
60116	16.69889	16.25	214.0407
61016	16.94889	16.5	212.7636
61916	17.19889	16.75	211.4864
62816	17.44889	17	212.7636
63716	17.69889	17.25	213.4021
64616	17.94889	17.5	210.2093
65516	18.19889	17.75	211.4864
66416	18.44889	18	208.9321
67316	18.69889	18.25	211.4864
68216	18.94889	18.5	207.0164
69116	19.19889	18.75	208.9321
70016	19.44889	19	208.9321

Time (s)	Time (hr)	Time (Corrected)	P (psig)
70916	19.69889	19.25	208.2936
71816	19.94889	19.5	207.655
72716	20.19889	19.75	208.2936
73616	20.44889	20	208.2936
74516	20.69889	20.25	206.3779
75416	20.94889	20.5	204.4622
76316	21.19889	20.75	205.7393
77216	21.44889	21	204.4622
78116	21.69889	21.25	205.7393
79016	21.94889	21.5	204.4622
79916	22.19889	21.75	206.3779
80816	22.44889	22	201.9079
81716	22.69889	22.25	203.8236
82616	22.94889	22.5	201.9079
83516	23.19889	22.75	203.8236
84416	23.44889	23	203.8236
85316	23.69889	23.25	203.185
86216	23.94889	23.5	199.3536
87116	24.19889	23.75	199.3536
88016	24.44889	24	201.9079
88916	24.69889	24.25	199.3536
89816	24.94889	24.5	198.715
90716	25.19889	24.75	198.715
91616	25.44889	25	199.9922
92516	25.69889	25.25	196.7993
93416	25.94889	25.5	198.715
94316	26.19889	25.75	198.0765
95216	26.44889	26	198.0765
96116	26.69889	26.25	198.0765
97016	26.94889	26.5	194.8836
97916	27.19889	26.75	199.3536
98816	27.44889	27	196.1608
99716	27.69889	27.25	198.715
100616	27.94889	27.5	194.2451
101516	28.19889	27.75	194.8836
102416	28.44889	28	194.8836
103316	28.69889	28.25	194.2451
104216	28.94889	28.5	192.3294
105116	29.19889	28.75	191.6908
106016	29.44889	29	191.6908
106916	29.69889	29.25	192.9679

Time (s)	Time (hr)	Time (Corrected)	P (psig)
107816	29.94889	29.5	191.6908
108716	30.19889	29.75	192.9679
109616	30.44889	30	191.6908
110516	30.69889	30.25	192.3294
111416	30.94889	30.5	191.6908
112316	31.19889	30.75	191.6908
113216	31.44889	31	191.6908
114116	31.69889	31.25	191.6908
115016	31.94889	31.5	189.1365
115916	32.19889	31.75	187.2208
116816	32.44889	32	187.8594
117716	32.69889	32.25	188.4979
118616	32.94889	32.5	189.7751
119516	33.19889	32.75	187.2208
120416	33.44889	33	186.5822
121316	33.69889	33.25	184.6665
122216	33.94889	33.5	184.028
123116	34.19889	33.75	185.9437
124016	34.44889	34	185.9437
124916	34.69889	34.25	182.7508
125816	34.94889	34.5	183.3894
126716	35.19889	34.75	184.028
127616	35.44889	35	182.7508
128516	35.69889	35.25	182.1123
129416	35.94889	35.5	180.8351
130316	36.19889	35.75	182.7508
131216	36.44889	36	180.8351
132116	36.69889	36.25	180.1966
133016	36.94889	36.5	178.2808
133916	37.19889	36.75	181.4737
134816	37.44889	37	178.2808
135716	37.69889	37.25	180.8351
136616	37.94889	37.5	178.2808
137516	38.19889	37.75	178.2808
138416	38.44889	38	177.6423
139316	38.69889	38.25	174.4494
140216	38.94889	38.5	173.8109
141116	39.19889	38.75	173.8109
142016	39.44889	39	172.5337
142916	39.69889	39.25	173.1723
143816	39.94889	39.5	172.5337

Time (s)	Time (hr)	Time (Corrected)	P (psig)
144716	40.19889	39.75	171.8952
145616	40.44889	40	171.8952
146516	40.69889	40.25	171.8952
147416	40.94889	40.5	167.4252
148316	41.19889	40.75	169.3409
149216	41.44889	41	165.5095
150116	41.69889	41.25	166.7866
151016	41.94889	41.5	167.4252
151916	42.19889	41.75	164.8709
152816	42.44889	42	163.5938
153716	42.69889	42.25	163.5938
154616	42.94889	42.5	159.7624
155516	43.19889	42.75	162.3166
156416	43.44889	43	159.7624
157316	43.69889	43.25	159.1238
158216	43.94889	43.5	157.8467
159116	44.19889	43.75	158.4852
160016	44.44889	44	159.7624
160916	44.69889	44.25	157.2081
161816	44.94889	44.5	157.2081
162716	45.19889	44.75	155.9309
163616	45.44889	45	154.0152
164516	45.69889	45.25	154.0152
165416	45.94889	45.5	154.6538
166316	46.19889	45.75	155.2924
167216	46.44889	46	152.7381
168116	46.69889	46.25	151.461
169016	46.94889	46.5	151.461
169916	47.19889	46.75	150.1838
170816	47.44889	47	150.1838
171716	47.69889	47.25	149.5453
172616	47.94889	47.5	147.6296
173516	48.19889	47.75	146.991
174416	48.44889	48	146.991
175316	48.69889	48.25	146.3524
176216	48.94889	48.5	147.6296
177116	49.19889	48.75	144.4367
178016	49.44889	49	146.991
178916	49.69889	49.25	145.7138
179816	49.94889	49.5	146.991
180716	50.19889	49.75	146.991

Time (s)	Time (hr)	Time (Corrected)	P (psig)
181616	50.44889	50	144.4367
182516	50.69889	50.25	144.4367
183416	50.94889	50.5	145.7138
184316	51.19889	50.75	145.0753
185216	51.44889	51	145.7138
186116	51.69889	51.25	143.7981
187016	51.94889	51.5	141.8824
187916	52.19889	51.75	143.1596
188816	52.44889	52	142.521
189716	52.69889	52.25	140.6053
190616	52.94889	52.5	143.1596
191516	53.19889	52.75	141.8824
192416	53.44889	53	140.6053
193316	53.69889	53.25	143.7981
194216	53.94889	53.5	141.8824
195116	54.19889	53.75	141.8824
196016	54.44889	54	141.8824
196916	54.69889	54.25	140.6053
197816	54.94889	54.5	141.8824
198716	55.19889	54.75	143.1596
199616	55.44889	55	140.6053
200516	55.69889	55.25	138.6896
201416	55.94889	55.5	139.3282
202316	56.19889	55.75	139.3282
203216	56.44889	56	141.2439
204116	56.69889	56.25	138.6896
205016	56.94889	56.5	140.6053
205916	57.19889	56.75	139.9667
206816	57.44889	57	138.051
207716	57.69889	57.25	139.9667
208616	57.94889	57.5	139.9667
209516	58.19889	57.75	138.051
210416	58.44889	58	139.9667
211316	58.69889	58.25	138.051
212216	58.94889	58.5	139.9667
213116	59.19889	58.75	139.9667
214016	59.44889	59	140.6053
214916	59.69889	59.25	139.3282
215816	59.94889	59.5	138.6896
216716	60.19889	59.75	139.9667
217616	60.44889	60	138.051

Time (s)	Time (hr)	Time (Corrected)	P (psig)
218516	60.69889	60.25	138.6896
219416	60.94889	60.5	138.6896
220316	61.19889	60.75	139.9667
221216	61.44889	61	139.9667
222116	61.69889	61.25	141.2439
223016	61.94889	61.5	138.051
223916	62.19889	61.75	140.6053
224816	62.44889	62	140.6053
225716	62.69889	62.25	138.6896
226616	62.94889	62.5	139.3282
227516	63.19889	62.75	139.3282
228416	63.44889	63	140.6053
229316	63.69889	63.25	138.6896
230216	63.94889	63.5	138.6896
231116	64.19889	63.75	137.4125
232016	64.44889	64	138.6896
232916	64.69889	64.25	138.6896
233816	64.94889	64.5	139.3282
234716	65.19889	64.75	140.6053
235616	65.44889	65	138.6896
236516	65.69889	65.25	138.6896
237416	65.94889	65.5	138.051
238316	66.19889	65.75	138.051
239216	66.44889	66	138.051
240116	66.69889	66.25	138.6896
241016	66.94889	66.5	140.6053
241916	67.19889	66.75	138.051
242816	67.44889	67	135.4968
243716	67.69889	67.25	137.4125
244616	67.94889	67.5	138.051
245516	68.19889	67.75	139.9667
246416	68.44889	68	138.051
247316	68.69889	68.25	137.4125
248216	68.94889	68.5	138.051
249116	69.19889	68.75	139.3282
250016	69.44889	69	139.3282
250916	69.69889	69.25	138.051
251816	69.94889	69.5	138.051
252716	70.19889	69.75	138.6896
253616	70.44889	70	137.4125
254516	70.69889	70.25	138.6896

Time (s)	Time (hr)	Time (Corrected)	P (psig)
255416	70.94889	70.5	137.4125
256316	71.19889	70.75	136.7739
257216	71.44889	71	138.6896
258116	71.69889	71.25	140.6053
259016	71.94889	71.5	138.051
259916	72.19889	71.75	137.4125
260816	72.44889	72	137.4125
261716	72.69889	72.25	138.6896
262616	72.94889	72.5	138.051
263516	73.19889	72.75	137.4125
264416	73.44889	73	138.051
265316	73.69889	73.25	136.7739
266216	73.94889	73.5	138.6896
267116	74.19889	73.75	138.6896
268016	74.44889	74	136.7739
268916	74.69889	74.25	139.3282
269816	74.94889	74.5	138.051
270716	75.19889	74.75	137.4125
271616	75.44889	75	138.6896
272516	75.69889	75.25	138.051
273416	75.94889	75.5	137.4125
274316	76.19889	75.75	138.051
275216	76.44889	76	137.4125
276116	76.69889	76.25	140.6053
277016	76.94889	76.5	138.051
277916	77.19889	76.75	138.051
278816	77.44889	77	139.9667
279716	77.69889	77.25	136.7739
280616	77.94889	77.5	136.7739
281516	78.19889	77.75	139.3282
282416	78.44889	78	138.051
283316	78.69889	78.25	138.051
284216	78.94889	78.5	139.3282
285116	79.19889	78.75	136.1353
286016	79.44889	79	139.3282
286916	79.69889	79.25	138.051
287816	79.94889	79.5	139.3282
288716	80.19889	79.75	137.4125
289616	80.44889	80	136.7739
290516	80.69889	80.25	139.3282
291416	80.94889	80.5	139.3282

Time (s)	Time (hr)	Time (Corrected)	P (psig)
292316	81.19889	80.75	138.051
293216	81.44889	81	136.7739
294116	81.69889	81.25	138.051
295016	81.94889	81.5	139.3282
295916	82.19889	81.75	138.051
296816	82.44889	82	137.4125
297716	82.69889	82.25	138.051
298616	82.94889	82.5	136.7739
299516	83.19889	82.75	136.7739
300416	83.44889	83	139.9667
301316	83.69889	83.25	138.6896
302216	83.94889	83.5	139.9667
303116	84.19889	83.75	136.7739
304016	84.44889	84	136.7739
304916	84.69889	84.25	138.051
305816	84.94889	84.5	139.3282
306716	85.19889	84.75	138.051
307616	85.44889	85	138.051
308516	85.69889	85.25	138.051
309416	85.94889	85.5	139.9667
310316	86.19889	85.75	138.051
311216	86.44889	86	138.6896
312116	86.69889	86.25	138.051
313016	86.94889	86.5	138.051
313916	87.19889	86.75	138.051
314816	87.44889	87	138.051
315716	87.69889	87.25	136.1353
316616	87.94889	87.5	138.051
317516	88.19889	87.75	138.051
318416	88.44889	88	138.051
319316	88.69889	88.25	136.7739
320216	88.94889	88.5	136.7739
321116	89.19889	88.75	138.051
322016	89.44889	89	139.3282
322916	89.69889	89.25	138.051
323816	89.94889	89.5	138.051
324716	90.19889	89.75	136.1353
325616	90.44889	90	138.6896
326516	90.69889	90.25	138.6896
328316	91.19889	90.75	138.6896
329216	91.44889	91	138.051

Time (s)	Time (hr)	Time (Corrected)	P (psig)
330116	91.69889	91.25	139.3282
331016	91.94889	91.5	138.6896
331916	92.19889	91.75	138.051
332816	92.44889	92	138.051
333716	92.69889	92.25	138.051
334616	92.94889	92.5	138.6896
335516	93.19889	92.75	137.4125
336416	93.44889	93	139.3282
337316	93.69889	93.25	138.051
338216	93.94889	93.5	136.7739
339116	94.19889	93.75	139.9667
340016	94.44889	94	138.051
340916	94.69889	94.25	138.051
341816	94.94889	94.5	138.051
342716	95.19889	94.75	136.1353
343616	95.44889	95	138.051
344516	95.69889	95.25	135.4968
345416	95.94889	95.5	136.1353
346316	96.19889	95.75	138.051
347216	96.44889	96	137.4125
348116	96.69889	96.25	136.7739
349016	96.94889	96.5	139.3282
349916	97.19889	96.75	138.051
350816	97.44889	97	137.4125
351716	97.69889	97.25	138.051
352616	97.94889	97.5	137.4125
353516	98.19889	97.75	137.4125
354416	98.44889	98	139.9667
355316	98.69889	98.25	138.6896
356216	98.94889	98.5	138.051
357116	99.19889	98.75	137.4125
358016	99.44889	99	139.3282
358916	99.69889	99.25	138.051
359816	99.94889	99.5	139.9667
360716	100.1989	99.75	138.051
361616	100.4489	100	137.4125
362516	100.6989	100.25	137.4125
363416	100.9489	100.5	137.4125
364316	101.1989	100.75	136.7739
365216	101.4489	101	136.7739
366116	101.6989	101.25	137.4125

Time (s)	Time (hr)	Time (Corrected)	P (psig)
367016	101.9489	101.5	136.1353
367916	102.1989	101.75	138.6896
368816	102.4489	102	138.051
369716	102.6989	102.25	136.1353
371516	103.1989	102.75	138.051
372416	103.4489	103	136.1353
373316	103.6989	103.25	138.6896
374216	103.9489	103.5	138.051
375116	104.1989	103.75	138.051
376016	104.4489	104	138.6896
376916	104.6989	104.25	136.1353
377816	104.9489	104.5	135.4968
378716	105.1989	104.75	138.051
379616	105.4489	105	138.6896
380516	105.6989	105.25	135.4968
381416	105.9489	105.5	139.9667
382316	106.1989	105.75	138.6896
383216	106.4489	106	138.6896
384116	106.6989	106.25	139.3282
385016	106.9489	106.5	138.051
385916	107.1989	106.75	138.051
386816	107.4489	107	139.3282
387716	107.6989	107.25	138.6896
388616	107.9489	107.5	137.4125
389516	108.1989	107.75	138.051
390416	108.4489	108	137.4125
391316	108.6989	108.25	136.7739
392216	108.9489	108.5	136.7739
393116	109.1989	108.75	138.6896
394916	109.6989	109.25	136.7739
395816	109.9489	109.5	139.9667
396716	110.1989	109.75	138.051
397616	110.4489	110	139.3282
398516	110.6989	110.25	136.7739
399416	110.9489	110.5	137.4125
400316	111.1989	110.75	138.051
401216	111.4489	111	138.6896
402116	111.6989	111.25	136.7739
403016	111.9489	111.5	136.7739
403916	112.1989	111.75	139.3282
404816	112.4489	112	136.1353
405716	112.6989	112.25	138.6896
406616	112.9489	112.5	138.6896
407516	113.1989	112.75	136.7739
408416	113.4489	113	138.6896
409316	113.6989	113.25	136.7739
410216	113.9489	113.5	138.051
411116	114.1989	113.75	137.4125
412016	114.4489	114	136.1353
412916	114.6989	114.25	137.4125
413816	114.9489	114.5	138.051
414716	115.1989	114.75	138.6896
415616	115.4489	115	139.3282
416516	115.6989	115.25	138.051
417416	115.9489	115.5	136.7739
418316	116.1989	115.75	137.4125
419216	116.4489	116	138.051
420116	116.6989	116.25	139.3282
421016	116.9489	116.5	138.051
422816	117.4489	117	139.3282
423716	117.6989	117.25	136.1353
424616	117.9489	117.5	138.6896
425516	118.1989	117.75	135.4968
426416	118.4489	118	135.4968
427316	118.6989	118.25	135.4968
428216	118.9489	118.5	138.051
429116	119.1989	118.75	138.6896
430016	119.4489	119	138.6896
431816	119.9489	119.5	136.7739
432716	120.1989	119.75	138.6896
433616	120.4489	120	137.4125

Pressure Decline Data
T = 65°C, $C_{3(g)}$-heavy oil

Time (s)	Time (hr)	Time (Corrected)	P (psig)
1451	0.403056	0	238.3063
3251	0.903056	0.5	224.8964
4151	1.153056	0.75	223.6192
5051	1.403056	1	216.5950
5951	1.653056	1.25	214.0407
6851	1.903056	1.5	208.2936
7751	2.153056	1.75	208.2936
8651	2.403056	2	203.8236
9551	2.653056	2.25	203.1850
10451	2.903056	2.5	199.9922
11351	3.153056	2.75	198.7150
12251	3.403056	3	198.0765
13151	3.653056	3.25	195.5222
14051	3.903056	3.5	192.9679
14951	4.153056	3.75	193.6065
15851	4.403056	4	192.3294
16751	4.653056	4.25	191.6908
17651	4.903056	4.5	188.4979
18551	5.153056	4.75	187.2208
19451	5.403056	5	186.5822
20351	5.653056	5.25	183.3894
21251	5.903056	5.5	183.3894
22151	6.153056	5.75	183.3894
23051	6.403056	6	182.1123
23951	6.653056	6.25	182.7508
24851	6.903056	6.5	178.2808
25751	7.153056	6.75	181.4737
26651	7.403056	7	178.2808
27551	7.653056	7.25	177.6423
28451	7.903056	7.5	176.3651
29351	8.153056	7.75	176.3651
30251	8.403056	8	177.0037
31151	8.653056	8.25	175.0880
32051	8.903056	8.5	173.8109
32951	9.153056	8.75	173.1723
33851	9.403056	9	171.2566
34751	9.653056	9.25	171.2566
35651	9.903056	9.5	170.6180
36551	10.15306	9.75	172.5337
37451	10.40306	10	170.6180
38351	10.65306	10.25	171.8952
39251	10.90306	10.5	167.4252
40151	11.15306	10.75	167.4252
41051	11.40306	11	169.9795
41951	11.65306	11.25	167.4252
42851	11.90306	11.5	168.0637
43751	12.15306	11.75	167.4252
44651	12.40306	12	165.5095
45551	12.65306	12.25	166.7866
46451	12.90306	12.5	164.2323
47351	13.15306	12.75	165.5095
48251	13.40306	13	164.8709
49151	13.65306	13.25	164.8709
50051	13.90306	13.5	162.9552
50951	14.15306	13.75	163.5938
51851	14.40306	14	164.2323
52751	14.65306	14.25	164.2323
53651	14.90306	14.5	161.0395
54551	15.15306	14.75	161.0395
55451	15.40306	15	161.6781
56351	15.65306	15.25	161.6781
57251	15.90306	15.5	162.9552
58151	16.15306	15.75	161.0395
59051	16.40306	16	160.4009
59951	16.65306	16.25	159.7624
60851	16.90306	16.5	159.7624
61751	17.15306	16.75	159.1238
62651	17.40306	17	157.2081
63551	17.65306	17.25	157.8467
64451	17.90306	17.5	155.9309
65351	18.15306	17.75	155.9309
66251	18.40306	18	157.8467
67151	18.65306	18.25	157.8467
68051	18.90306	18.5	156.5695
68951	19.15306	18.75	155.9309
69851	19.40306	19	155.9309
70751	19.65306	19.25	155.9309

Time (s)	Time (hr)	Time (Corrected)	P (psig)
71651	19.90306	19.5	153.3767
72551	20.15306	19.75	157.2081
73451	20.40306	20	154.6538
74351	20.65306	20.25	154.0152
75251	20.90306	20.5	154.6538
76151	21.15306	20.75	155.2924
77051	21.40306	21	154.6538
77951	21.65306	21.25	154.6538
78851	21.90306	21.5	152.7381
79751	22.15306	21.75	153.3767
80651	22.40306	22	152.7381
81551	22.65306	22.25	151.4610
82451	22.90306	22.5	148.2681
83351	23.15306	22.75	152.7381
84251	23.40306	23	150.8224
85151	23.65306	23.25	147.6296
86051	23.90306	23.5	149.5453
86951	24.15306	23.75	146.9910
87851	24.40306	24	148.2681
88751	24.65306	24.25	150.1838
89651	24.90306	24.5	145.7138
90551	25.15306	24.75	145.7138
91451	25.40306	25	148.9067
92351	25.65306	25.25	145.7138
93251	25.90306	25.5	149.5453
94151	26.15306	25.75	147.6296
95051	26.40306	26	144.4367
95951	26.65306	26.25	145.7138
96851	26.90306	26.5	145.7138
97751	27.15306	26.75	146.9910
98651	27.40306	27	143.7981
99551	27.65306	27.25	143.7981
100451	27.90306	27.5	145.0753
101351	28.15306	27.75	143.7981
102251	28.40306	28	142.5210
103151	28.65306	28.25	142.5210
104051	28.90306	28.5	145.7138
104951	29.15306	28.75	141.2439
105851	29.40306	29	144.4367
106751	29.65306	29.25	143.1596
107651	29.90306	29.5	142.5210
108551	30.15306	29.75	143.7981
109451	30.40306	30	143.1596
110351	30.65306	30.25	141.8824
111251	30.90306	30.5	143.7981
112151	31.15306	30.75	141.2439
113051	31.40306	31	142.5210
113951	31.65306	31.25	143.1596
114851	31.90306	31.5	141.8824
115751	32.15306	31.75	140.6053
116651	32.40306	32	143.1596
117551	32.65306	32.25	139.9667
118451	32.90306	32.5	142.5210
119351	33.15306	32.75	140.6053
120251	33.40306	33	139.3282
121151	33.65306	33.25	141.8824
122051	33.90306	33.5	139.9667
122951	34.15306	33.75	142.5210
123851	34.40306	34	141.2439
124751	34.65306	34.25	139.9667
125651	34.90306	34.5	137.4125
126551	35.15306	34.75	138.0510
127451	35.40306	35	138.6896
128351	35.65306	35.25	136.1353
129251	35.90306	35.5	139.3282
130151	36.15306	35.75	138.6896
131051	36.40306	36	134.8582
131951	36.65306	36.25	138.0510
132851	36.90306	36.5	140.6053
133751	37.15306	36.75	136.1353
134651	37.40306	37	136.1353
135551	37.65306	37.25	137.4125
136451	37.90306	37.5	133.5810
137351	38.15306	37.75	135.4968
138251	38.40306	38	136.1353
139151	38.65306	38.25	134.2196
140051	38.90306	38.5	134.8582
140951	39.15306	38.75	137.4125
141851	39.40306	39	138.0510
142751	39.65306	39.25	134.2196
143651	39.90306	39.5	133.5810
144551	40.15306	39.75	132.9425

Time (s)	Time (hr)	Time (Corrected)	P (psig)
145451	40.40306	40	131.6653
146351	40.65306	40.25	132.9425
147251	40.90306	40.5	132.3039
148151	41.15306	40.75	134.2196
149051	41.40306	41	130.3882
149951	41.65306	41.25	130.3882
150851	41.90306	41.5	134.2196
151751	42.15306	41.75	130.3882
152651	42.40306	42	133.5810
153551	42.65306	42.25	134.8582
154451	42.90306	42.5	132.9425
155351	43.15306	42.75	132.9425
156251	43.40306	43	131.0268
157151	43.65306	43.25	129.1111
158051	43.90306	43.5	130.3882
158951	44.15306	43.75	129.1111
159851	44.40306	44	132.3039
160751	44.65306	44.25	128.4725
161651	44.90306	44.5	130.3882
162551	45.15306	44.75	129.7496
163451	45.40306	45	127.1954
164351	45.65306	45.25	129.1111
165251	45.90306	45.5	129.7496
166151	46.15306	45.75	127.1954
167051	46.40306	46	132.9425
167951	46.65306	46.25	129.7496
168851	46.90306	46.5	131.0268
169751	47.15306	46.75	129.7496
170651	47.40306	47	127.1954
171551	47.65306	47.25	130.3882
172451	47.90306	47.5	130.3882
173351	48.15306	47.75	126.5568
174251	48.40306	48	128.4725
175151	48.65306	48.25	129.1111
176051	48.90306	48.5	125.2797
176951	49.15306	48.75	129.7496
177851	49.40306	49	126.5568
178751	49.65306	49.25	127.8339
179651	49.90306	49.5	127.1954
180551	50.15306	49.75	123.3639
181451	50.40306	50	127.8339
182351	50.65306	50.25	125.9182
183251	50.90306	50.5	127.1954
184151	51.15306	50.75	127.1954
185051	51.40306	51	128.4725
185951	51.65306	51.25	127.1954
186851	51.90306	51.5	127.8339
187751	52.15306	51.75	124.0025
188651	52.40306	52	122.7254
189551	52.65306	52.25	125.2797
190451	52.90306	52.5	125.9182
191351	53.15306	52.75	124.0025
192251	53.40306	53	127.1954
193151	53.65306	53.25	128.4725
194051	53.90306	53.5	122.0868
194951	54.15306	53.75	124.0025
195851	54.40306	54	122.7254
196751	54.65306	54.25	124.6411
197651	54.90306	54.5	121.4482
198551	55.15306	54.75	122.7254
199451	55.40306	55	125.2797
200351	55.65306	55.25	125.2797
201251	55.90306	55.5	123.3639
202151	56.15306	55.75	121.4482
203051	56.40306	56	122.7254
203951	56.65306	56.25	122.7254
204851	56.90306	56.5	121.4482
205751	57.15306	56.75	120.8097
206651	57.40306	57	122.7254
207551	57.65306	57.25	125.2797
208451	57.90306	57.5	121.4482
209351	58.15306	57.75	126.5568
210251	58.40306	58	119.5325
211151	58.65306	58.25	120.1711
212051	58.90306	58.5	124.6411
212951	59.15306	58.75	119.5325
213851	59.40306	59	124.6411
214751	59.65306	59.25	124.6411
215651	59.90306	59.5	118.8940
216551	60.15306	59.75	127.1954
217451	60.40306	60	121.4482
218351	60.65306	60.25	118.2554

Time (s)	Time (hr)	Time (Corrected)	P (psig)
219251	60.90306	60.5	124.0025
220151	61.15306	60.75	124.6411
221051	61.40306	61	121.4482
221951	61.65306	61.25	116.9783
222851	61.90306	61.5	124.6411
223751	62.15306	61.75	122.0868
224651	62.40306	62	118.2554
225551	62.65306	62.25	118.8940
226451	62.90306	62.5	121.4482
227351	63.15306	62.75	114.4240
228251	63.40306	63	121.4482
229151	63.65306	63.25	120.8097
230051	63.90306	63.5	117.6168
230951	64.15306	63.75	117.6168
231851	64.40306	64	122.7254
232751	64.65306	64.25	116.9783
233651	64.90306	64.5	117.6168
234551	65.15306	64.75	118.2554
235451	65.40306	65	118.8940
236351	65.65306	65.25	120.1711
237251	65.90306	65.5	117.6168
238151	66.15306	65.75	119.5325
239051	66.40306	66	118.2554
239951	66.65306	66.25	119.5325
240851	66.90306	66.5	117.6168
241751	67.15306	66.75	116.9783
242651	67.40306	67	119.5325
243551	67.65306	67.25	118.2554
244451	67.90306	67.5	119.5325
245351	68.15306	67.75	115.7011
246251	68.40306	68	115.7011
247151	68.65306	68.25	118.8940
248051	68.90306	68.5	118.2554
248951	69.15306	68.75	120.1711
249851	69.40306	69	116.9783
250751	69.65306	69.25	118.2554
251651	69.90306	69.5	116.3397
252551	70.15306	69.75	120.1711
253451	70.40306	70	115.0626
254351	70.65306	70.25	120.8097
255251	70.90306	70.5	116.9783

Time (s)	Time (hr)	Time (Corrected)	P (psig)
256151	71.15306	70.75	117.6168
257051	71.40306	71	119.5325
257951	71.65306	71.25	116.3397
258851	71.90306	71.5	120.1711
259751	72.15306	71.75	117.6168
260651	72.40306	72	116.3397
261551	72.65306	72.25	113.7854
262451	72.90306	72.5	113.7854
263351	73.15306	72.75	117.6168
264251	73.40306	73	112.5083
265151	73.65306	73.25	114.4240
266051	73.90306	73.5	116.9783
266951	74.15306	73.75	115.0626
267851	74.40306	74	116.3397
268751	74.65306	74.25	112.5083
269651	74.90306	74.5	111.8697
270551	75.15306	74.75	114.4240
271451	75.40306	75	114.4240
272351	75.65306	75.25	113.7854
273251	75.90306	75.5	111.2311
274151	76.15306	75.75	114.4240
275051	76.40306	76	111.8697
275951	76.65306	76.25	118.8940
276851	76.90306	76.5	111.2311
277751	77.15306	76.75	111.8697
278651	77.40306	77	112.5083
279551	77.65306	77.25	113.1468
280451	77.90306	77.5	114.4240
281351	78.15306	77.75	111.8697
282251	78.40306	78	113.1468
283151	78.65306	78.25	112.5083
284051	78.90306	78.5	112.5083
284951	79.15306	78.75	113.7854
285851	79.40306	79	117.6168
286751	79.65306	79.25	113.7854
287651	79.90306	79.5	112.5083
288551	80.15306	79.75	110.5926
289451	80.40306	80	109.9540
290351	80.65306	80.25	111.2311
291251	80.90306	80.5	112.5083
292151	81.15306	80.75	114.4240

Time (s)	Time (hr)	Time (Corrected)	P (psig)
293051	81.40306	81	113.1468
293951	81.65306	81.25	111.2311
294851	81.90306	81.5	112.5083
295751	82.15306	81.75	113.1468
296651	82.40306	82	108.0383
297551	82.65306	82.25	108.0383
298451	82.90306	82.5	113.1468
299351	83.15306	82.75	111.8697
300251	83.40306	83	113.1468
301151	83.65306	83.25	111.2311
302051	83.90306	83.5	108.0383
302951	84.15306	83.75	111.8697
303851	84.40306	84	108.0383
304751	84.65306	84.25	113.1468
305651	84.90306	84.5	109.9540
306551	85.15306	84.75	113.7854
307451	85.40306	85	106.7612
308351	85.65306	85.25	110.5926
309251	85.90306	85.5	109.9540
310151	86.15306	85.75	109.9540
311051	86.40306	86	108.0383
311951	86.65306	86.25	107.3997
312851	86.90306	86.5	112.5083
313751	87.15306	86.75	106.7612
314651	87.40306	87	111.8697
315551	87.65306	87.25	109.3154
316451	87.90306	87.5	110.5926
317351	88.15306	87.75	109.9540
318251	88.40306	88	111.2311
319151	88.65306	88.25	109.9540
320051	88.90306	88.5	111.8697
320951	89.15306	88.75	109.3154
321851	89.40306	89	109.3154
322751	89.65306	89.25	108.6769
323651	89.90306	89.5	109.3154
324551	90.15306	89.75	108.0383
325451	90.40306	90	108.0383
326351	90.65306	90.25	108.6769
327251	90.90306	90.5	111.2311
328151	91.15306	90.75	104.8455
329051	91.40306	91	108.0383

Time (s)	Time (hr)	Time (Corrected)	P (psig)
329951	91.65306	91.25	106.7612
330851	91.90306	91.5	111.8697
331751	92.15306	91.75	108.6769
332651	92.40306	92	111.8697
333551	92.65306	92.25	109.3154
334451	92.90306	92.5	106.1226
335351	93.15306	92.75	104.2069
336251	93.40306	93	102.9298
337151	93.65306	93.25	106.7612
338051	93.90306	93.5	111.2311
338951	94.15306	93.75	106.7612
339851	94.40306	94	106.7612
340751	94.65306	94.25	108.0383
341651	94.90306	94.5	106.7612
342551	95.15306	94.75	106.1226
343451	95.40306	95	106.7612
344351	95.65306	95.25	106.7612
345251	95.90306	95.5	107.3997
346151	96.15306	95.75	108.0383
347051	96.40306	96	106.1226
347951	96.65306	96.25	107.3997
348851	96.90306	96.5	104.8455
349751	97.15306	96.75	108.0383
350651	97.40306	97	104.2069
351551	97.65306	97.25	104.8455
352451	97.90306	97.5	106.7612
353351	98.15306	97.75	106.7612
354251	98.40306	98	103.5683
355151	98.65306	98.25	107.3997
356051	98.90306	98.5	106.1226
356951	99.15306	98.75	106.1226
357851	99.40306	99	106.1226
358751	99.65306	99.25	107.3997
359651	99.90306	99.5	105.4840
360551	100.1531	99.75	104.2069
361451	100.4031	100	105.4840
362351	100.6531	100.25	104.8455
363251	100.9031	100.5	106.1226
364151	101.1531	100.75	103.5683
365051	101.4031	101	103.5683
365951	101.6531	101.25	103.5683

Time (s)	Time (hr)	Time (Corrected)	P (psig)
366851	101.9031	101.5	104.2069
367751	102.1531	101.75	103.5683
368651	102.4031	102	106.1226
369551	102.6531	102.25	104.2069
370451	102.9031	102.5	105.4840
371351	103.1531	102.75	104.8455
372251	103.4031	103	104.2069
373151	103.6531	103.25	106.1226
374051	103.9031	103.5	104.2069
374951	104.1531	103.75	101.6526
375851	104.4031	104	104.2069
376751	104.6531	104.25	106.1226
377651	104.9031	104.5	105.4840
378551	105.1531	104.75	104.2069
379451	105.4031	105	104.2069
380351	105.6531	105.25	102.2912
381251	105.9031	105.5	101.6526
382151	106.1531	105.75	104.2069
383051	106.4031	106	102.9298
383951	106.6531	106.25	102.9298
384851	106.9031	106.5	104.8455
385751	107.1531	106.75	103.5683
386651	107.4031	107	104.8455
387551	107.6531	107.25	102.9298
388451	107.9031	107.5	101.0140
389351	108.1531	107.75	102.9298
390251	108.4031	108	102.9298
391151	108.6531	108.25	101.0140
392051	108.9031	108.5	104.2069
392951	109.1531	108.75	104.2069
393851	109.4031	109	102.9298
394751	109.6531	109.25	102.2912
395651	109.9031	109.5	101.0140
396551	110.1531	109.75	104.2069
397451	110.4031	110	102.2912
398351	110.6531	110.25	102.2912
399251	110.9031	110.5	101.6526
400151	111.1531	110.75	103.5683
401051	111.4031	111	101.6526
401951	111.6531	111.25	104.2069
402851	111.9031	111.5	101.6526

Time (s)	Time (hr)	Time (Corrected)	P (psig)
403751	112.1531	111.75	101.6526
404651	112.4031	112	99.7369
405551	112.6531	112.25	101.0140
406451	112.9031	112.5	100.3755
407351	113.1531	112.75	102.9298
408251	113.4031	113	101.0140
409151	113.6531	113.25	102.2912
410051	113.9031	113.5	101.6526
410951	114.1531	113.75	102.2912
411851	114.4031	114	101.6526
412751	114.6531	114.25	101.6526
413651	114.9031	114.5	101.0140
414551	115.1531	114.75	102.2912
415451	115.4031	115	101.6526
416351	115.6531	115.25	101.0140
417251	115.9031	115.5	99.7369
418151	116.1531	115.75	100.3755
419051	116.4031	116	101.0140
419951	116.6531	116.25	102.2912
420851	116.9031	116.5	102.9298
421751	117.1531	116.75	99.7369
422651	117.4031	117	101.6526
423551	117.6531	117.25	100.3755
424451	117.9031	117.5	100.3755
425351	118.1531	117.75	102.2912
426251	118.4031	118	99.7369
427151	118.6531	118.25	100.3755
428051	118.9031	118.5	99.0983
428951	119.1531	118.75	99.0983
429851	119.4031	119	99.7369
430751	119.6531	119.25	100.3755
431651	119.9031	119.5	99.0983
432551	120.1531	119.75	97.8212
433451	120.4031	120	99.7369
434351	120.6531	120.25	101.6526
435251	120.9031	120.5	99.7369
436151	121.1531	120.75	99.7369
437051	121.4031	121	97.8212
437951	121.6531	121.25	99.0983
438851	121.9031	121.5	97.8212
439751	122.1531	121.75	99.0983

Time (s)	Time (hr)	Time (Corrected)	P (psig)
440651	122.4031	122	97.1826
441551	122.6531	122.25	100.3755
442451	122.9031	122.5	99.7369
443351	123.1531	122.75	98.4598
444251	123.4031	123	99.0983
445151	123.6531	123.25	99.0983
446051	123.9031	123.5	98.4598
446951	124.1531	123.75	97.1826
447851	124.4031	124	99.7369
448751	124.6531	124.25	96.5441
449651	124.9031	124.5	99.7369
450551	125.1531	124.75	98.4598
451451	125.4031	125	98.4598
452351	125.6531	125.25	99.7369
453251	125.9031	125.5	99.7369
454151	126.1531	125.75	99.7369
455051	126.4031	126	99.7369
455951	126.6531	126.25	99.7369
456851	126.9031	126.5	96.5441
457751	127.1531	126.75	99.7369
458651	127.4031	127	99.7369
459551	127.6531	127.25	97.8212
460451	127.9031	127.5	99.0983
461351	128.1531	127.75	99.0983
462251	128.4031	128	98.4598
463151	128.6531	128.25	99.0983
464051	128.9031	128.5	97.1826
464951	129.1531	128.75	99.0983
465851	129.4031	129	96.5441
466751	129.6531	129.25	96.5441
467651	129.9031	129.5	98.4598
468551	130.1531	129.75	97.8212
469451	130.4031	130	95.2669
470351	130.6531	130.25	96.5441
471251	130.9031	130.5	96.5441
472151	131.1531	130.75	97.1826
473051	131.4031	131	96.5441
473951	131.6531	131.25	94.6284
474851	131.9031	131.5	98.4598
475751	132.1531	131.75	95.2669
476651	132.4031	132	97.8212

Time (s)	Time (hr)	Time (Corrected)	P (psig)
477551	132.6531	132.25	94.6284
478451	132.9031	132.5	96.5441
479351	133.1531	132.75	95.9055
480251	133.4031	133	96.5441
481151	133.6531	133.25	96.5441
482051	133.9031	133.5	97.1826
482951	134.1531	133.75	93.9898
483851	134.4031	134	93.9898
484751	134.6531	134.25	94.6284
485651	134.9031	134.5	97.1826
486551	135.1531	134.75	95.9055
487451	135.4031	135	97.1826
488351	135.6531	135.25	97.1826
489251	135.9031	135.5	97.1826
490151	136.1531	135.75	95.9055
491051	136.4031	136	93.9898
491951	136.6531	136.25	95.9055
492851	136.9031	136.5	95.9055
493751	137.1531	136.75	95.9055
494651	137.4031	137	97.1826
495551	137.6531	137.25	95.2669
496451	137.9031	137.5	95.9055
497351	138.1531	137.75	94.6284
498251	138.4031	138	95.2669
499151	138.6531	138.25	93.3512
500051	138.9031	138.5	95.2669
500951	139.1531	138.75	93.3512
501851	139.4031	139	96.5441
502751	139.6531	139.25	94.6284
503651	139.9031	139.5	93.9898
504551	140.1531	139.75	95.9055
505451	140.4031	140	96.5441
506351	140.6531	140.25	96.5441
507251	140.9031	140.5	95.9055
508151	141.1531	140.75	93.3512
509051	141.4031	141	94.6284
509951	141.6531	141.25	93.9898
510851	141.9031	141.5	95.9055
511751	142.1531	141.75	94.6284
512651	142.4031	142	95.9055
513551	142.6531	142.25	92.7127

Time (s)	Time (hr)	Time (Corrected)	P (psig)
514451	142.9031	142.5	93.9898
515351	143.1531	142.75	92.7127
516251	143.4031	143	95.9055
517151	143.6531	143.25	92.7127
518051	143.9031	143.5	93.9898
518951	144.1531	143.75	93.9898
519851	144.4031	144	93.9898
520751	144.6531	144.25	93.9898
521651	144.9031	144.5	94.6284
522551	145.1531	144.75	93.9898
523451	145.4031	145	94.6284
524351	145.6531	145.25	92.7127
525251	145.9031	145.5	93.9898
526151	146.1531	145.75	93.3512
527051	146.4031	146	95.2669
528851	146.9031	146.5	93.9898
529751	147.1531	146.75	93.3512
530651	147.4031	147	93.3512
532451	147.9031	147.5	93.3512
533351	148.1531	147.75	93.9898
534251	148.4031	148	93.3512
536951	149.1531	148.75	93.3512
541451	150.4031	150	93.9898
542351	150.6531	150.25	93.9898
543251	150.9031	150.5	92.7127
544151	151.1531	150.75	89.5198
545051	151.4031	151	93.3512
545951	151.6531	151.25	92.7127
546851	151.9031	151.5	92.0741
547751	152.1531	151.75	92.0741
548651	152.4031	152	90.7969
549551	152.6531	152.25	90.1584
550451	152.9031	152.5	95.9055
551351	153.1531	152.75	92.7127
552251	153.4031	153	93.3512
553151	153.6531	153.25	91.4355
554051	153.9031	153.5	96.5441
554951	154.1531	153.75	88.8812
555851	154.4031	154	88.2427
556751	154.6531	154.25	90.7969
557651	154.9031	154.5	88.2427

Time (s)	Time (hr)	Time (Corrected)	P (psig)
558551	155.1531	154.75	87.6041
559451	155.4031	155	92.0741
560351	155.6531	155.25	92.7127
561251	155.9031	155.5	94.6284
562151	156.1531	155.75	88.8812
563051	156.4031	156	91.4355
563951	156.6531	156.25	89.5198
564851	156.9031	156.5	93.3512
565751	157.1531	156.75	92.7127
566651	157.4031	157	92.0741
567551	157.6531	157.25	92.7127
568451	157.9031	157.5	88.8812
569351	158.1531	157.75	92.0741
570251	158.4031	158	92.7127
571151	158.6531	158.25	88.8812
572051	158.9031	158.5	88.8812
572951	159.1531	158.75	93.3512
573851	159.4031	159	90.7969
574751	159.6531	159.25	89.5198
575651	159.9031	159.5	95.9055
576551	160.1531	159.75	95.2669
577451	160.4031	160	89.5198
578351	160.6531	160.25	88.8812
579251	160.9031	160.5	91.4355
580151	161.1531	160.75	91.4355
581051	161.4031	161	89.5198
581951	161.6531	161.25	92.0741
582851	161.9031	161.5	93.3512
583751	162.1531	161.75	89.5198
584651	162.4031	162	90.1584
585551	162.6531	162.25	91.4355
586451	162.9031	162.5	91.4355
587351	163.1531	162.75	91.4355
588251	163.4031	163	92.7127
589151	163.6531	163.25	91.4355
590051	163.9031	163.5	90.1584
590951	164.1531	163.75	93.9898
591851	164.4031	164	90.7969
592751	164.6531	164.25	94.6284
593651	164.9031	164.5	92.7127
594551	165.1531	164.75	91.4355

Time (s)	Time (hr)	Time (Corrected)	P (psig)
595451	165.4031	165	92.0741
596351	165.6531	165.25	92.7127
597251	165.9031	165.5	91.4355
598151	166.1531	165.75	93.9898
599051	166.4031	166	90.7969
599951	166.6531	166.25	92.0741
600851	166.9031	166.5	91.4355
601751	167.1531	166.75	89.5198
602651	167.4031	167	88.8812
603551	167.6531	167.25	89.5198
604451	167.9031	167.5	86.9655
605351	168.1531	167.75	88.8812
606251	168.4031	168	92.7127
607151	168.6531	168.25	89.5198
608051	168.9031	168.5	92.7127
608951	169.1531	168.75	86.9655
609851	169.4031	169	88.2427
610751	169.6531	169.25	90.1584
611651	169.9031	169.5	89.5198
612551	170.1531	169.75	87.6041
613451	170.4031	170	90.7969
614351	170.6531	170.25	89.5198
615251	170.9031	170.5	90.7969
616151	171.1531	170.75	91.4355
617051	171.4031	171	89.5198
617951	171.6531	171.25	90.7969
618851	171.9031	171.5	88.8812
619751	172.1531	171.75	88.2427
620651	172.4031	172	86.9655
621551	172.6531	172.25	88.8812
622451	172.9031	172.5	90.7969
623351	173.1531	172.75	89.5198
624251	173.4031	173	88.2427
625151	173.6531	173.25	91.4355
626051	173.9031	173.5	85.6884
626951	174.1531	173.75	89.5198
627851	174.4031	174	91.4355
628751	174.6531	174.25	90.1584
629651	174.9031	174.5	89.5198
630551	175.1531	174.75	86.3270
631451	175.4031	175	88.8812
632351	175.6531	175.25	86.3270
633251	175.9031	175.5	89.5198
634151	176.1531	175.75	84.4113
635051	176.4031	176	85.0498
635951	176.6531	176.25	86.9655
636851	176.9031	176.5	88.8812
637751	177.1531	176.75	90.1584
638651	177.4031	177	86.3270
639551	177.6531	177.25	86.9655
640451	177.9031	177.5	88.2427
641351	178.1531	177.75	92.0741
642251	178.4031	178	90.7969
643151	178.6531	178.25	91.4355
644051	178.9031	178.5	89.5198
644951	179.1531	178.75	88.8812
645851	179.4031	179	86.9655
646751	179.6531	179.25	86.3270
647651	179.9031	179.5	85.0498
648551	180.1531	179.75	87.6041
649451	180.4031	180	88.8812
650351	180.6531	180.25	88.2427
651251	180.9031	180.5	84.4113
652151	181.1531	180.75	85.6884
653051	181.4031	181	88.2427
653951	181.6531	181.25	85.6884
654851	181.9031	181.5	90.7969
655751	182.1531	181.75	83.7727
656651	182.4031	182	84.4113
657551	182.6531	182.25	85.0498
658451	182.9031	182.5	86.9655
659351	183.1531	182.75	88.2427
660251	183.4031	183	86.3270
661151	183.6531	183.25	88.2427
662051	183.9031	183.5	88.2427
662951	184.1531	183.75	86.9655
663851	184.4031	184	84.4113
664751	184.6531	184.25	84.4113
665651	184.9031	184.5	84.4113
666551	185.1531	184.75	86.9655
667451	185.4031	185	88.8812
668351	185.6531	185.25	87.6041

Time (s)	Time (hr)	Time (Corrected)	P (psig)
669251	185.9031	185.5	85.0498
670151	186.1531	185.75	83.7727
671051	186.4031	186	86.3270
671951	186.6531	186.25	86.3270
672851	186.9031	186.5	81.8570
673751	187.1531	186.75	85.0498
674651	187.4031	187	86.9655
675551	187.6531	187.25	86.3270
676451	187.9031	187.5	81.2184
677351	188.1531	187.75	88.8812
678251	188.4031	188	82.4956
679151	188.6531	188.25	88.8812
680051	188.9031	188.5	89.5198
680951	189.1531	188.75	84.4113
681851	189.4031	189	86.3270
682751	189.6531	189.25	81.8570
683651	189.9031	189.5	83.7727
684551	190.1531	189.75	85.6884
685451	190.4031	190	84.4113
686351	190.6531	190.25	81.2184
687251	190.9031	190.5	86.9655
688151	191.1531	190.75	83.7727
689051	191.4031	191	86.3270
689951	191.6531	191.25	83.7727
690851	191.9031	191.5	83.1341
691751	192.1531	191.75	86.9655
692651	192.4031	192	83.1341
693551	192.6531	192.25	83.1341
694451	192.9031	192.5	82.4956
695351	193.1531	192.75	83.7727
696251	193.4031	193	86.9655
697151	193.6531	193.25	83.1341
698051	193.9031	193.5	83.7727
698951	194.1531	193.75	81.2184
699851	194.4031	194	82.4956
700751	194.6531	194.25	83.7727
701651	194.9031	194.5	84.4113
702551	195.1531	194.75	83.7727
703451	195.4031	195	81.2184
704351	195.6531	195.25	83.7727

Pressure Decline Data
T = 130°C, $C_{4(g)}$-heavy oil

Time (s)	Time (hr)	Time (Corrected)	P (psig)
2786	0.773889	0	300.24745
3686	1.023889	0.25	285.560372
4586	1.273889	0.5	279.174686
5486	1.523889	0.75	272.150431
6386	1.773889	1	267.041883
7286	2.023889	1.25	261.933334
8186	2.273889	1.5	256.824785
9086	2.523889	1.75	254.270511
9986	2.773889	2	249.161962
10886	3.023889	2.25	243.414844
11786	3.273889	2.5	237.667727
12686	3.523889	2.75	236.39059
13586	3.773889	3	229.366335
14486	4.023889	3.25	226.173492
15386	4.273889	3.5	224.896355
16286	4.523889	3.75	220.426375
17186	4.773889	4	218.510669
18086	5.023889	4.25	217.8721
18986	5.273889	4.5	215.956394
19886	5.523889	4.75	215.317826
20786	5.773889	5	215.317826
21686	6.023889	5.25	212.763551
22586	6.273889	5.5	212.763551
23486	6.523889	5.75	212.124983
24386	6.773889	6	210.209277
25286	7.023889	6.25	209.570708
26186	7.273889	6.5	206.377865
27086	7.523889	6.75	207.655003
27986	7.773889	7	205.100728
28886	8.023889	7.25	205.100728
29786	8.273889	7.5	201.907885
30686	8.523889	7.75	203.823591
31586	8.773889	8	201.907885
32486	9.023889	8.25	199.992179
33386	9.273889	8.5	198.715042
34286	9.523889	8.75	199.992179
35186	9.773889	9	196.799336
36086	10.02389	9.25	196.160768
36986	10.27389	9.5	198.715042
37886	10.52389	9.75	197.437905
38786	10.77389	10	198.715042
39686	11.02389	10.25	194.245062
40586	11.27389	10.5	196.160768
41486	11.52389	10.75	196.799336
42386	11.77389	11	191.052219
43286	12.02389	11.25	193.606493
44186	12.27389	11.5	191.052219
45086	12.52389	11.75	191.052219
45986	12.77389	12	192.967925
46886	13.02389	12.25	191.690788
47786	13.27389	12.5	189.136513
48686	13.52389	12.75	189.775082
49586	13.77389	13	190.41365
50486	14.02389	13.25	184.666533
51386	14.27389	13.5	190.41365
52286	14.52389	13.75	189.136513
53186	14.77389	14	187.859376
54086	15.02389	14.25	185.305102
54986	15.27389	14.5	184.666533
55886	15.52389	14.75	185.94367
56786	15.77389	15	187.220807
57686	16.02389	15.25	182.750827
58586	16.27389	15.5	182.112259
59486	16.52389	15.75	184.027964
60386	16.77389	16	183.389396
61286	17.02389	16.25	183.389396
62186	17.27389	16.5	180.835121
63086	17.52389	16.75	181.47369
63986	17.77389	17	178.919416
64886	18.02389	17.25	179.557984
65786	18.27389	17.5	178.919416
66686	18.52389	17.75	179.557984
67586	18.77389	18	174.449435
68486	19.02389	18.25	178.280847
69386	19.27389	18.5	175.726573
70286	19.52389	18.75	177.642278
71186	19.77389	19	177.00371

Time (s)	Time (hr)	Time (Corrected)	P (psig)
72086	20.02389	19.25	171.256592
72986	20.27389	19.5	171.895161
73886	20.52389	19.75	173.810867
74786	20.77389	20	173.810867
75686	21.02389	20.25	174.449435
76586	21.27389	20.5	172.533729
77486	21.52389	20.75	172.533729
78386	21.77389	21	171.256592
79286	22.02389	21.25	173.172298
80186	22.27389	21.5	168.702318
81086	22.52389	21.75	169.979455
81986	22.77389	22	169.340886
82886	23.02389	22.25	168.702318
83786	23.27389	22.5	166.786612
84686	23.52389	22.75	165.509475
85586	23.77389	23	164.870906
86486	24.02389	23.25	159.123789
87386	24.27389	23.5	161.039495
88286	24.52389	23.75	155.930946
89186	24.77389	24	157.846652
90086	25.02389	24.25	157.208083
90986	25.27389	24.5	155.292377
91886	25.52389	24.75	150.822397
92786	25.77389	25	148.906691
93686	26.02389	25.25	150.822397
94586	26.27389	25.5	150.822397
95486	26.52389	25.75	146.352417
96386	26.77389	26	146.352417
97286	27.02389	26.25	145.07528
98186	27.27389	26.5	142.521005
99086	27.52389	26.75	140.605299
99986	27.77389	27	141.243868
100886	28.02389	27.25	138.689594
101786	28.27389	27.5	140.605299
102686	28.52389	27.75	141.243868
103586	28.77389	28	139.328162
104486	29.02389	28.25	140.605299
105386	29.27389	28.5	141.882437
106286	29.52389	28.75	138.051025
107186	29.77389	29	139.966731
108086	30.02389	29.25	140.605299
108986	30.27389	29.5	140.605299
109886	30.52389	29.75	139.966731
110786	30.77389	30	138.689594
111686	31.02389	30.25	139.966731
112586	31.27389	30.5	142.521005
113486	31.52389	30.75	139.966731
114386	31.77389	31	143.798142
115286	32.02389	31.25	143.798142
116186	32.27389	31.5	143.159574
117086	32.52389	31.75	139.966731
117986	32.77389	32	141.882437
118886	33.02389	32.25	141.882437
119786	33.27389	32.5	139.966731
120686	33.52389	32.75	141.882437
121586	33.77389	33	138.689594
122486	34.02389	33.25	139.966731
123386	34.27389	33.5	139.966731
124286	34.52389	33.75	138.051025
125186	34.77389	34	141.882437
126086	35.02389	34.25	139.966731
126986	35.27389	34.5	141.243868
127886	35.52389	34.75	139.966731
128786	35.77389	35	143.159574
129686	36.02389	35.25	140.605299
130586	36.27389	35.5	141.243868
131486	36.52389	35.75	139.966731
132386	36.77389	36	142.521005
133286	37.02389	36.25	138.051025
134186	37.27389	36.5	139.966731
135086	37.52389	36.75	142.521005
135986	37.77389	37	142.521005
136886	38.02389	37.25	139.328162
137786	38.27389	37.5	139.966731
138686	38.52389	37.75	140.605299
139586	38.77389	38	140.605299
140486	39.02389	38.25	138.051025
141386	39.27389	38.5	143.798142
142286	39.52389	38.75	143.159574
143186	39.77389	39	141.243868
144086	40.02389	39.25	141.882437
144986	40.27389	39.5	138.051025

Time (s)	Time (hr)	Time (Corrected)	P (psig)
145886	40.52389	39.75	143.159574
146786	40.77389	40	141.882437
147686	41.02389	40.25	140.605299
148586	41.27389	40.5	141.243868
149486	41.52389	40.75	140.605299
150386	41.77389	41	140.605299
151286	42.02389	41.25	140.605299
152186	42.27389	41.5	141.243868
153086	42.52389	41.75	140.605299
153986	42.77389	42	140.605299
154886	43.02389	42.25	141.882437
155786	43.27389	42.5	140.605299
156686	43.52389	42.75	140.605299
157586	43.77389	43	140.605299
158486	44.02389	43.25	139.966731
159386	44.27389	43.5	141.882437
160286	44.52389	43.75	143.159574
161186	44.77389	44	139.966731
162086	45.02389	44.25	141.243868
162986	45.27389	44.5	139.328162
163886	45.52389	44.75	140.605299
164786	45.77389	45	143.159574
165686	46.02389	45.25	139.966731
166586	46.27389	45.5	141.882437
167486	46.52389	45.75	139.328162
168386	46.77389	46	139.966731
169286	47.02389	46.25	140.605299
170186	47.27389	46.5	139.966731
171086	47.52389	46.75	140.605299
171986	47.77389	47	139.966731
172886	48.02389	47.25	140.605299
173786	48.27389	47.5	139.328162
174686	48.52389	47.75	142.521005
175586	48.77389	48	142.521005
176486	49.02389	48.25	138.689594
177386	49.27389	48.5	138.051025
178286	49.52389	48.75	138.689594
179186	49.77389	49	139.966731
180086	50.02389	49.25	141.243868
180986	50.27389	49.5	142.521005
181886	50.52389	49.75	139.328162
182786	50.77389	50	138.689594
183686	51.02389	50.25	140.605299
184586	51.27389	50.5	139.966731
185486	51.52389	50.75	138.689594
186386	51.77389	51	138.051025
187286	52.02389	51.25	138.689594
188186	52.27389	51.5	142.521005
189086	52.52389	51.75	138.051025
189986	52.77389	52	141.882437
190886	53.02389	52.25	139.966731
191786	53.27389	52.5	141.243868
192686	53.52389	52.75	139.328162
193586	53.77389	53	139.328162
194486	54.02389	53.25	139.966731
195386	54.27389	53.5	143.798142
196286	54.52389	53.75	139.966731
197186	54.77389	54	140.605299
198086	55.02389	54.25	140.605299
198986	55.27389	54.5	143.159574
199886	55.52389	54.75	141.882437
200786	55.77389	55	140.605299
201686	56.02389	55.25	142.521005
202586	56.27389	55.5	137.412456
203486	56.52389	55.75	140.605299
204386	56.77389	56	138.689594
205286	57.02389	56.25	139.966731
206186	57.27389	56.5	141.243868
207086	57.52389	56.75	138.051025
207986	57.77389	57	136.773888
208886	58.02389	57.25	138.051025
209786	58.27389	57.5	140.605299
210686	58.52389	57.75	139.328162
211586	58.77389	58	138.689594
212486	59.02389	58.25	140.605299
213386	59.27389	58.5	137.412456
214286	59.52389	58.75	136.773888
215186	59.77389	59	137.412456
216086	60.02389	59.25	141.882437
216986	60.27389	59.5	139.966731
217886	60.52389	59.75	138.689594
218786	60.77389	60	139.966731

Time (s)	Time (hr)	Time (Corrected)	P (psig)
219686	61.02389	60.25	140.605299
220586	61.27389	60.5	139.328162

Appendix B: Compositional Analysis of Heavy Oil

Table B-1: Compositional analysis of heavy oil by simulated distillation method (Eghbali and Dehghanpour, 2018)

Carbon Number	Tb (^{O}C)	Weight Fraction	Carbon Number	Tb (^{O}C)	Weight Fraction
11	196	0.0034	56	600	0.0059
12	216	0.0076	57	604	0.0055
13	235	0.0137	58	608	0.0055
14	254	0.0169	59	612	0.005
15	271	0.0196	60	615	0.005
16	287	0.0205	61	619	0.005
17	302	0.0195	62	622	0.0054
18	316	0.0209	63	625	0.0046
19	330	0.02	64	629	0.005
20	344	0.0205	65	632	0.0046
21	356	0.0188	66	635	0.0047
22	369	0.0187	67	638	0.0047
23	380	0.0176	68	641	0.0047
24	391	0.0172	69	644	0.0048
25	401	0.0162	70	647	0.0049
26	412	0.0161	71	650	0.0045
27	422	0.0156	72	653	0.0045
28	431	0.0164	73	655	0.005
29	440	0.0166	74	658	0.0046
30	449	0.016	75	661	0.0051

31	458	0.0141	76	664	0.0047
32	466	0.0137	77	667	0.0053
33	474	0.0126	78	670	0.0054
34	481	0.0122	79	673	0.005
35	489	0.0115	80	675	0.0051
36	496	0.012	81	678	0.0057
37	503	0.0102	82	681	0.0054
38	509	0.01	83	683	0.0055
39	516	0.0103	84	686	0.0062
40	522	0.0097	85	688	0.0057
41	528	0.009	86	691	0.0059
42	534	0.0083	87	693	0.0061
43	540	0.0087	88	695	0.0063
44	545	0.0085	89	697	0.0064
45	550	0.0075	90	700	0.0065
46	556	0.0069	91	702	0.0066
47	561	0.0073	92	704	0.0069
48	566	0.0072	93	706	0.0064
49	570	0.0067	94	708	0.0072
50	575	0.0066	95	710	0.0072
51	579	0.0065	96	712	0.0064
52	584	0.0061	97	714	0.0075
53	588	0.006	98	716	0.0072
54	592	0.006	99	718	0.0074
55	596	0.0056	100+	-	0.198

Appendix C: Viscosity Modelling

Following is the viscosity model developed by Eghbali and Dehghanpour, 2017.

$$\ln \mu_L = \sum_{i=1}^{n} x_i ln\mu_{iL}$$

They replaced the weighting factor with $N_k x_k$ for for the key components and with $N_{nk} x_k$ for the non-key components. Their viscosity model is referred as nonlinear mixing model.

$$\ln \mu_L = \sum_{i=k\ and\ nk} N_i x_i ln\mu_{iL}$$

Where,

$$N_{nk} = \frac{1 - N_k x_k}{\sum_{i=nk} x_i}$$

$$N_k = 1 + \alpha_1 \left[\frac{(1 - x_k) \times (1 - (1 - x_k)^{\alpha_2}}{x_k} \right]$$

Table C-1: Optimized coefficients for key components in viscosity modelling (Eghbali and Dehghanpour, 2018)

System	α_1	α_2
C_3-bitumen	0.4702	6.9718
C_4-bitumen	0.2909	10.1969

Appendix D: Matlab Code For Data Clustering

```
close all; clear; clc; tic
Data = xlsread('data.xlsx','130c');
E = 100; % length of data points [130c: 100]
Cl = 3;
sd = 300; % Seed of Matlab random number generator
l_SDs = 30;
Considered_Clusters = [];
%--------------------------------------------------------------------------
% Read data
T = Data(1:min(E,length(Data)),3);
ln_p = Data(1:min(E,length(Data)),8);
% Plot data
figure(1)
plot(T,ln_p,'or')
hold on
%--------------------------------------------------------------------------
rng('default');
rng(sd);
SDs = randi(1000,l_SDs,1);
Results = zeros(l_SDs, 3+Cl);
for n = 1:l_SDs
rng('default');
rng(SDs(n));
Results(n,1) = n;
Results(n,2) = SDs(n);
% Clustering:
% Idx = clusterdata([T, ln_p],2); % Idx of clustered data
Idx = kmeans([T, ln_p],Cl);
Num_Clus = max(Idx); % Number of Clusters
for i = 1:Num_Clus
iX = T(Idx == i); iY = ln_p(Idx == i); L_ix = length(iX);
% Fit data:
md = fitlm(iX,iY);
Results(n,i+2) = md.Rsquared.Ordinary;
end % for i = 1:Num_Clus
if ~isempty(Considered_Clusters)
R2_Des = sort((Results(n,3:3+Cl-1)),'descend');
cR2 = mean(R2_Des(1:Considered_Clusters));
else
cR2 = mean(Results(n,3:3+Cl-1));
end
Results(n,end) = cR2;
end % for n = 1:l_SDs
% Idx of best results:
[val, idx] = max(Results(:,end));
rng('default');
rng(SDs(idx));
%--------------------------------------------------------------------------
Idx = kmeans([T, ln_p],Cl);
Num_Clus = max(Idx);
```

```
Coc = hsv(Num_Clus);
for i = 1:Num_Clus
iX = T(Idx == i); iY = ln_p(Idx == i); L_ix = length(iX);
plot(iX,iY,'o', 'color',Coc(i,:),'MarkerSize',10)
hold on
% Fit data:
md = fitlm(iX,iY);
plot(md,'color',Coc(i,:))
% write on plot
txt = [' R^{2}= ', num2str(md.Rsquared.Ordinary)];
text(iX(ceil(L_ix/2)),iY(ceil(L_ix/3)),txt,'FontSize',14)
end % for i = 1:Num_Clus
```

Appendix E: Plots After Data Clustering

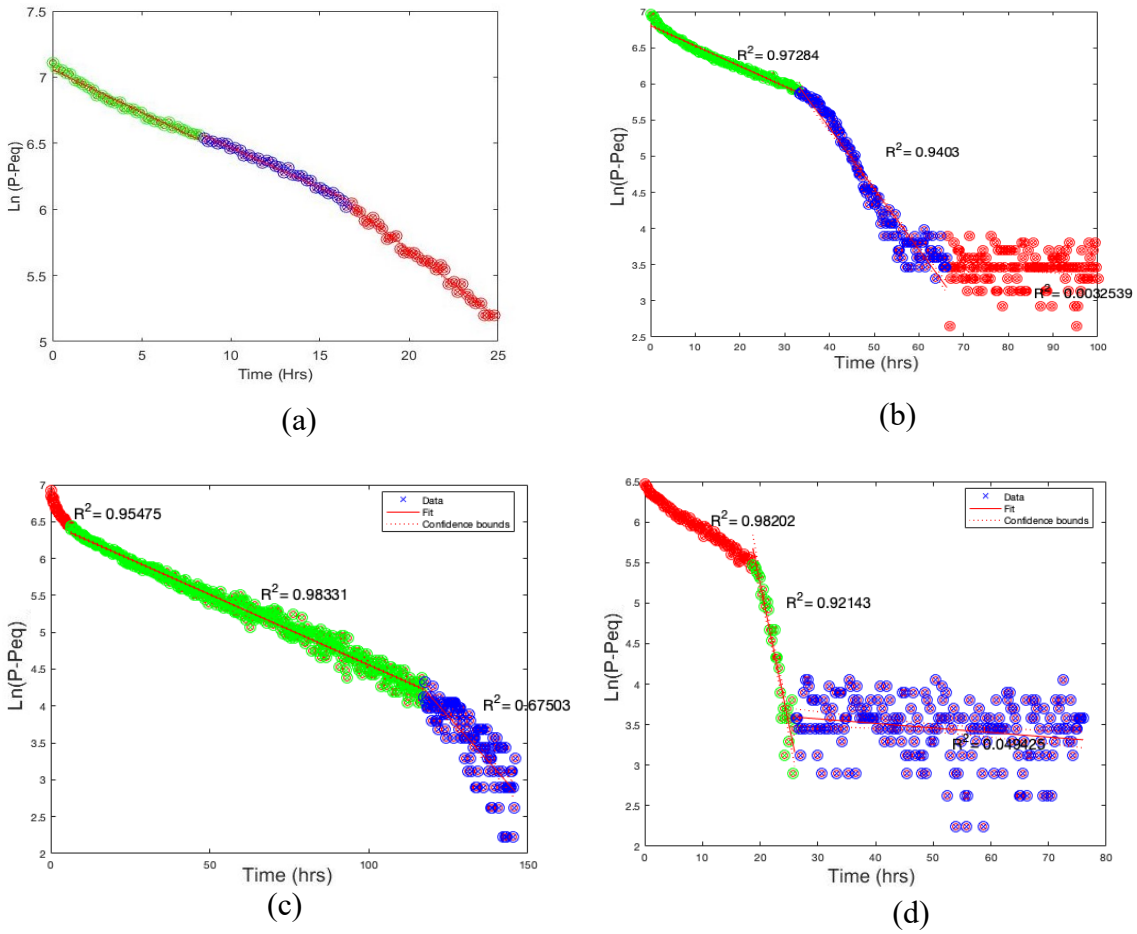

Figure E-1: Plot of Ln(P-P_{eq}) vs Time for C_3-heavy oil system at (a) 100°C, (b) 85°C, (c) 65°C and (d) for C_4-heavy oil system at 130°C. Green, blue and red color represents early, transition and late time region.

Copyrights Permissions

Chapter 4

License Number	4519410474051
License date	Jan 30, 2019
Licensed content publisher	Society of Petroleum Engineers
Licensed content title	SPE International Heavy Oil Conference and Exhibition
Licensed content date	Jan 1, 2018
Type of Use	Thesis/Dissertation
Requestor type	Academic institution
Format	Electronic
Portion	chapter/article
Number of pages in chapter/article	10
The requesting person/organization is:	Khan Athar
Title or numeric reference of the portion(s)	Chapter 1, Chapter 4
Title of the article or chapter the portion is from	Estimating Diffusion Coefficients and Visualizing Interactions in Propane-Heavy Oil Systems
Editor of portion(s)	Khan Athar
Author of portion(s)	Khan Athar
Volume of serial or monograph.	N/A
Page range of the portion	1-10
Publication date of portion	2019
Rights for	Main product
Duration of use	Life of current and all future editions
Creation of copies for the disabled	no
With minor editing privileges	yes
For distribution to	Worldwide
In the following language(s)	Original language of publication
With incidental promotional use	no
The lifetime unit quantity of new product	More than 2,000,000
Title	Estimating Diffusion Coefficients and Visualizing Interactions in Propane-Heavy Oil Systems
Institution name	University of Alberta
Expected presentation date	Jan 2019
Billing Type	Invoice
Billing Address	Khan S Athar 1125 Lakewood Road North North West Edmonton, AB T6K 3A9 Canada